LA-3235

LOS ALAMOS SCIENTIFIC LABORATORY
LOS ALAMOS of the NEW MEXICO
University of California

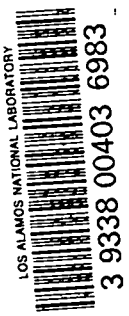

THE TWO-DIMENSIONAL HYDRODYNAMIC HOT SPOT
VOLUME II

UNITED STATES
ATOMIC ENERGY COMMISSION
CONTRACT W-7405-ENG. 36

This report expresses the opinions of the author or authors and does not necessarily reflect the opinions or views of the Los Alamos Scientific Laboratory.

Printed in USA. Price $ 4.00. Available from the

Clearinghouse for Federal Scientific
and Technical Information,
National Bureau of Standards,
U. S. Department of Commerce,
Springfield, Virginia

LA-3235
UC-4, CHEMISTRY
TID-4500 (37th Ed.)

LOS ALAMOS SCIENTIFIC LABORATORY
LOS ALAMOS of the NEW MEXICO
University of California

Report written: November 20, 1964
Report distributed: April 3, 1965

THE TWO-DIMENSIONAL HYDRODYNAMIC HOT SPOT
VOLUME II

by

Charles L. Mader

ABSTRACT

The basic processes in the shock initiation of inhomogeneous explosives are investigated theoretically using the model of a cylinder of nitromethane containing either a cylindrical or a biconical void, or a sphere or cylinder of aluminum. The interaction of a shock with these density discontinuities, the resulting formation of a hot spot, and the buildup to propagating detonation are computed using two-dimensional numerical hydrodynamics of the PIC type. For the aluminum density discontinuities, the calculations exhibit failure or propagation of detonation from the hot spot in approximately the same manner as does the one-dimensional hydrodynamic hot spot model.

The interaction of a shock with corners of aluminum and Plexiglas in nitromethane is discussed.

Radiographs of a shock interacting with a spherical bubble in water are compared with theoretical calculations and confirm the validity of the computations.

ACKNOWLEDGMENT

The author gratefully acknowledges the assistance and contributions of F. H. Harlow, Jr. of T-3, and of D. Venable, T. J. Boyd, Jr., J. R. Ruhe, W. C. Davis, J. R. Travis, B. G. Craig, W. Fickett, W. Gage, and L. C. Smith of the GMX Division of the Los Alamos Scientific Laboratory.

CONTENTS

APPENDICES

FIGURES

FIGURES - Continued

TABLES

I. INTRODUCTION

The mechanism of shock initiation of detonation of inhomogeneous explosives has been considered both experimentally and theoretically by numerous investigators. Initiation of inhomogeneous explosives is a result of shock interactions with the inhomogeneities, which produces numerous local hot spots in the bulk of the shocked explosive. The local hot spots decompose and result in nonpropagating explosions which strengthen the shock sufficiently that when it interacts with other inhomogeneities the hot spots are hotter and more of the explosive is decomposed. The shock wave grows stronger and stronger, releasing more and more energy, until it becomes strong enough to produce temperatures at which all the explosive reacts, and detonation begins. An experimental description of this process is presented in Appendix D. This initiation process is too complicated to describe with existing numerical computing techniques, and as described in Appendix D it can not even be empirically reproduced with a one-dimensional model if one uses realistic rates of homogeneous decomposition of the explosive.

In order to increase our understanding of the basic processes involved in the shock initiation of inhomogeneous explosives we have studied the formation of hot spots from shocks interacting with spherical, cylindrical, or conical voids and with cylinders and spheres of aluminum in the belief that they will exhibit the approximate features of real density discontinuities in heterogeneous explosives.

It is assumed that the reader is acquainted with the contents of the first volume describing the initial studies of the two-dimensional hydrodynamic hot spot[1].

In the first volume we described the results of our two-dimensional approach to studying heterogeneous shock initiation using the model of a shock in a cylinder of nitromethane interacting with a spherical void. We computed the interaction of a shock with the spherical void, the formation of the hot spot, and buildup to propagating detonation. In this volume, we describe the results for a shock interacting with cylindrical and conical voids in nitromethane. We also describe the results for a shock interacting with a sphere and with a cylinder of aluminum. The details of how the EIC (Explosive-In-a-Cell) code handles two components are described in Appendices A and B. In the case of a shock interacting with an aluminum discontinuity in nitromethane, the hot spot is formed behind the shock front and is at a lower temperature than the hot spot formed by a shock interacting with a void. The one-dimensional hydrodynamic hot spot model is appropriate, and the two-dimensional calculations show failure and propagation in approximately the same manner as does the one-dimensional hydrodynamic hot spot model[2,3].

The experimentally observed early initiation of nitromethane from the interaction of a shock with corners of Plexiglas and aluminum is also shown to be a result of the hydrodynamic flow.

In Appendix C we describe the recent radiographs of bubble closure in water. Comparison with EIC calculations for this system yields further evidence of the validity of the computed results.

II. CYLINDRICAL VOIDS IN NITROMETHANE

The initial and boundary conditions of the calculation were chosen to match the model shown in Figure 1. A cylinder of nitromethane contains a cylindrical void centered on the axis. The axial symmetry of the system allows a two-dimensional description of the process in terms of the usual axial and radial coordinates.

The results of a nonreactive EIC calculation are presented in the form of pictures in Figure 2 for a 0.064-cm-radius, 0.128-cm-high cylinder of nitromethane containing a 0.032-cm-radius, 0.032-cm-high cylindrical void. A piston is applied to the bottom of the cylinder, shocking the nitromethane to 85 kbar and 1200°K.

The 85-kbar, 1200°K shock arrives at the lower surface of the void traveling with a shock velocity of 0.45 cm/μsec and a particle velocity of 0.171 cm/μsec. The free surface velocity of the surface fluid becomes 0.342 cm/μsec with a temperature of 530°K. Since the shock in the nitromethane is going faster than the nitromethane free surface in the void, the surface fluid at the side of the cylinder starts moving toward the axis with a velocity of 0.1 cm/μsec as well as toward the top of the void. This results in a jet with a velocity that increases

as the jet approaches the top of the void. For a 0.032-cm-radius, 0.032-cm-high void the jet velocity is 0.48 cm/μsec upon arriving at the top of the void, and for a 0.048-cm-high void of the same radius the jet velocity is 0.52 cm/μsec upon arriving at the top of the void.

The convergence and shocks of the system also increase the velocity of the nitromethane between the jet and the center of the void. Near the center of the void the velocity of the surface nitromethane at collapse is 0.4 cm/μsec for a 0.032-cm-high void and 0.48 cm/μsec for a 0.048-cm-high void.

For a given radius, a taller cylindrical void gives a hotter hot spot. For a given height, a larger radius cylindrical void produces a cooler hot spot at the axis, but the size of the hot spot is about the same.

The results of a reactive EIC calculation for a 0.032-cm-radius, 0.032-cm-high cylindrical void are presented in Figure 3. Reaction occurs first in the region between the jet and the side of the void, and then in the region where the jet collides with the upper surface of the void. The formation of a propagating detonation occurs in much the same manner as in spherical voids[1].

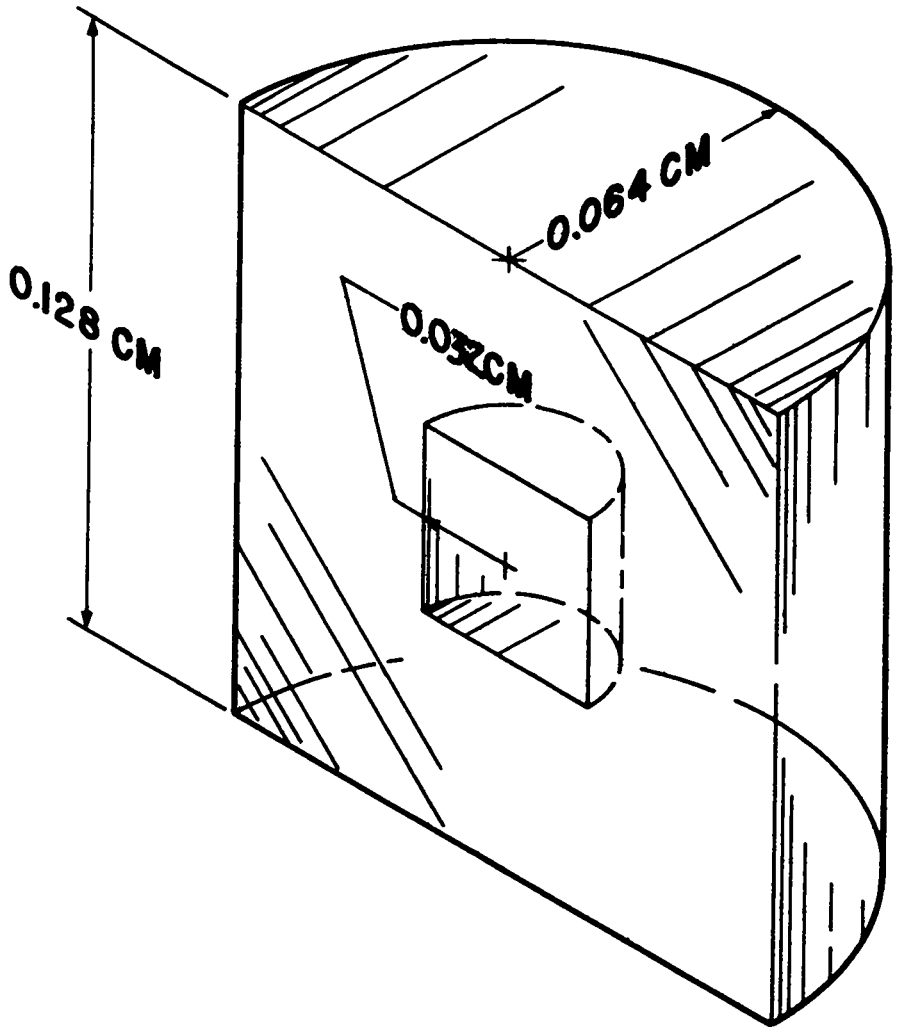

Figure 1. A cross section of a cylinder of nitromethane containing a cylindrical void centered on the axis.

Figure 2

THE FORMATION OF A HOT SPOT FROM A 0.032-cm-RADIUS, 0.032-cm-HIGH CYLINDRICAL VOID

The right sides of the following pictures show the shapes, wave positions, and fluid element (particle) positions for a cylinder of nitromethane containing a cylindrical void. A piston is applied to the bottom of the cylinder, shocking the nitromethane to 85 kbar and 1200°K. Chemical reaction is not permitted. The position of those cells with a temperature greater than 1400°K is shown on the left half of the picture with an "x". Isotherm plots are shown for the hot spot at 0.22 μsec for the left half of the cylinder. The dashed line represents the position of the interface between the top of the void and the nitromethane that filled the void. This position is also visible in the particle position plots since the resolution is only one cell width. The void is actually completely closed at the later times.

0.005μ sec.

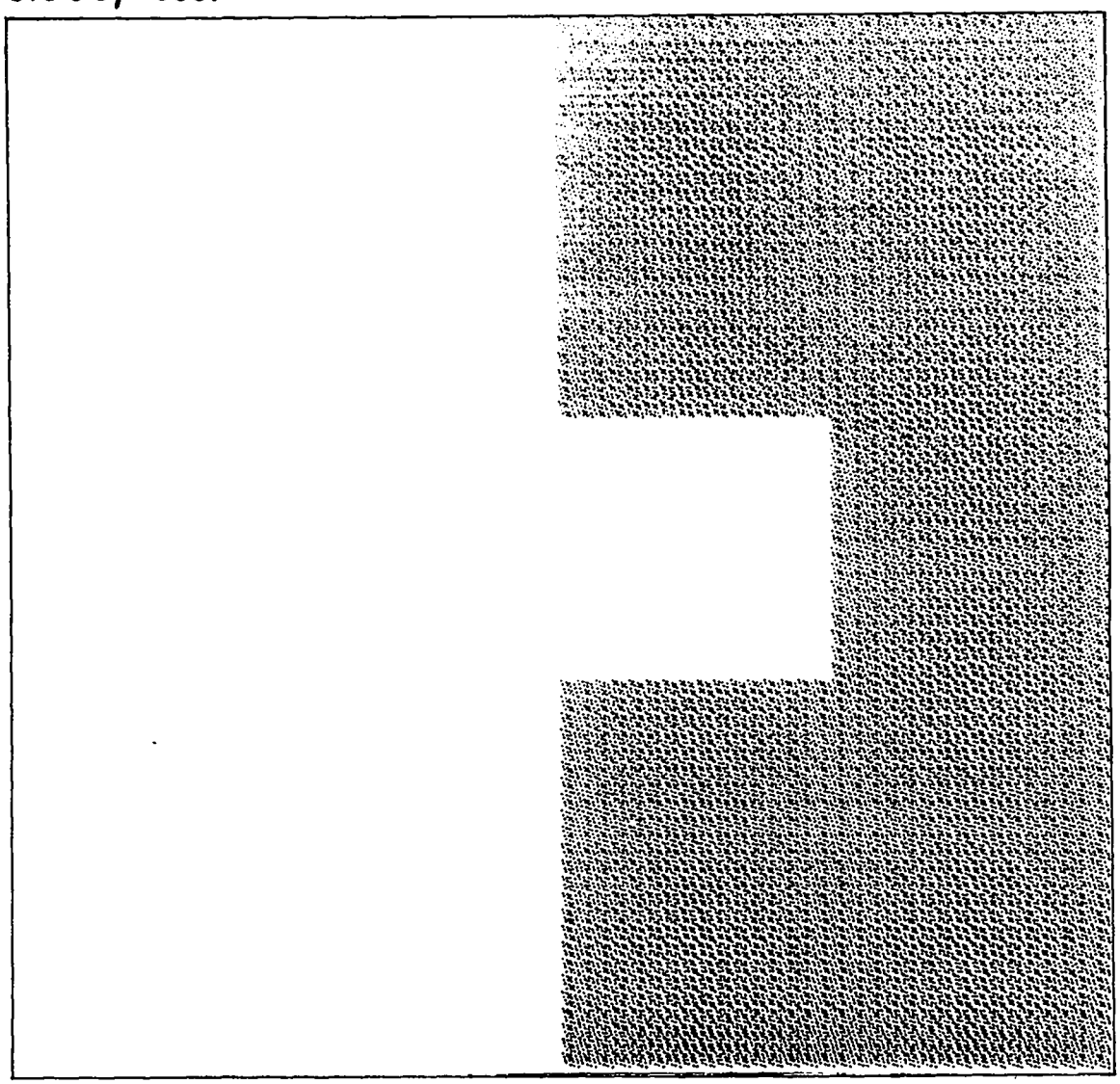

THE TIME IS 5.00000-003 MICROSECONDS AND THE CYCLE NUMBER IS 1.00000+001

0.125μ sec.

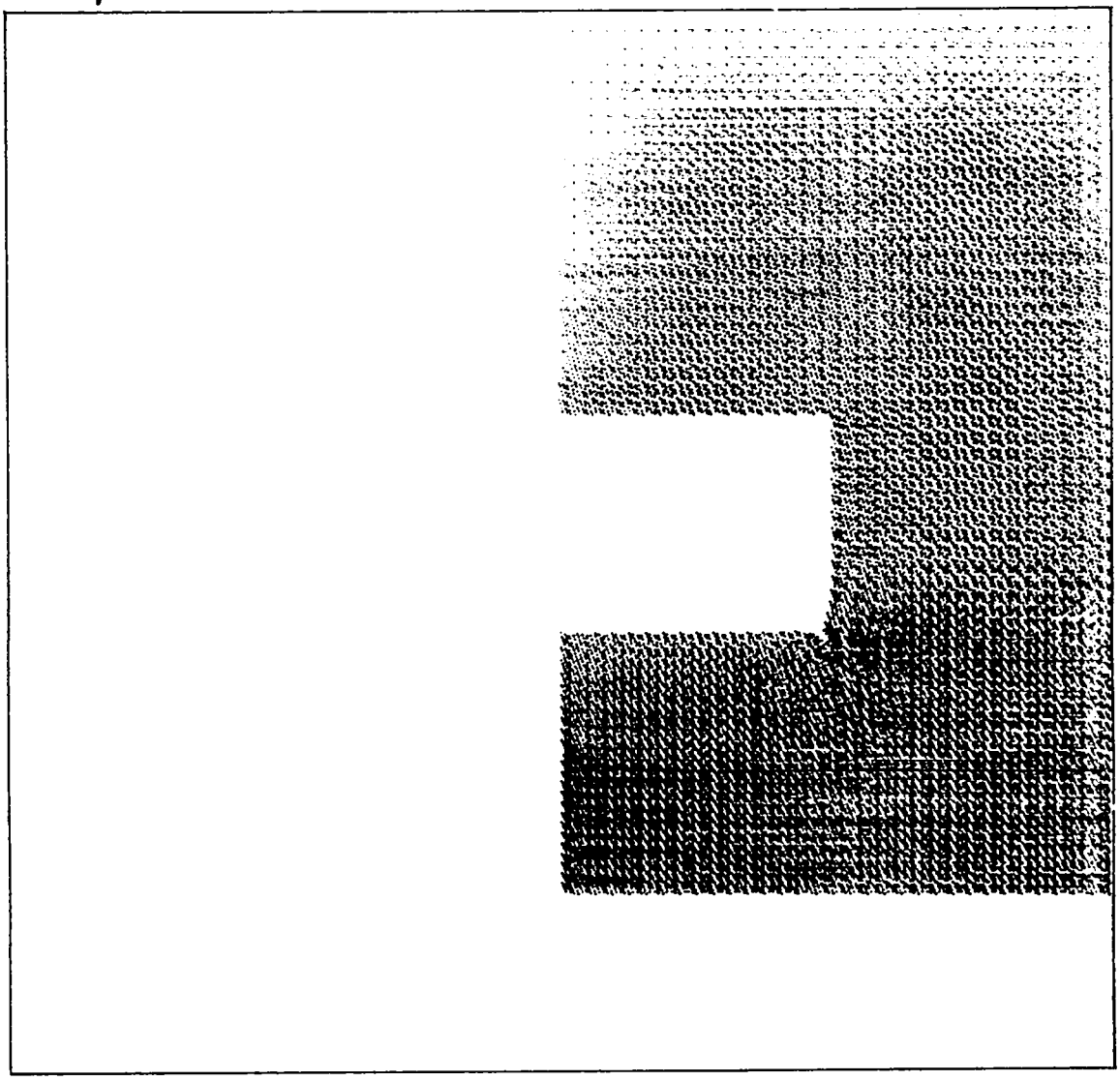

THE TIME IS 1.25000-001 MICROSECONDS AND THE CYCLE NUMBER IS 2.50000+002

0.150μ sec.

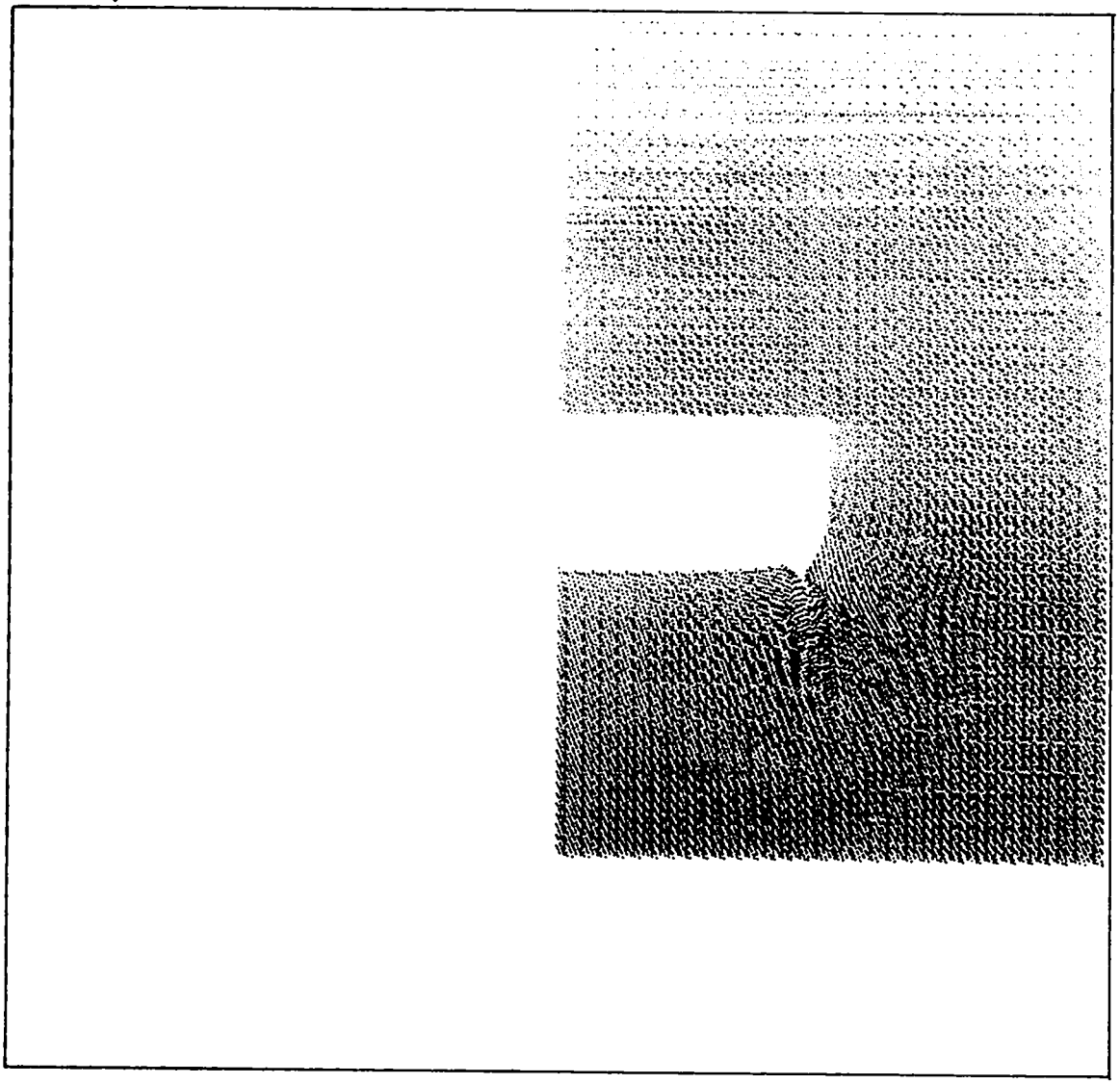

THE TIME IS 1.50000-001 MICROSECONDS AND THE CYCLE NUMBER IS 3.00000+002

0.180μ sec.

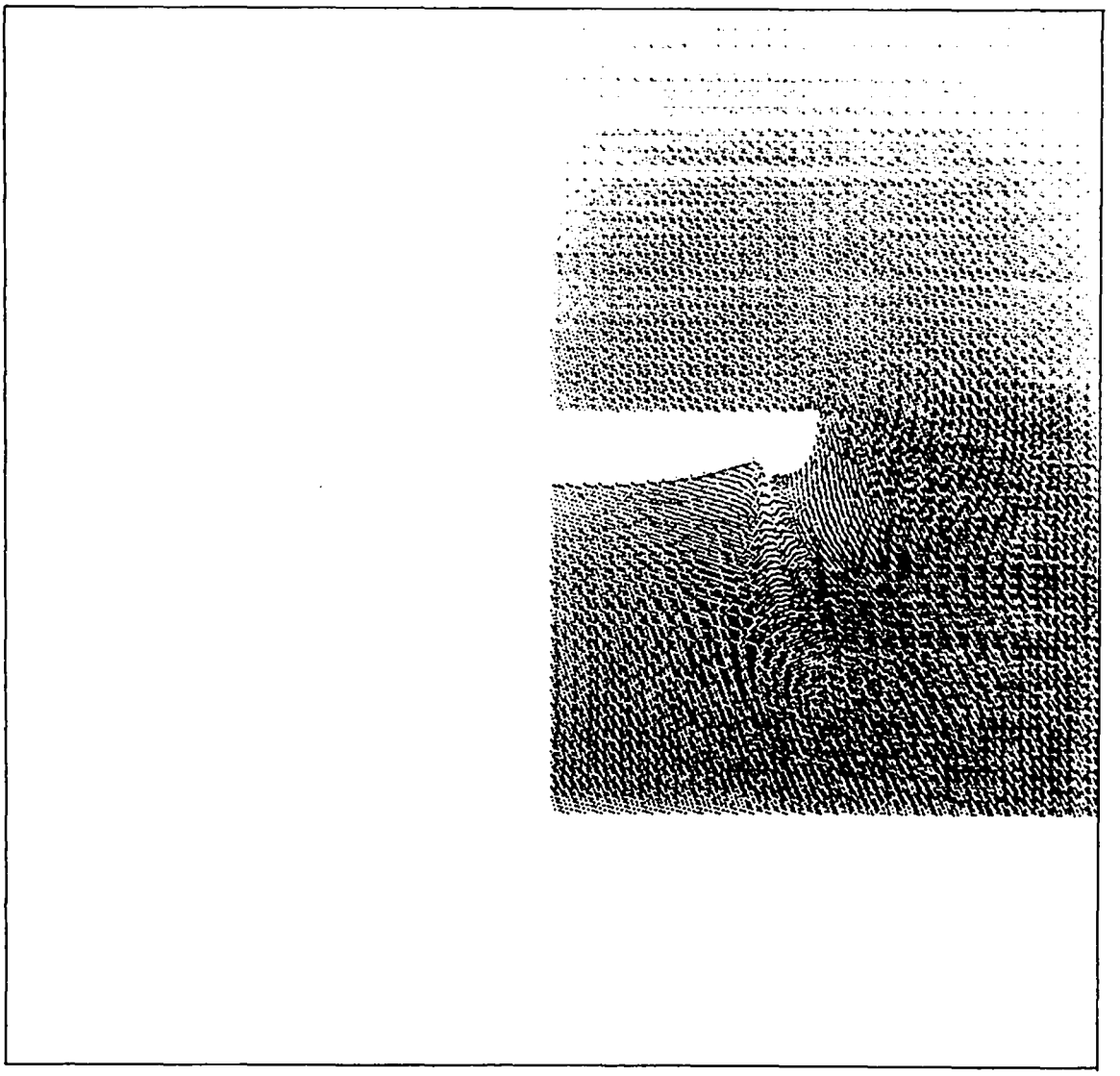

THE TIME IS 1.80000-001 MICROSECONDS AND THE CYCLE NUMBER IS 3.60000+002

0.190μ sec.

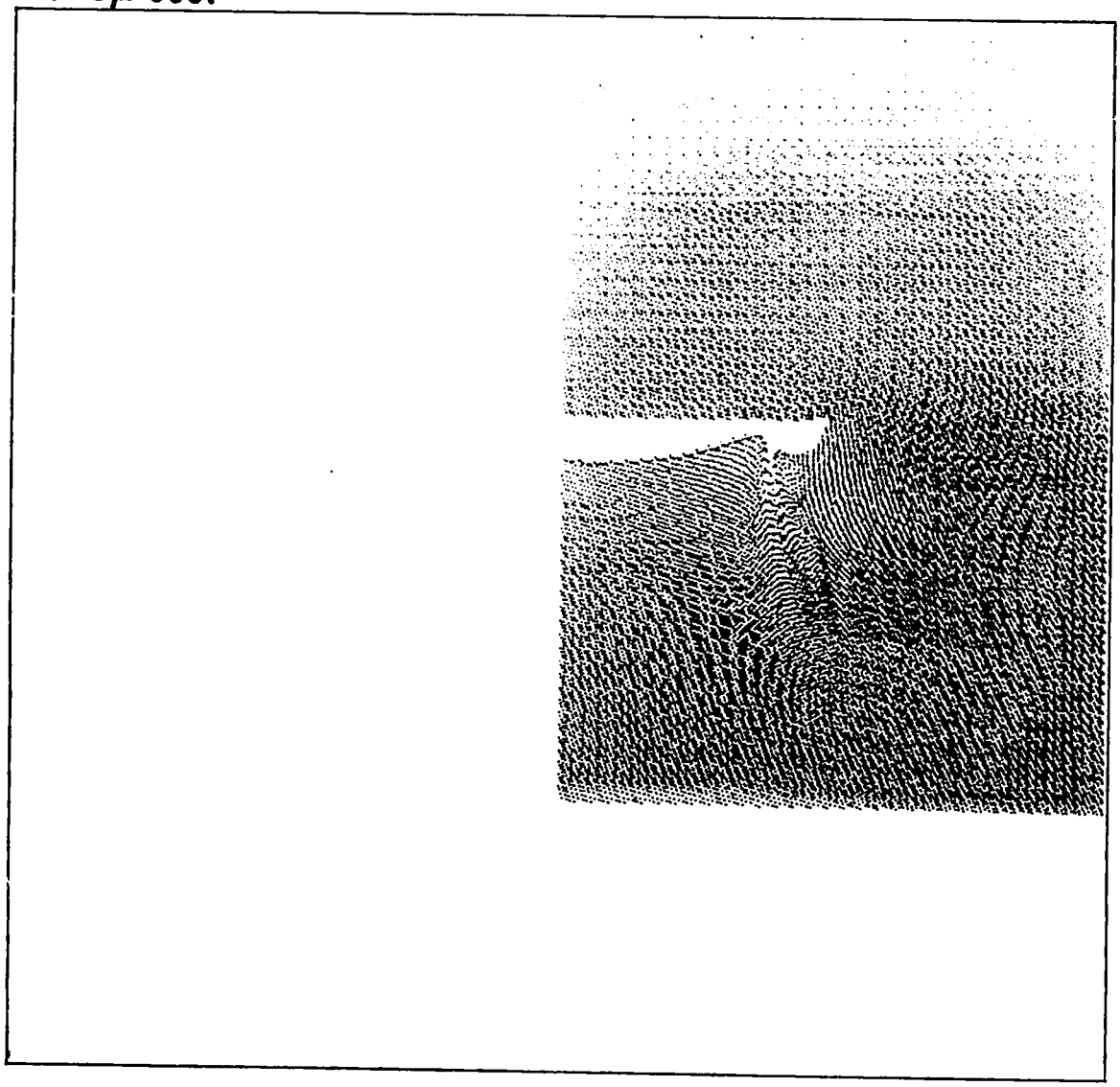

THE TIME IS 1.90000-001 MICROSECONDS AND THE CYCLE NUMBER IS 3.80000+002

0.195μ sec.

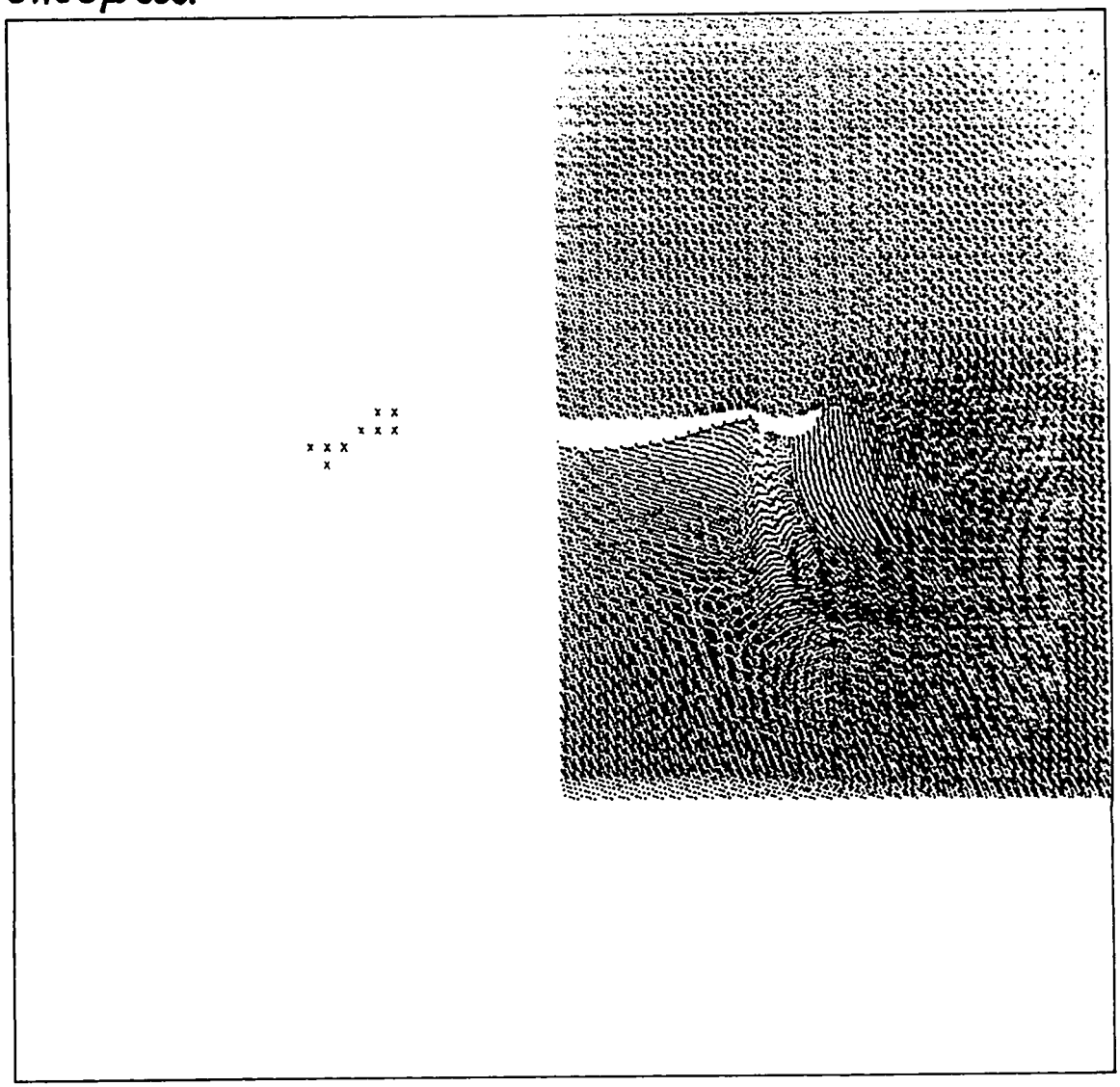

THE TIME IS 1.95000-001 MICROSECONDS AND THE CYCLE NUMBER IS 3.90000+002

0.200μ sec.

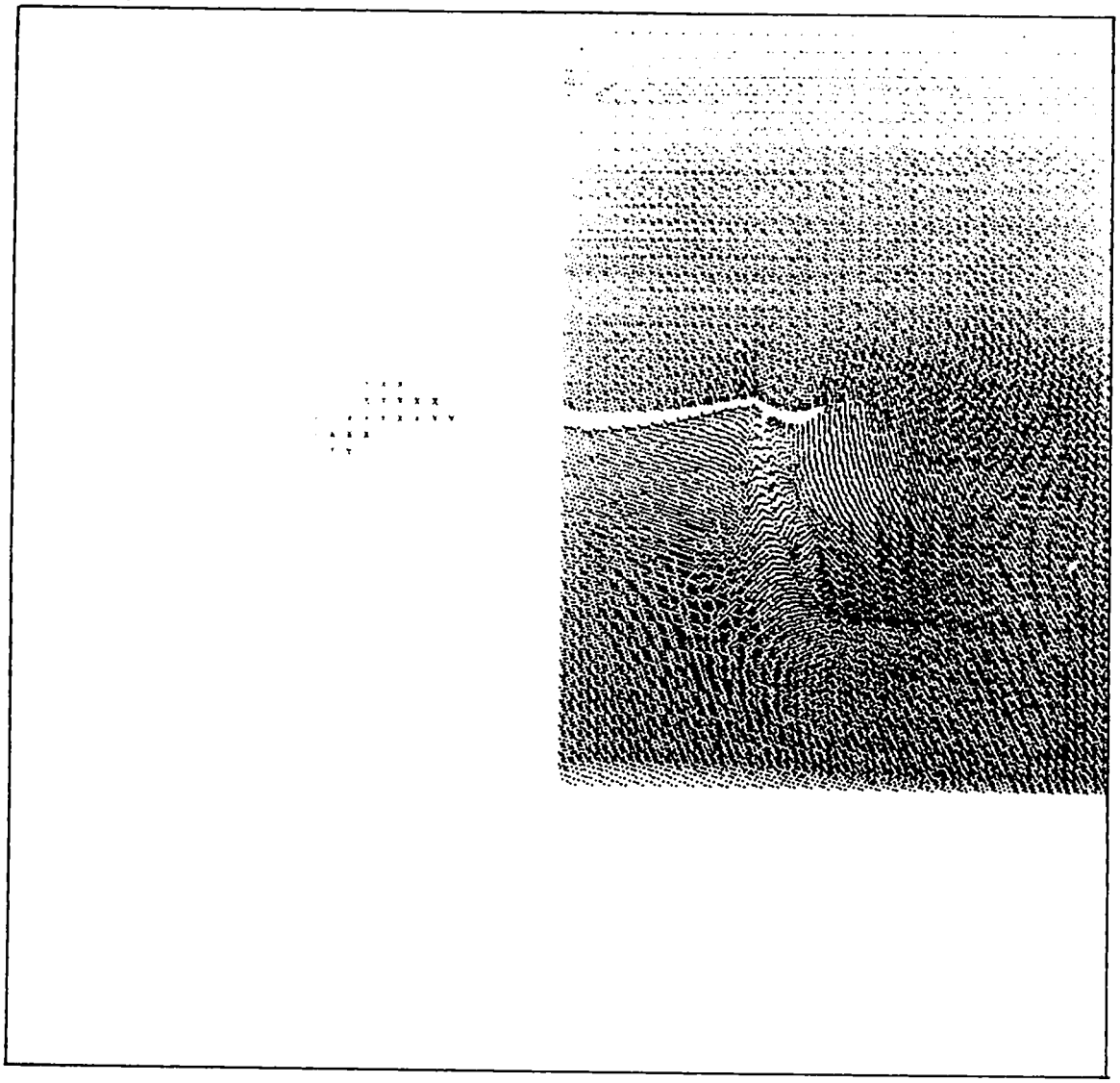

THE TIME IS 2.00000-001 MICROSECONDS AND THE CYCLE NUMBER IS 4.00000+002

0.210μ sec.

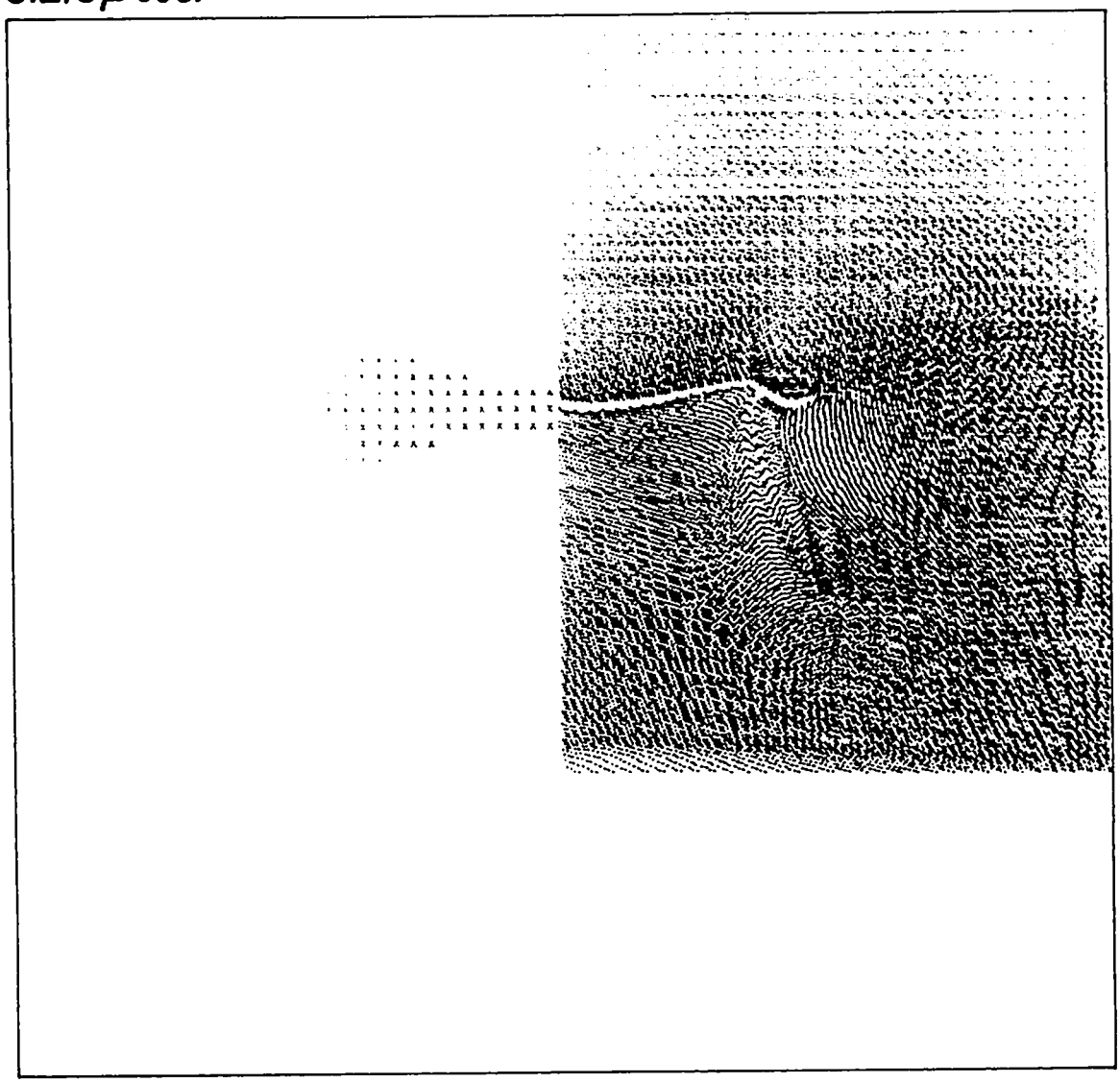

THE TIME IS 2.10000-001 MICROSECONDS AND THE CYCLE NUMBER IS 4.20000+002

0.220μ sec.

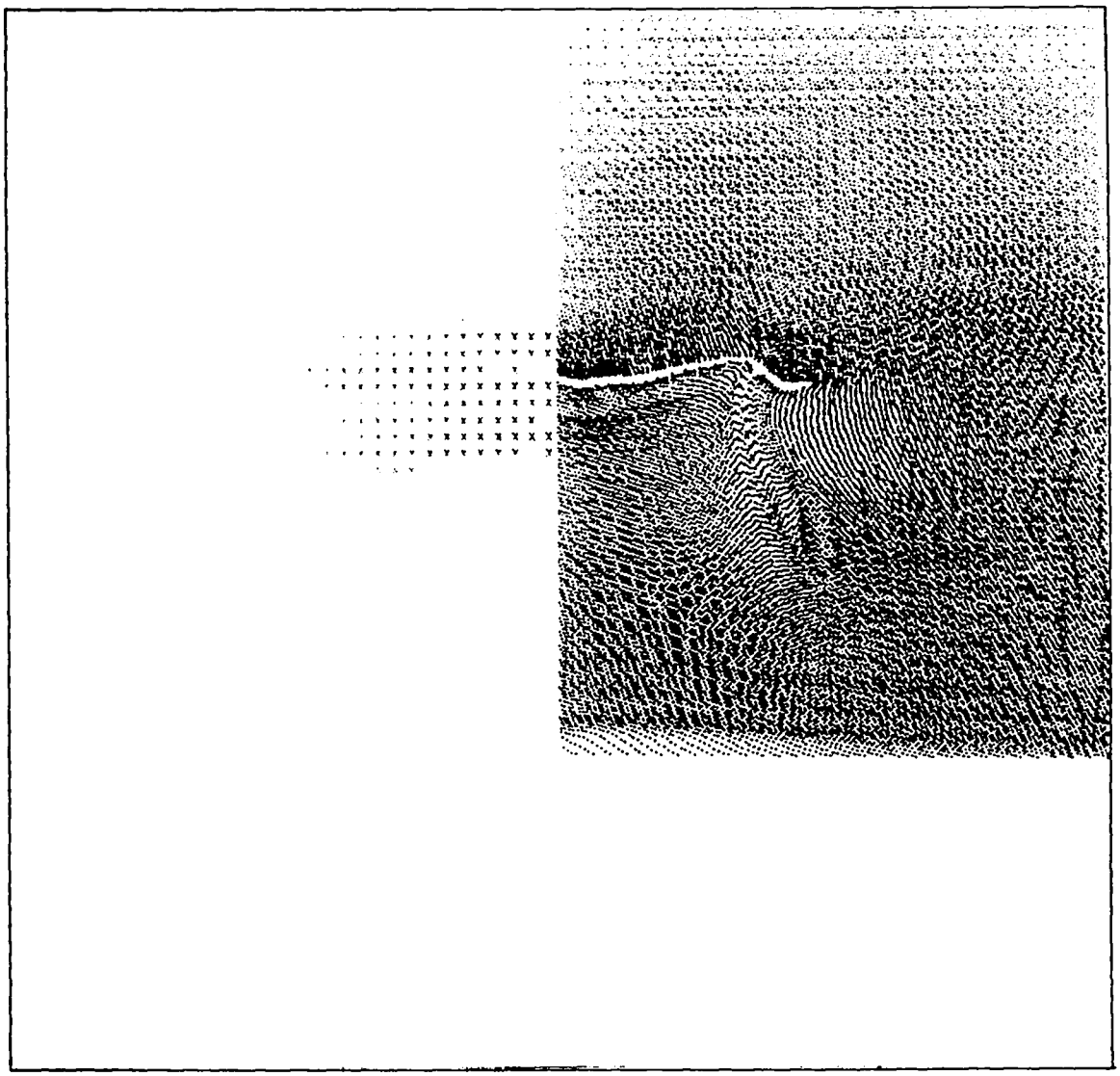

THE TIME IS 2.20000-001 MICROSECONDS AND THE CYCLE NUMBER IS 4.40000+002

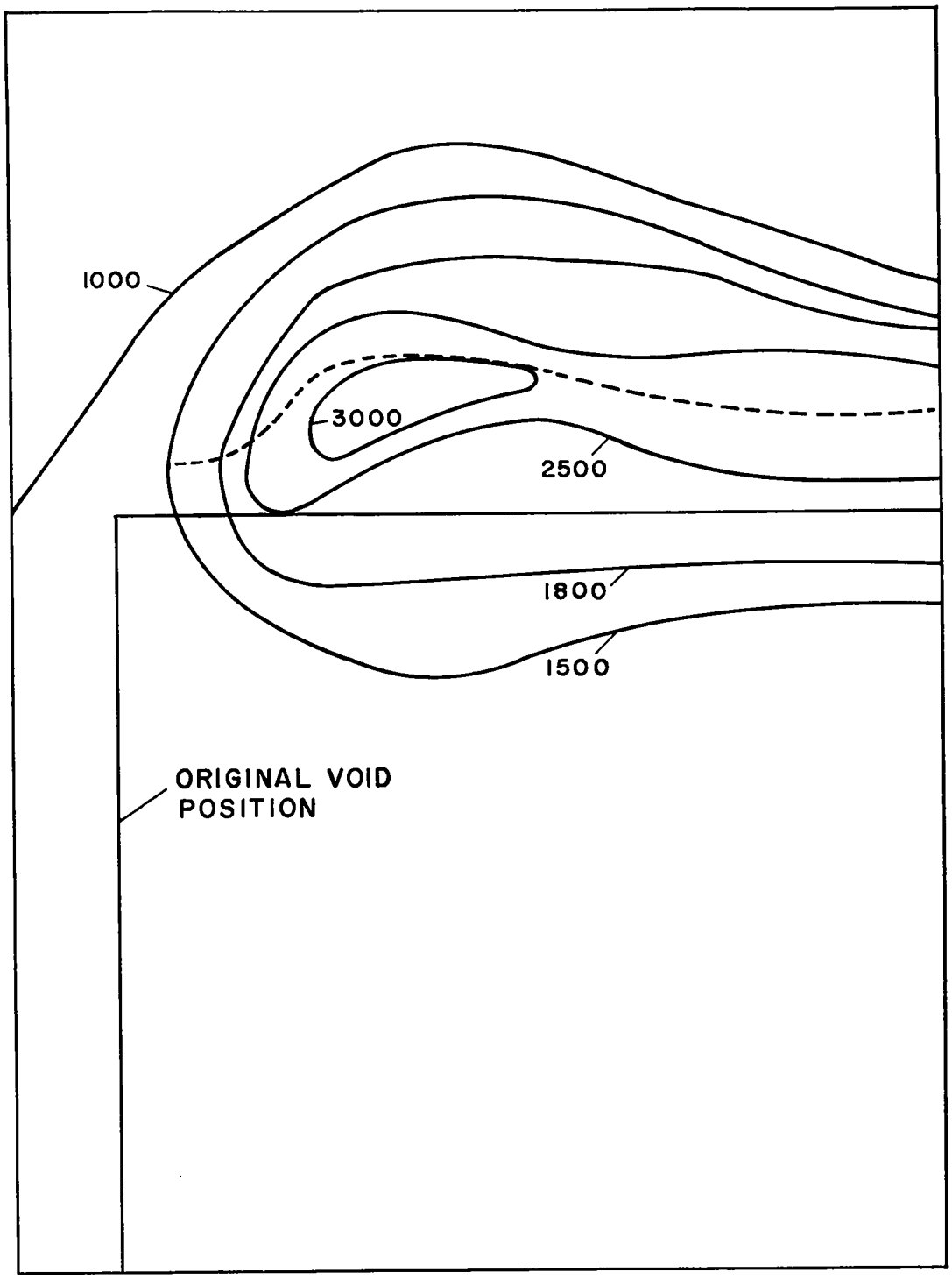

Hot Spot Isotherms At 0.22 μsec

0.240μ sec.

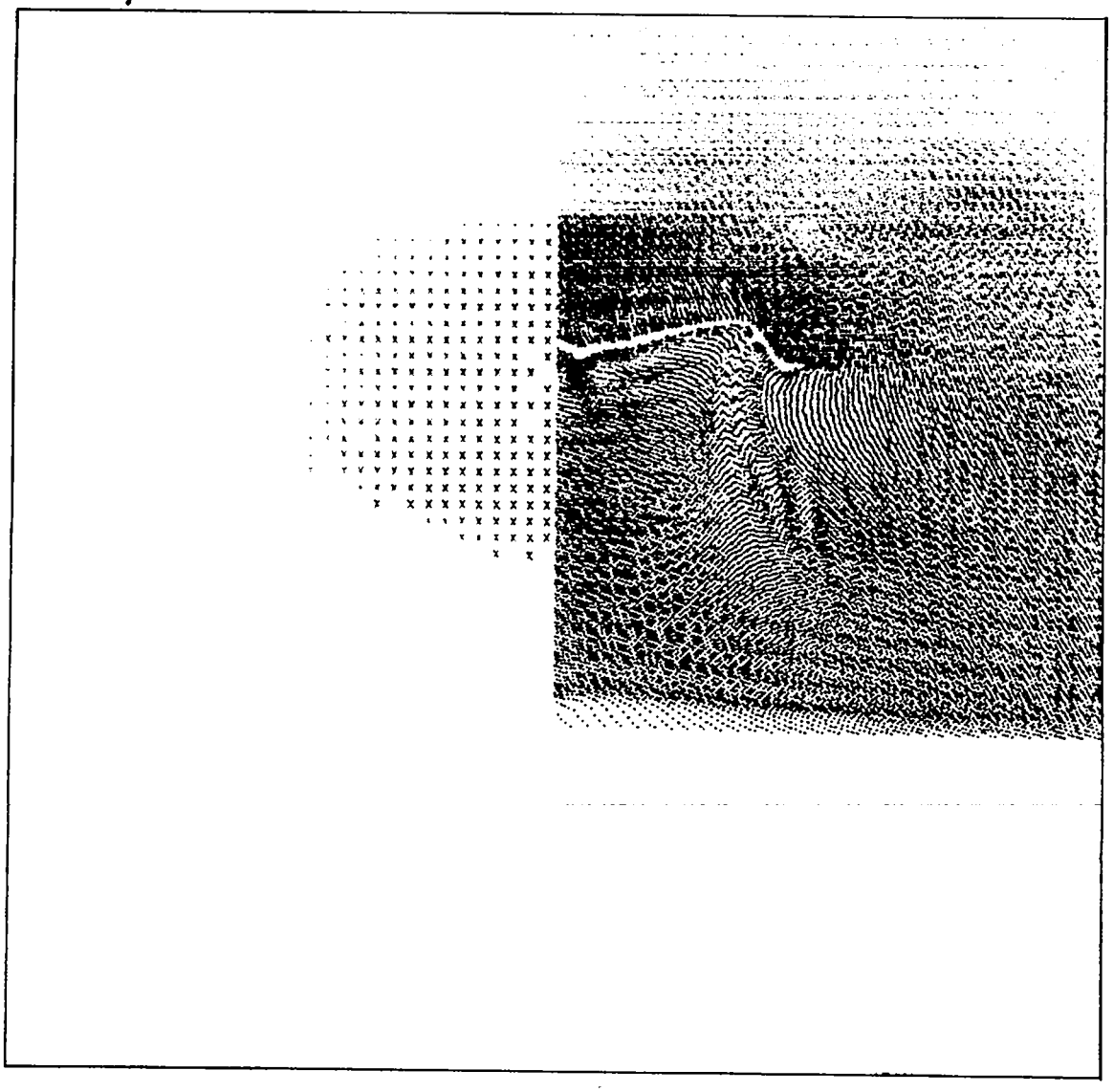

THE TIME IS 2.40000-001 MICROSECONDS AND THE CYCLE NUMBER IS 4.80000+002

Figure 3

THE FORMATION OF A HOT SPOT AND RESULTING PROPAGATING DETONATION FROM A 0.032-cm-RADIUS, 0.032-cm-HIGH CYLINDRICAL VOID

The right sides of the following pictures show the particle cross section of the cylinder. The positions of those cells that have completely decomposed are shown with an "x".

0.190μ sec.

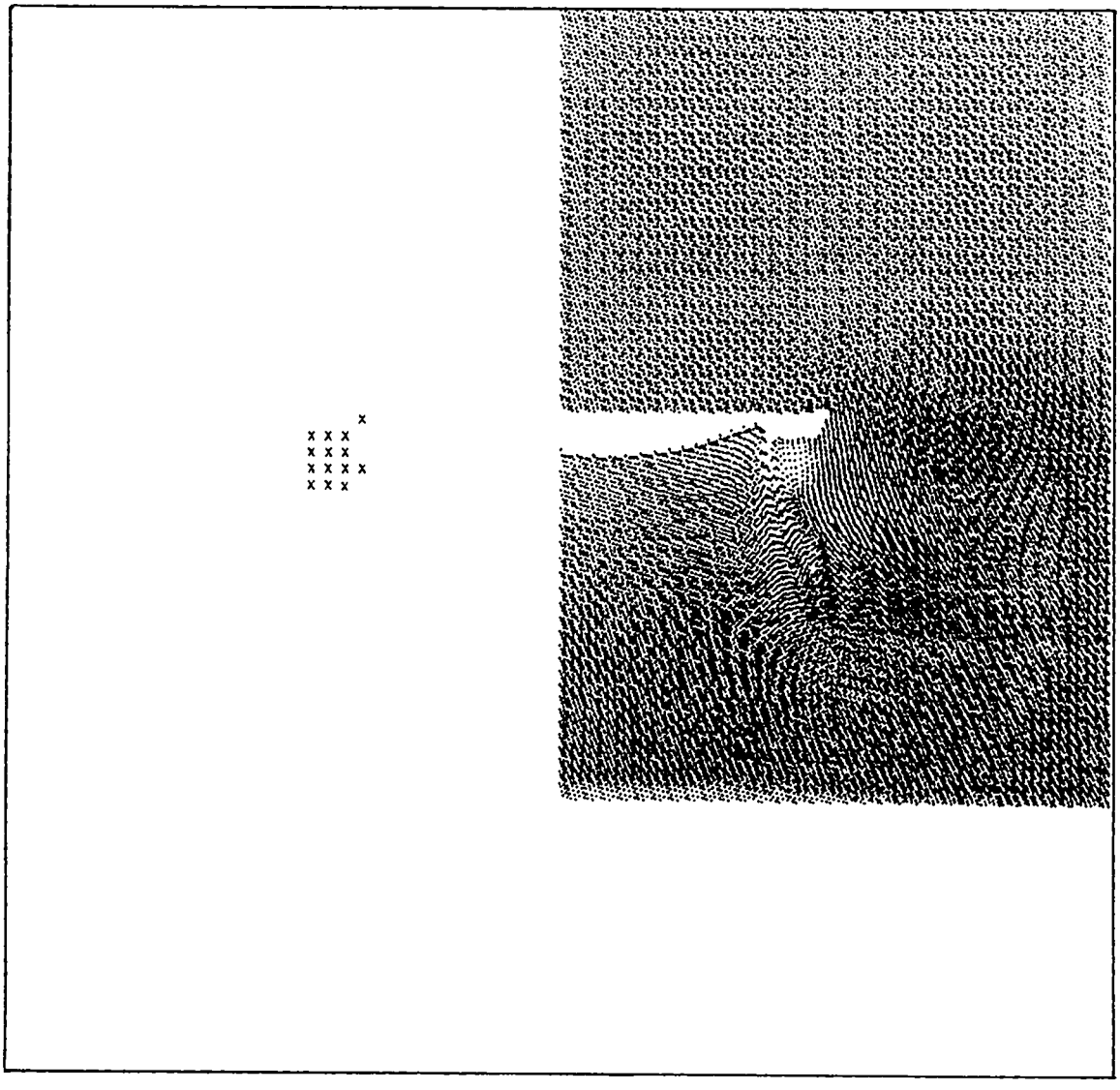

THE TIME IS 1.90000-001 MICROSECONDS AND THE CYCLE NUMBER IS 3.80000+002

0.200μ sec.

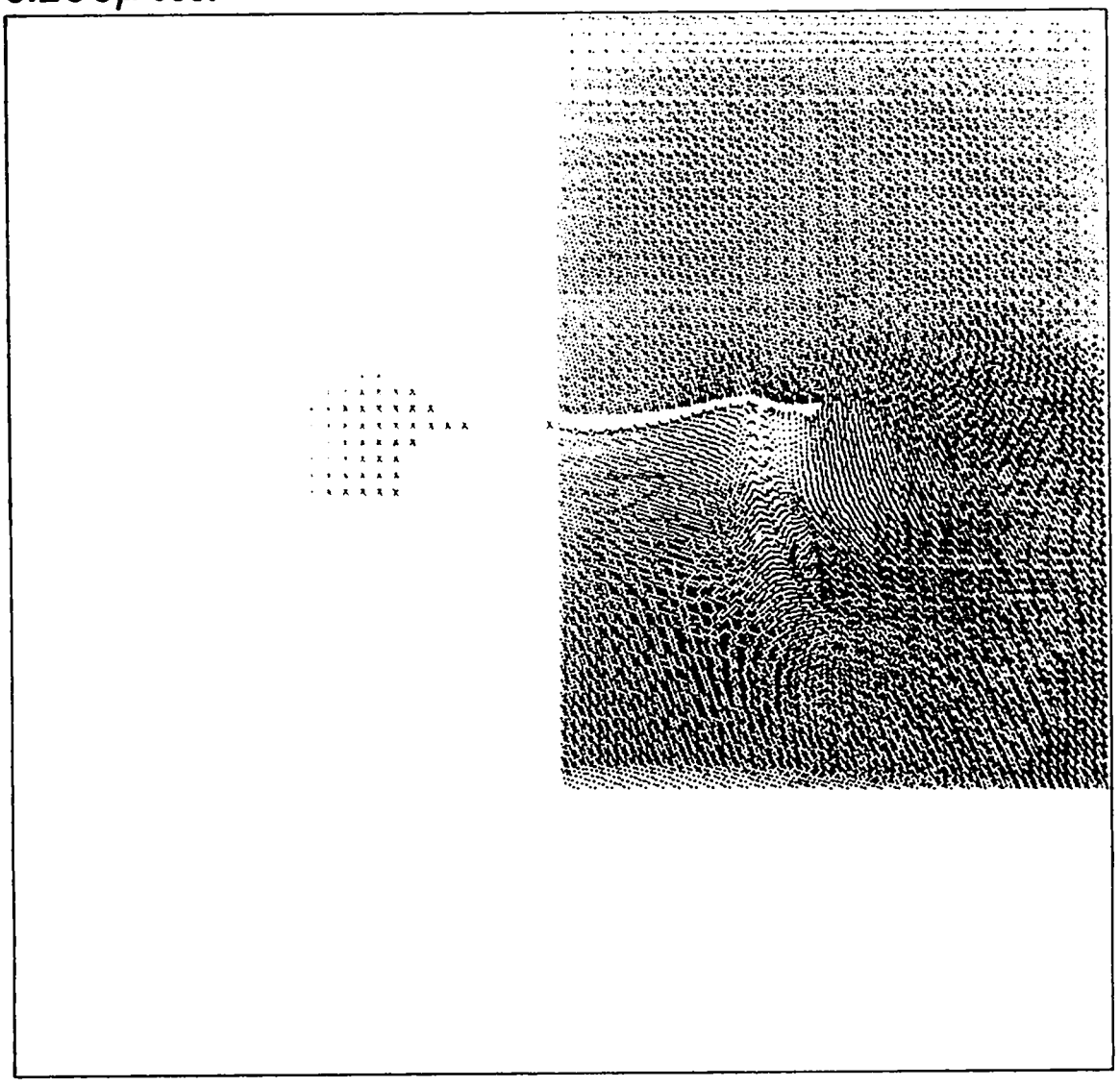

THE TIME IS 2.00000-001 MICROSECONDS AND THE CYCLE NUMBER IS 4.00000+002

0.210μ sec.

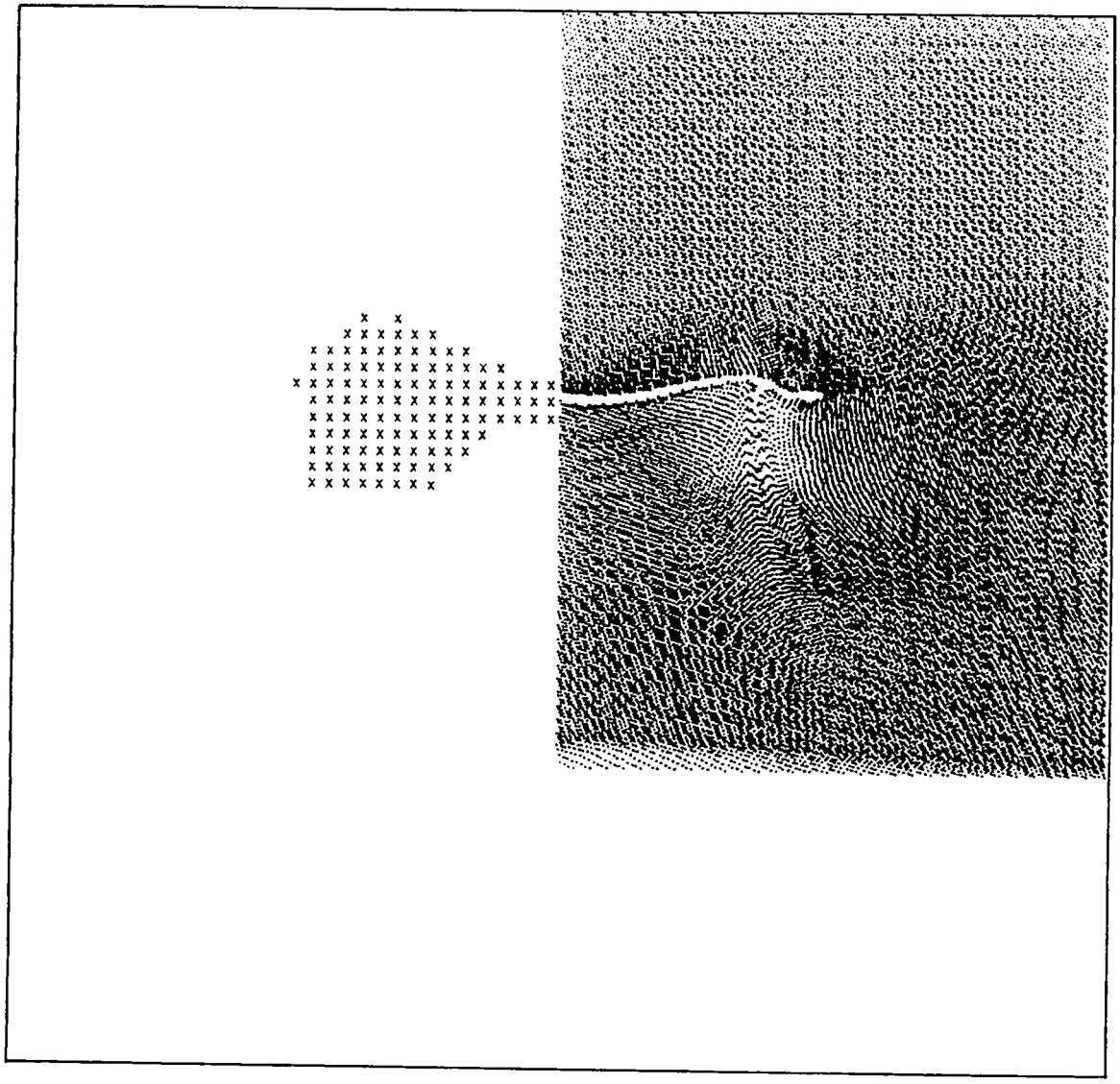

THE TIME IS 2.10000-001 MICROSECONDS AND THE CYCLE NUMBER IS 4.20000+002

0.220μ sec.

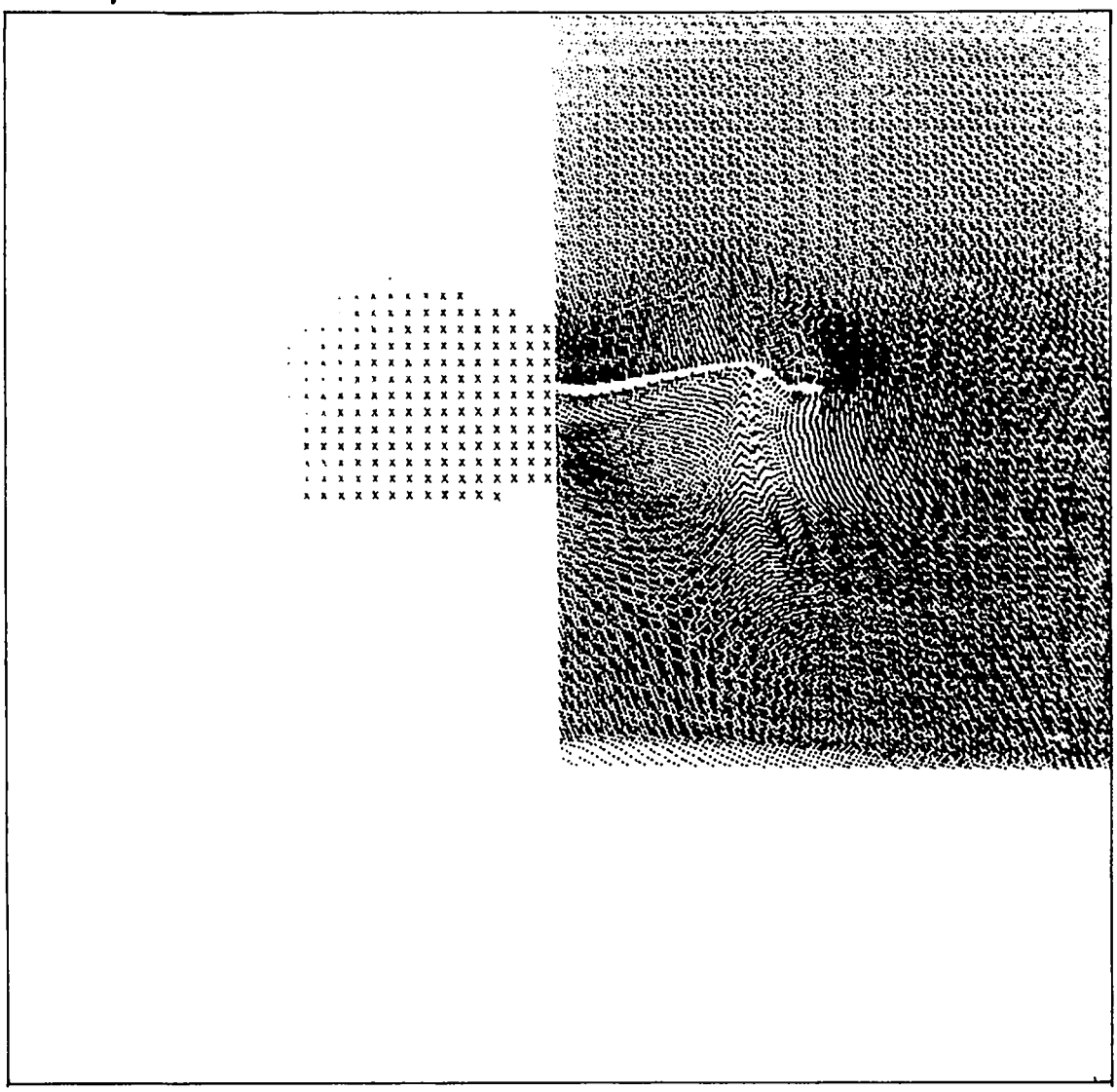

THE TIME IS 2.20000-001 MICROSECONDS AND THE CYCLE NUMBER IS 4.40000+002

0.240μ sec.

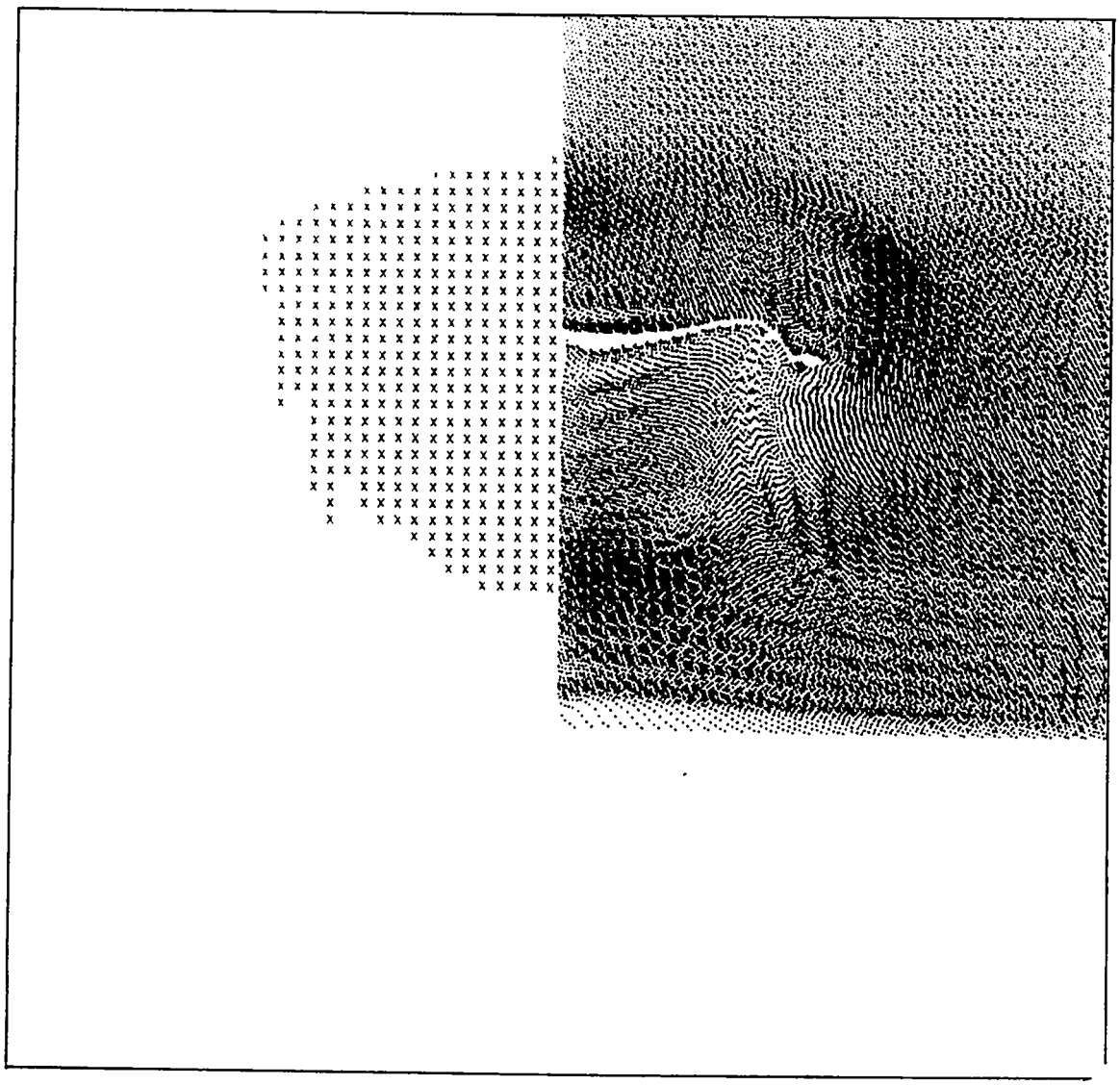

THE TIME IS 2.40000-001 MICROSECONDS AND THE CYCLE NUMBER IS 4.80000+002

0.250μ sec.

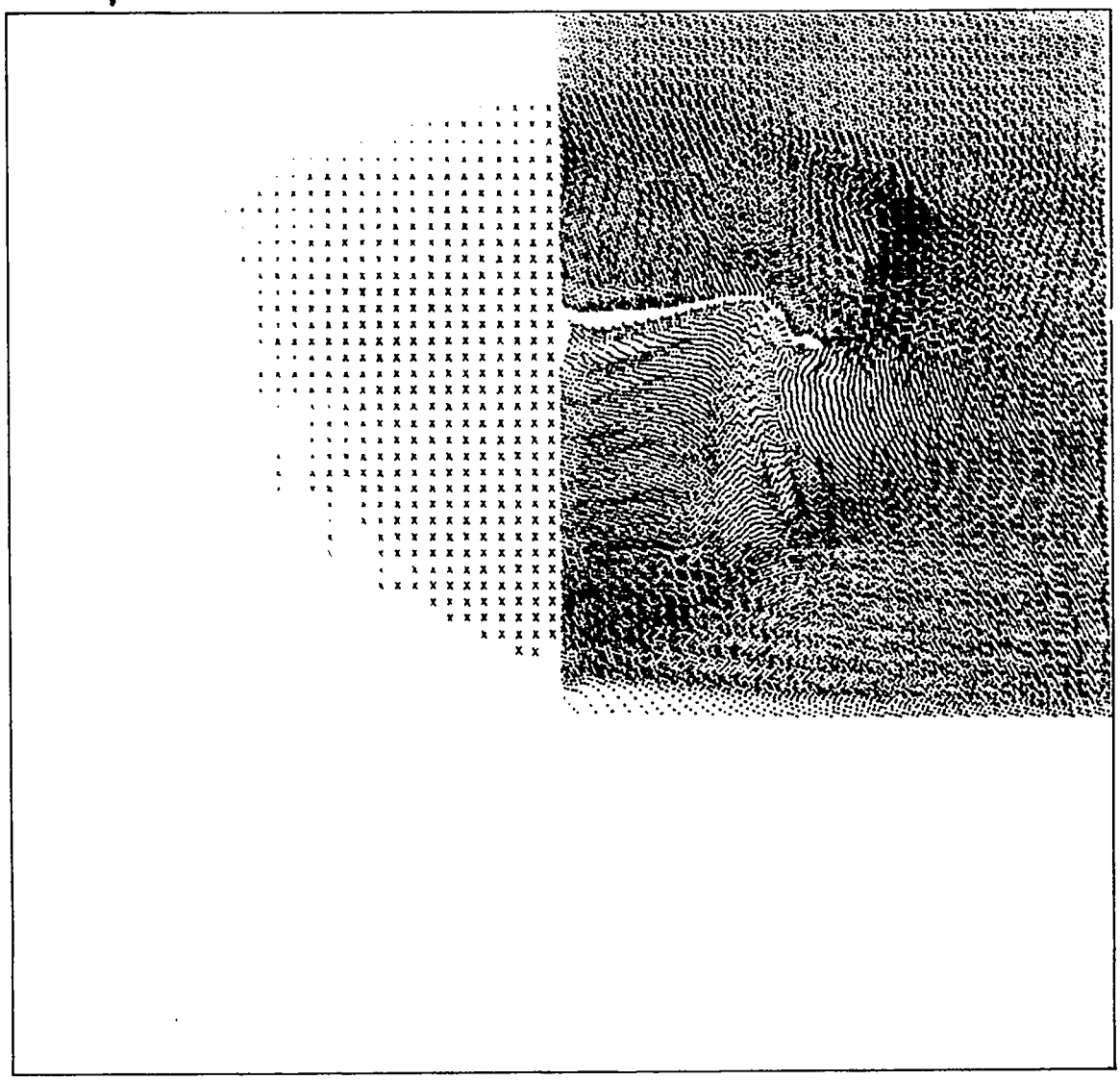

THE TIME IS 2.50000-001 MICROSECONDS AND THE CYCLE NUMBER IS 5.00000+002

III. CONICAL VOIDS IN NITROMETHANE

The initial and boundary conditions of the calculation were chosen to match the model shown in Figure 4. A cylinder of nitromethane contains a biconical void centered on the axis. The axial symmetry of the system allows a two-dimensional description of the process in terms of the usual axial and radial coordinates.

The results of a nonreactive EIC calculation are presented in the form of pictures in Figure 5 for a 0.064-cm-radius, 0.128-cm-high cylinder of nitromethane containing a 0.03-cm-radius, 0.03-cm-half-height biconical void. Pictures for a void of the same half height and 0.0225-cm radius are presented in Figure 6.

A piston is applied to the bottom of the cylinder, shocking the nitromethane to 85 kbar and 1200°K. The 85-kbar, 1200°K shock arrives at the lower surface of the void traveling with a shock velocity of 0.45 cm/μsec and a particle velocity of 0.171 cm/μsec. The free surface velocity of the surface fluid becomes 0.342 cm/μsec with a temperature of 530°K. Since the shock in the nitromethane is going faster than the nitromethane free surface in the void, the surface fluid at the side of the cone starts converging on the axis as well as moving toward the top of the cone. This results in a jet with a velocity that increases as the jet approaches the top of the cone. For a 0.03-cm-radius, 0.03-cm-half-height cone, the jet velocity is 0.54 cm/μsec upon arriving at the top of the void, and for a 0.0225-cm-radius cone of the same half height,

the jet velocity is 0.57 cm/μsec upon arriving at the top of the void (Figure 6). A 0.04-cm-radius, 0.02-cm-half-height cone has a jet velocity of 0.45 cm/μsec upon closure of the void.

For a given radius, a taller conical void gives a hotter hot spot. For a given height, the larger radius conical void results in a cooler, but larger, hot spot.

The results of a reactive EIC calculation for a 0.03-cm-radius, 0.03-cm-half-height conical void are shown in Figure 7. The first regions to react are just above the equator of the void at its outer rim (which became hot from void closure) and at the axis (which became hot from convergence). The formation of a propagating detonation occurs in much the same manner as in spherical voids[1].

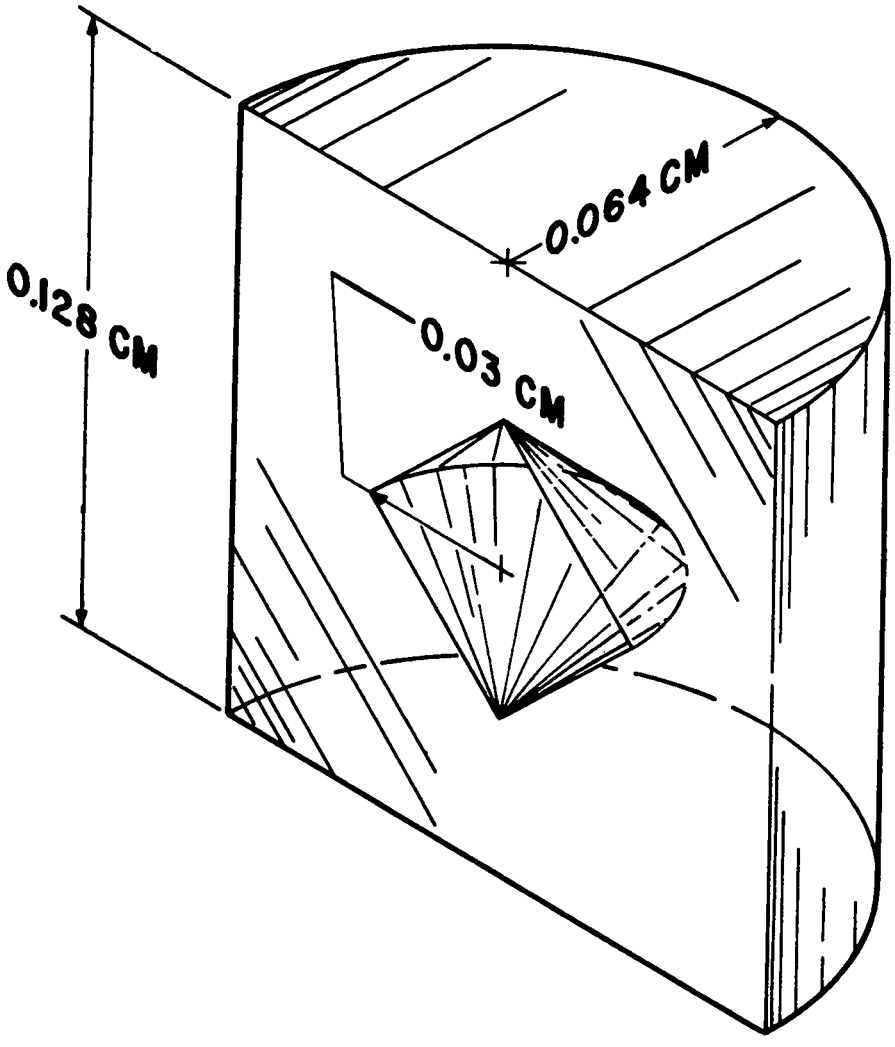

Figure 4. A cross section of a cylinder of nitromethane containing a biconical void centered on the axis.

Figure 5

THE FORMATION OF A HOT SPOT FROM A 0.03-cm-RADIUS, 0.03-cm-HALF-HEIGHT BICONICAL VOID

The right sides of the following pictures show the shapes, wave positions, and fluid element (particle) positions for a cylinder of nitromethane containing a biconical void. A piston is applied to the bottom of the cylinder, shocking the nitromethane to 85 kbar and 1200°K. Chemical reaction is not permitted. The position of those cells with a temperature greater than 1400°K is shown on the left half of the picture with an "x". Isotherm plots are shown for the hot spot at 0.24 μsec.

0.100μ sec.

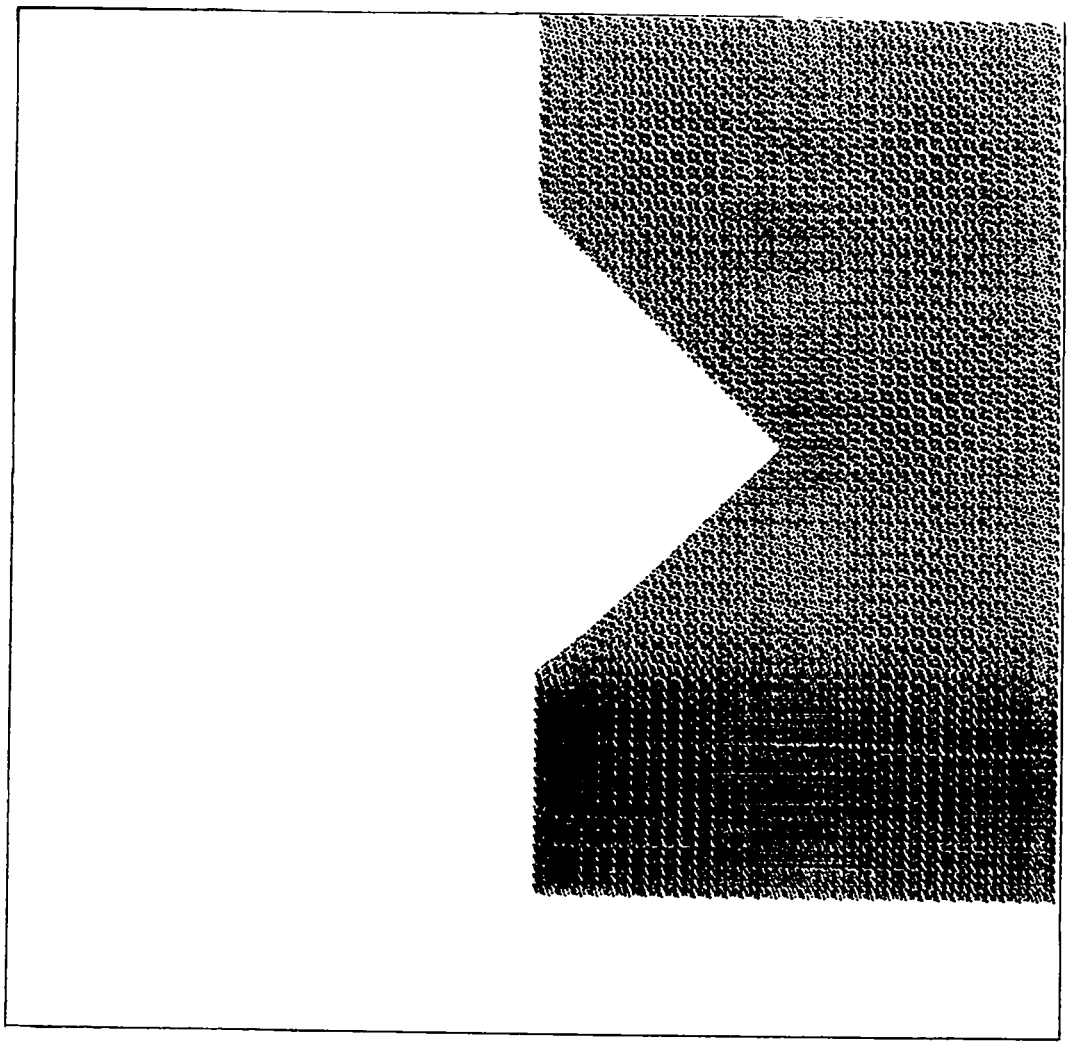

THE TIME IS 1.00000-001 MICROSECONDS AND THE CYCLE NUMBER IS 2.00000+002

0.120μ sec.

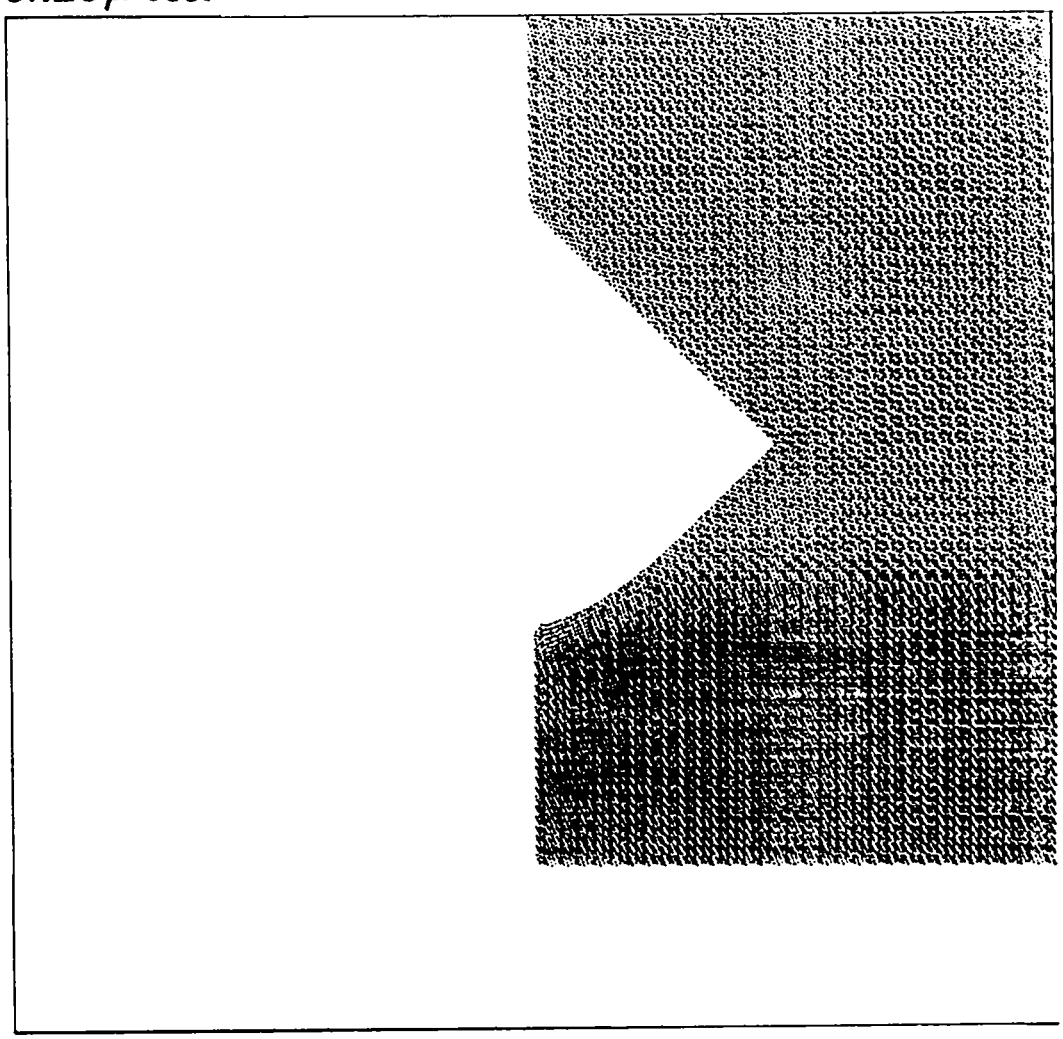

THE TIME IS 1.20000-001 MICROSECONDS AND THE CYCLE NUMBER IS 2.40000+002

0.150μ sec.

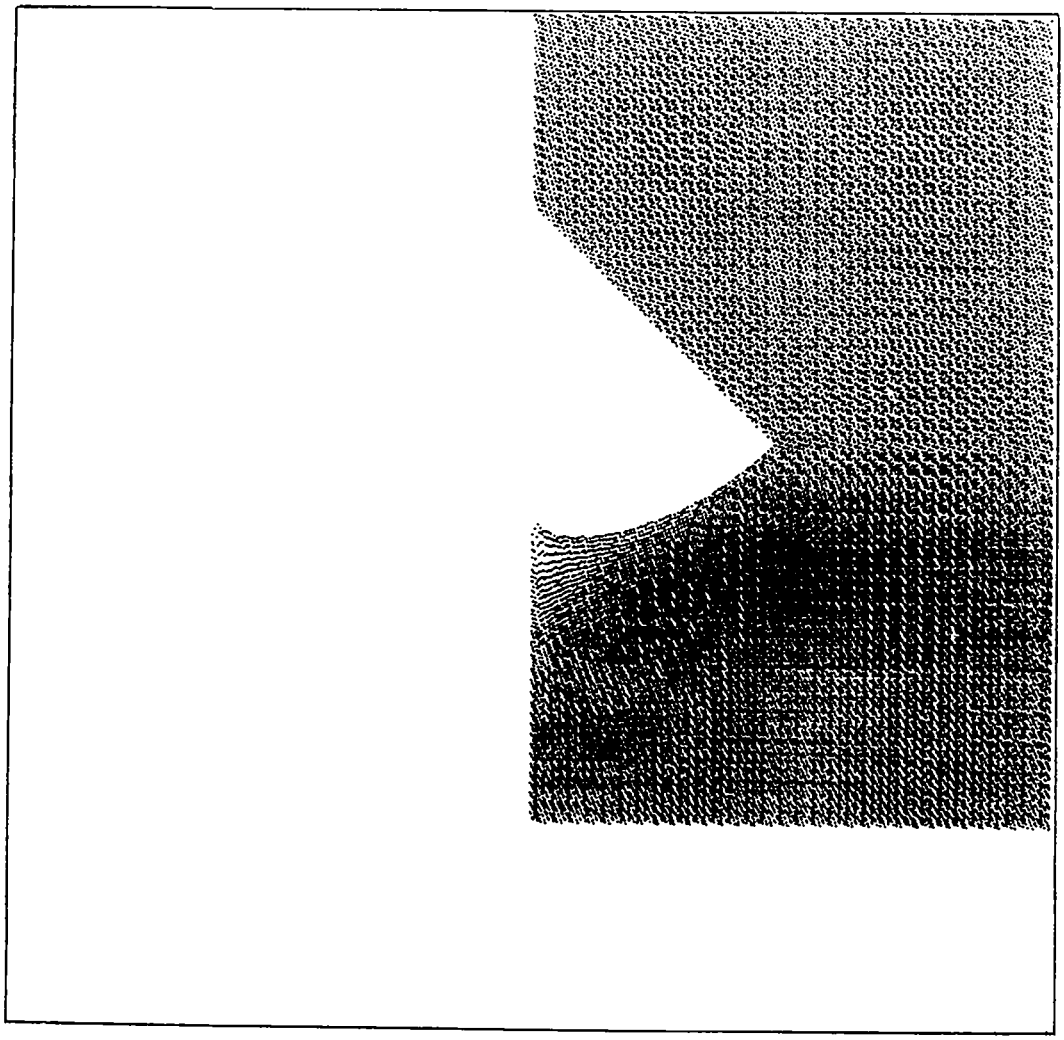

THE TIME IS 1.50000-001 MICROSECONDS AND THE CYCLE NUMBER IS 3.00000+002

0.170μ sec.

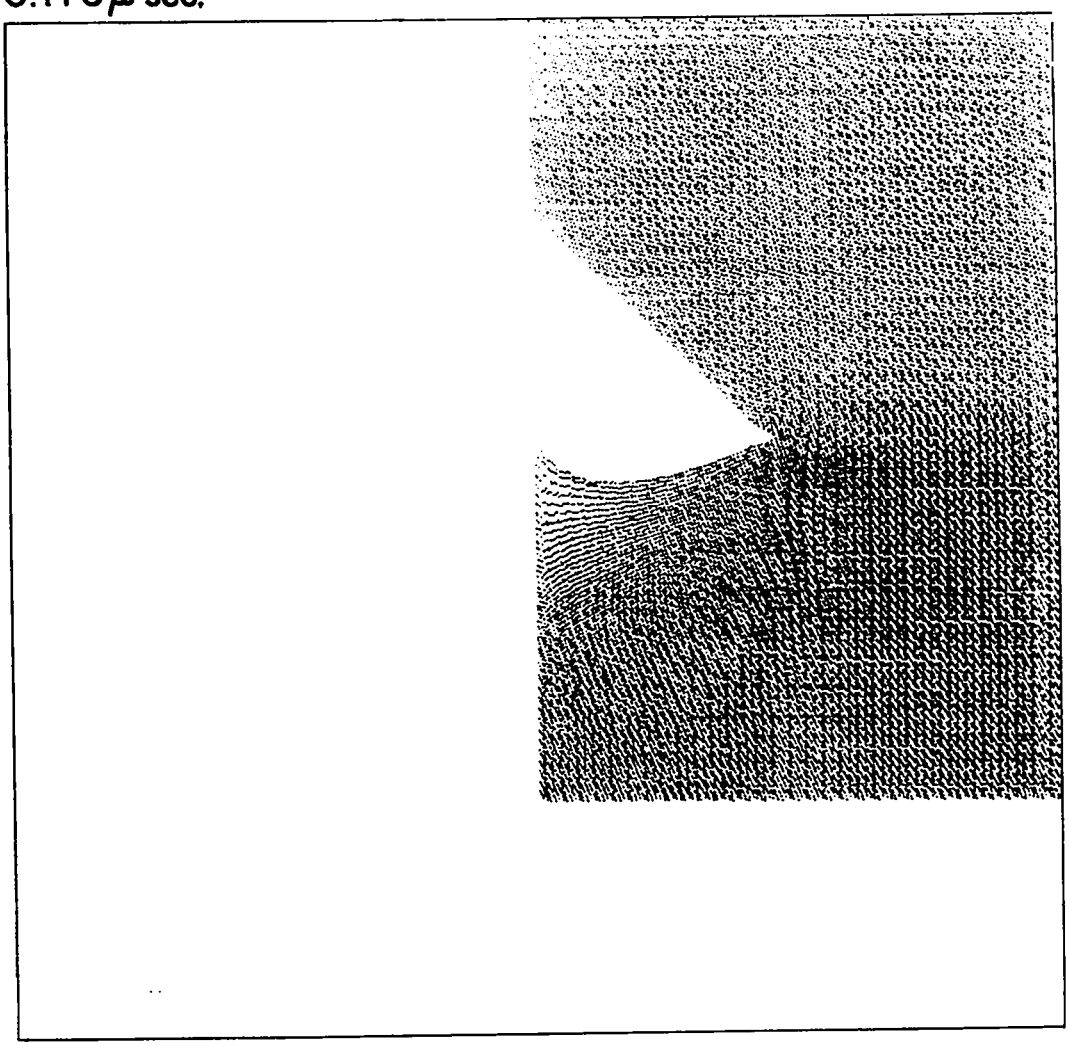

THE TIME IS 1.70000-001 MICROSECONDS AND THE CYCLE NUMBER IS 3.40000+002

0.200μ sec.

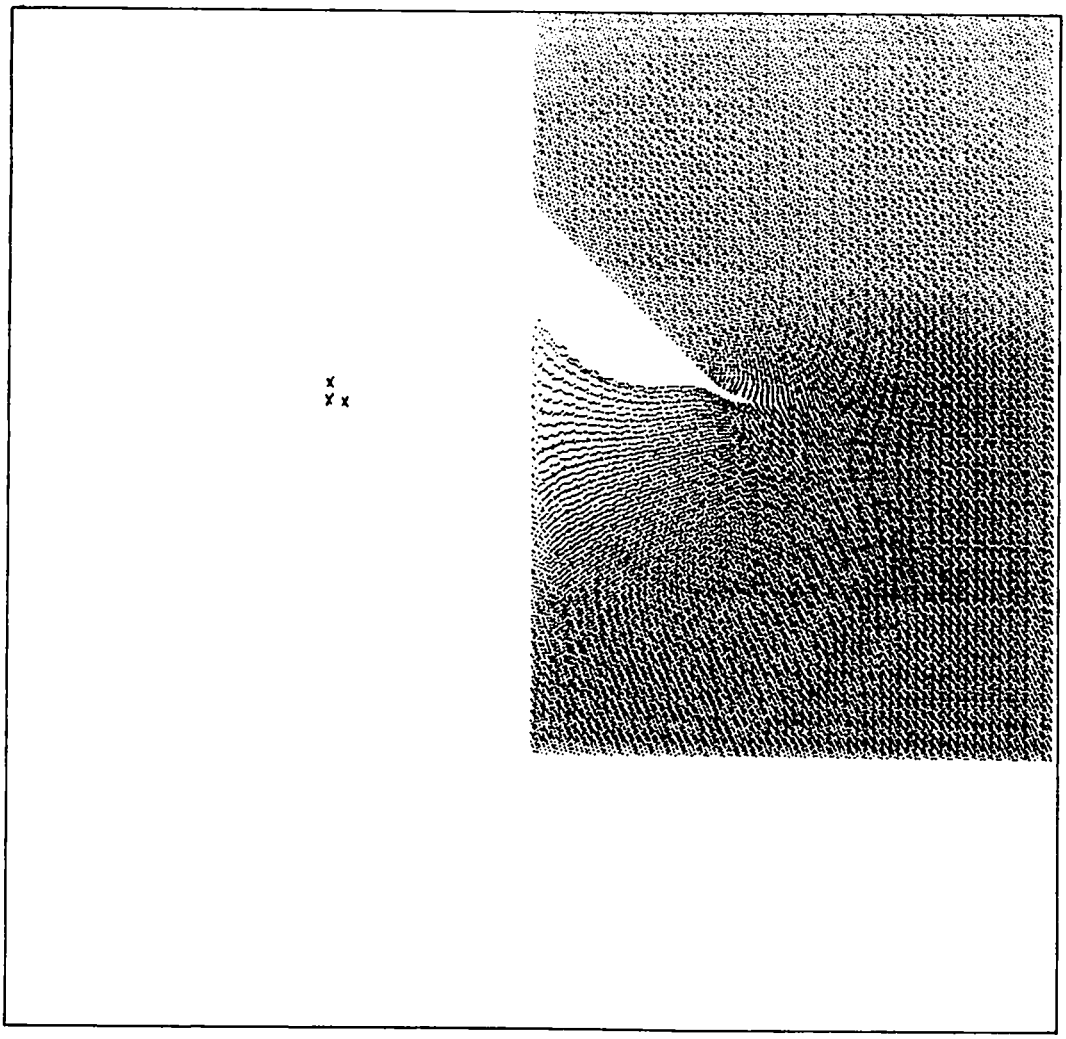

THE TIME IS 2.00000-001 MICROSECONDS AND THE CYCLE NUMBER IS 4.00000+002

0.210μ sec.

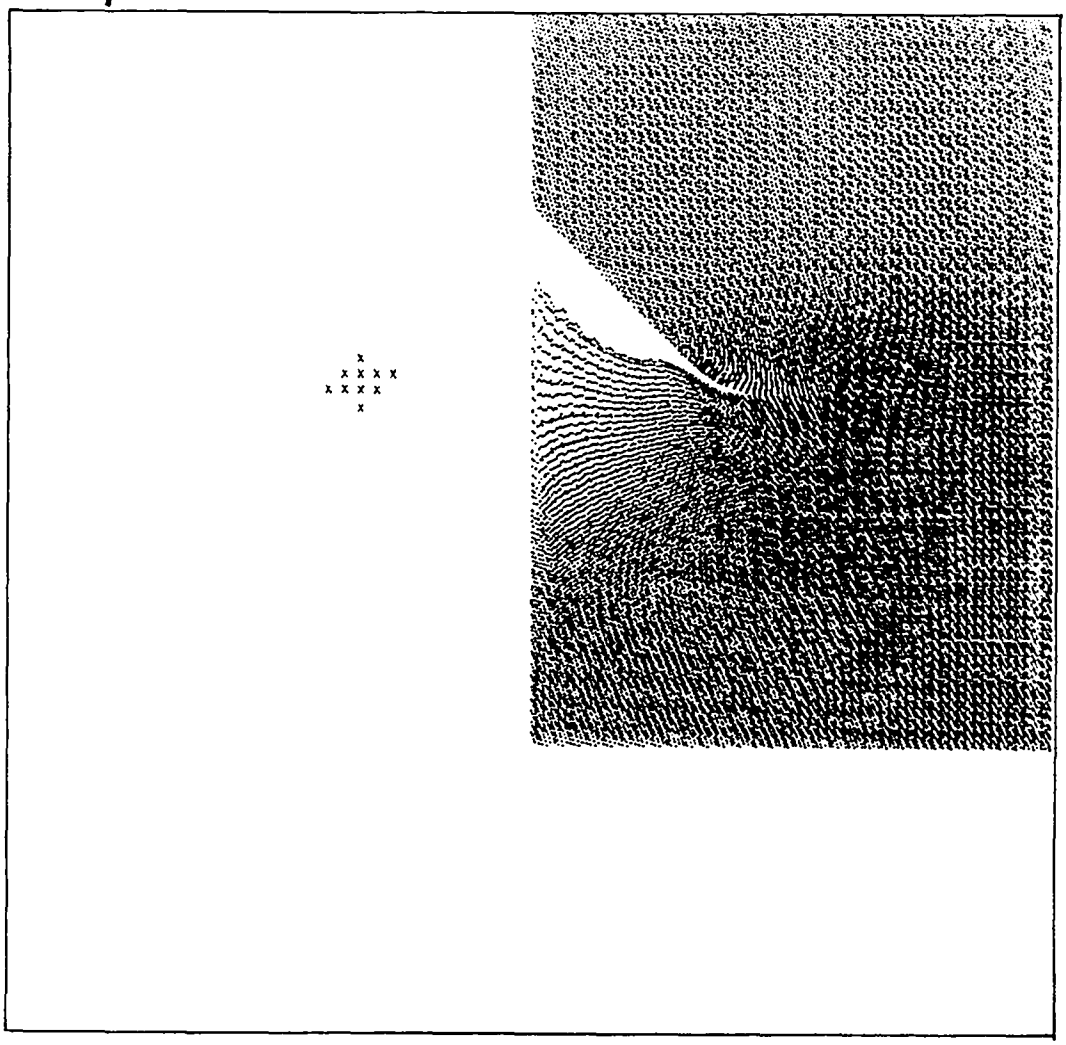

THE TIME IS 2.10000-001 MICROSECONDS AND THE CYCLE NUMBER IS 4.20000+002

0.220μ sec.

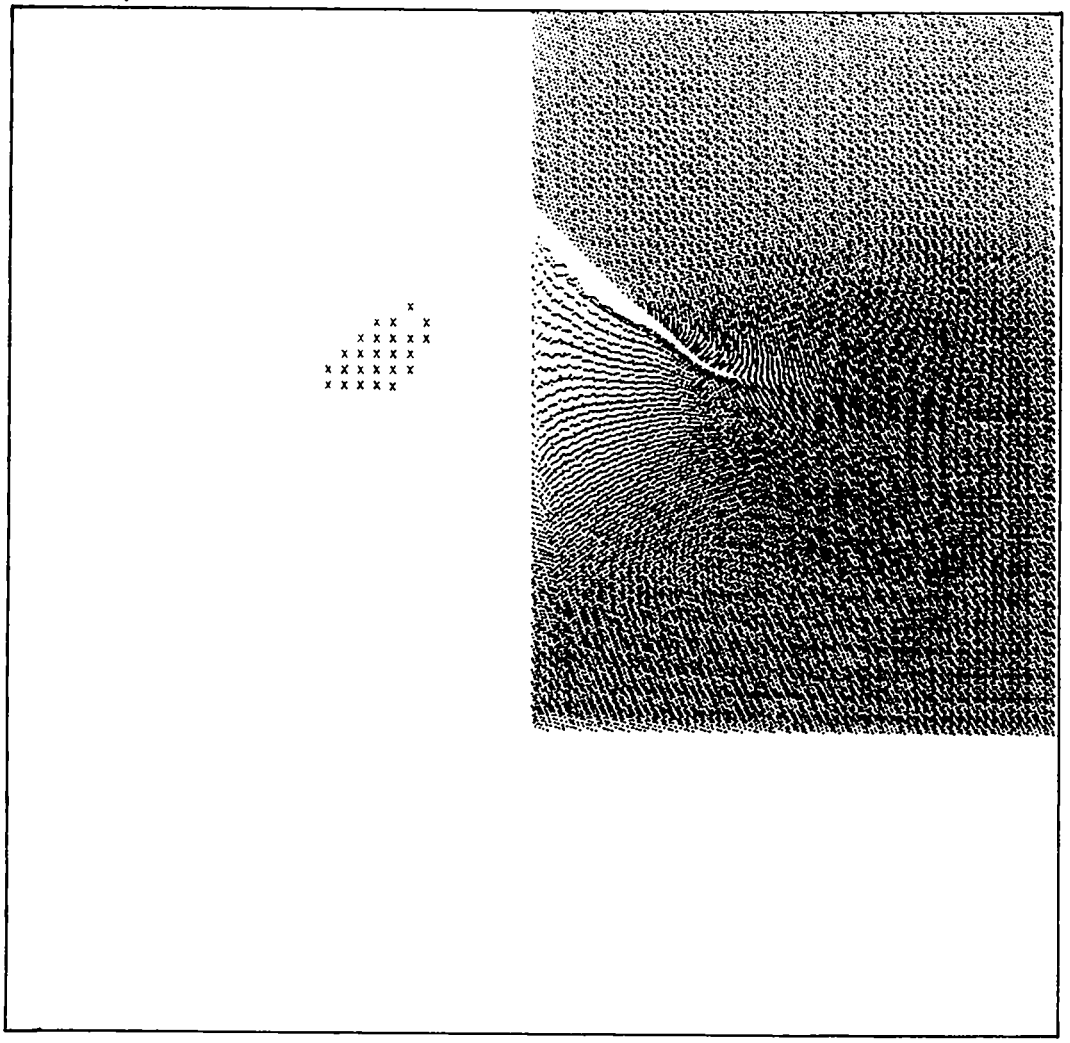

THE TIME IS 2.20000-001 MICROSECONDS AND THE CYCLE NUMBER IS 4.40000+002

0.230 μ sec.

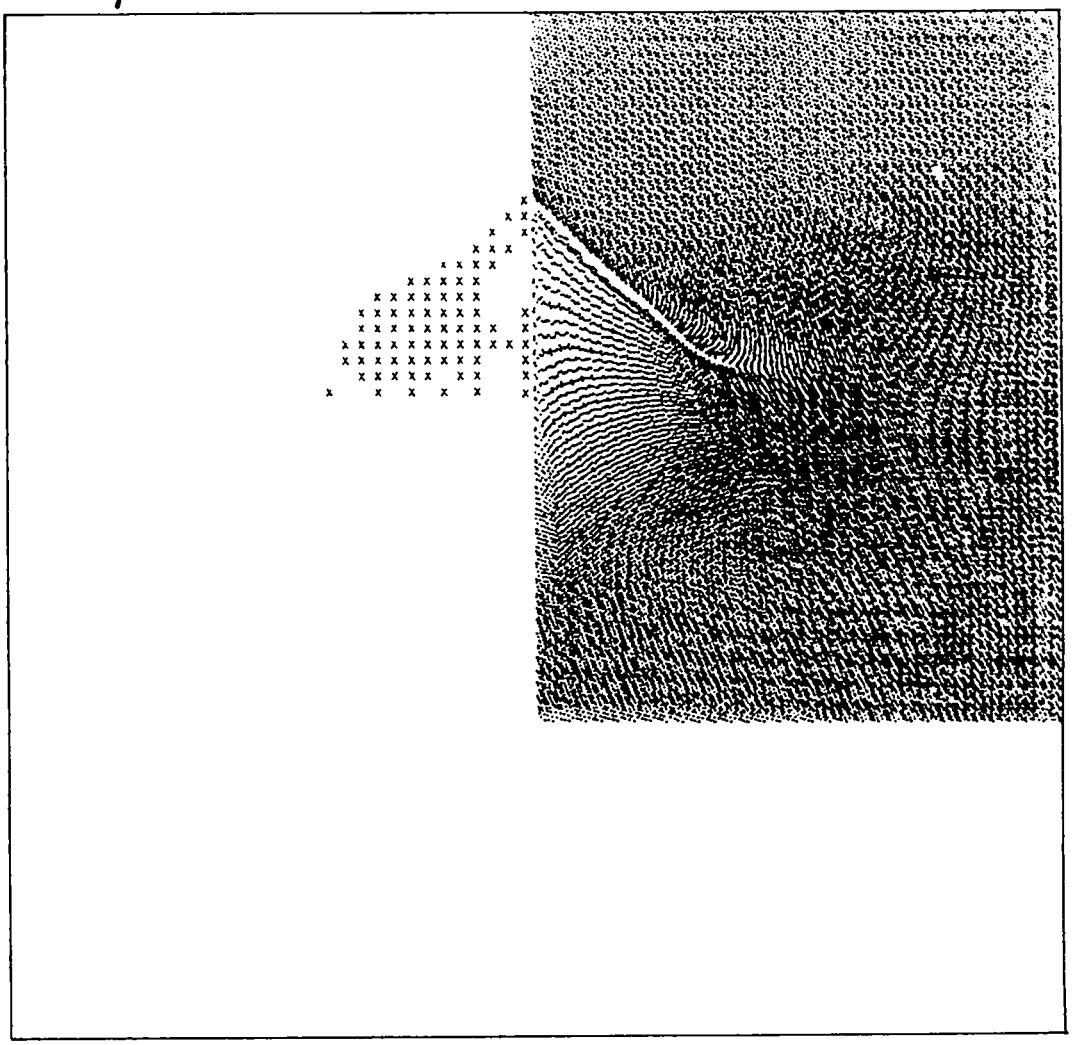

THE TIME IS 2.30000-001 MICROSECONDS AND THE CYCLE NUMBER IS 4.60000+002

0.240μ sec.

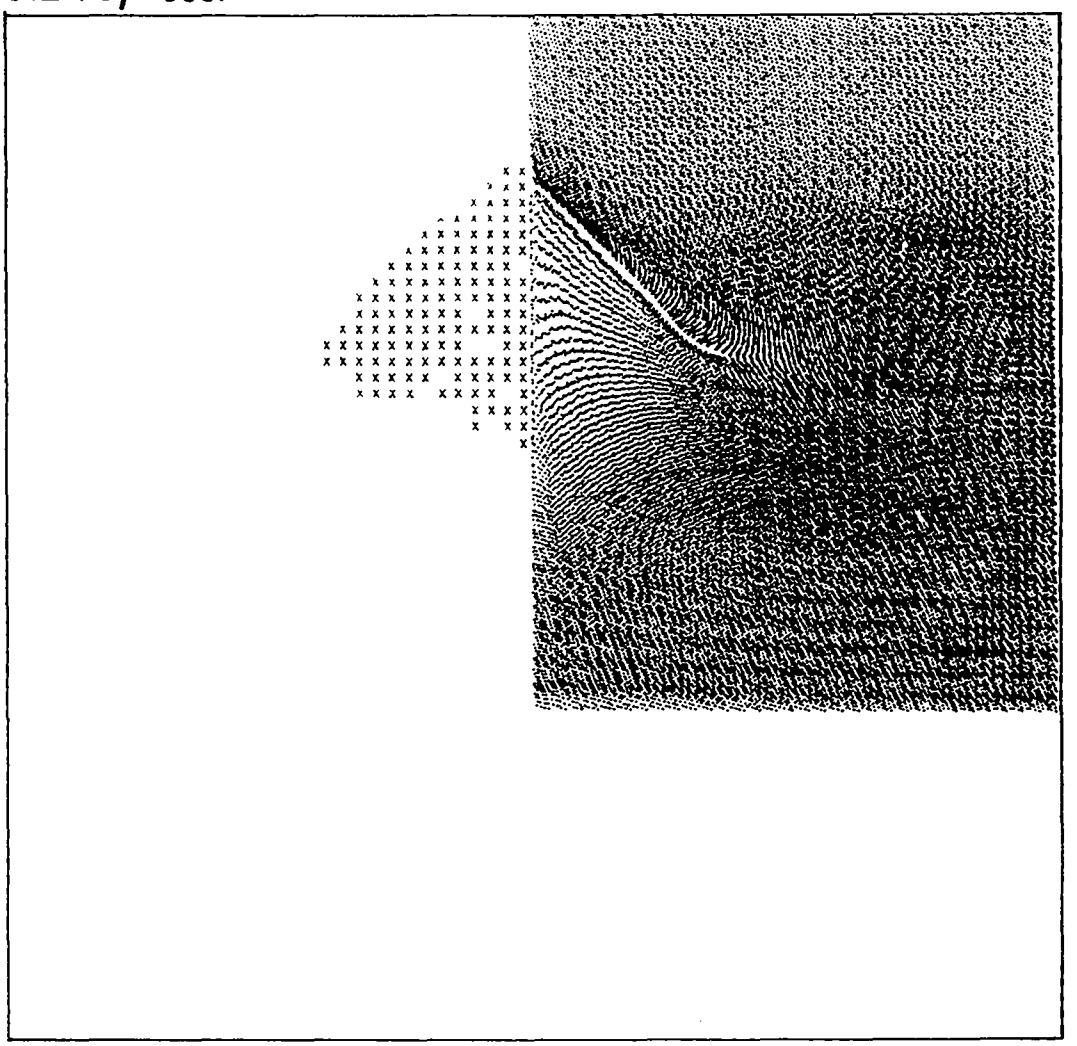

THE TIME IS 2.40000-001 MICROSECONDS AND THE CYCLE NUMBER IS 4.80000+002

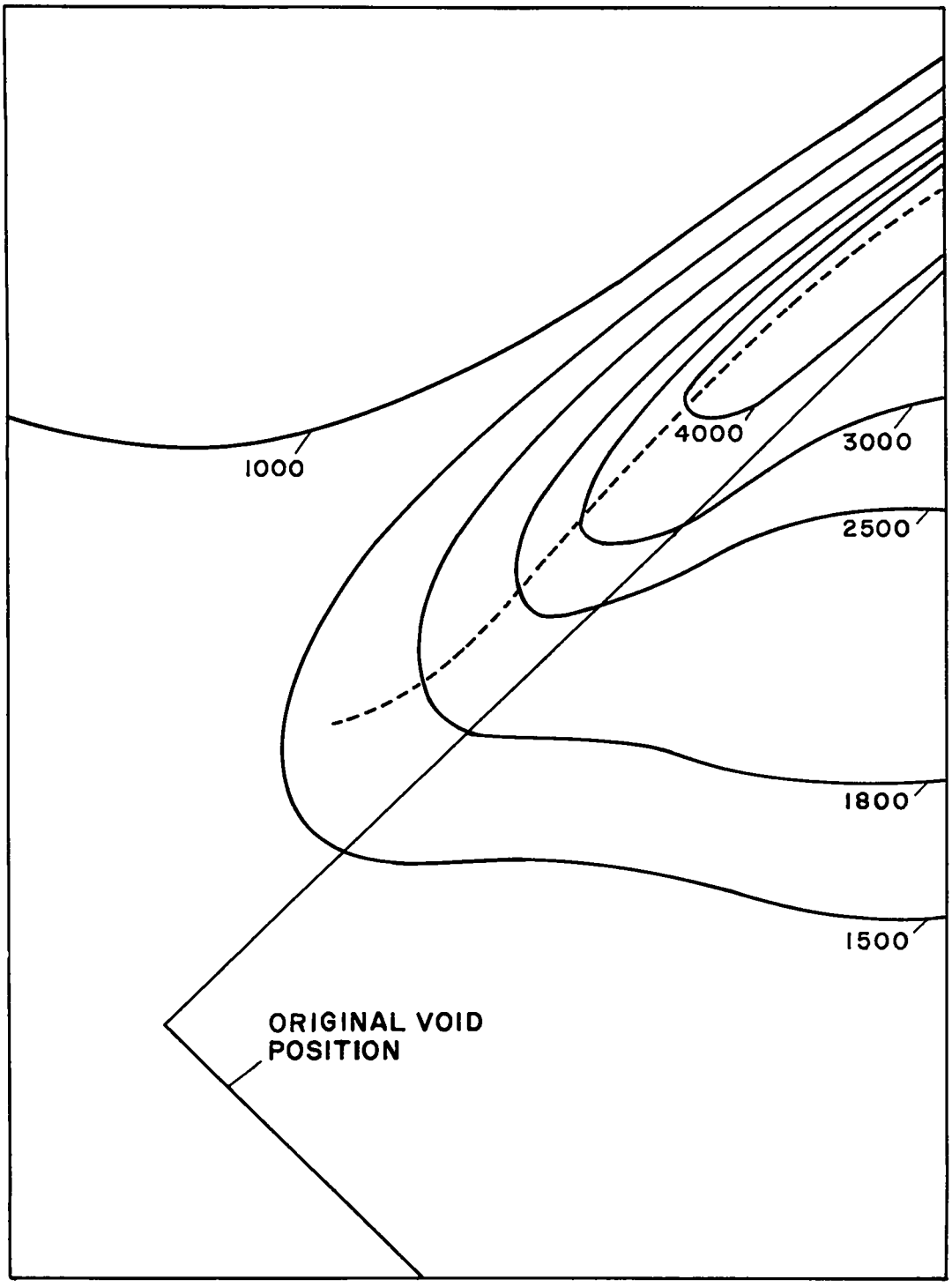

Hot Spot Isotherms At 0.24 μsec

0.250μ sec.

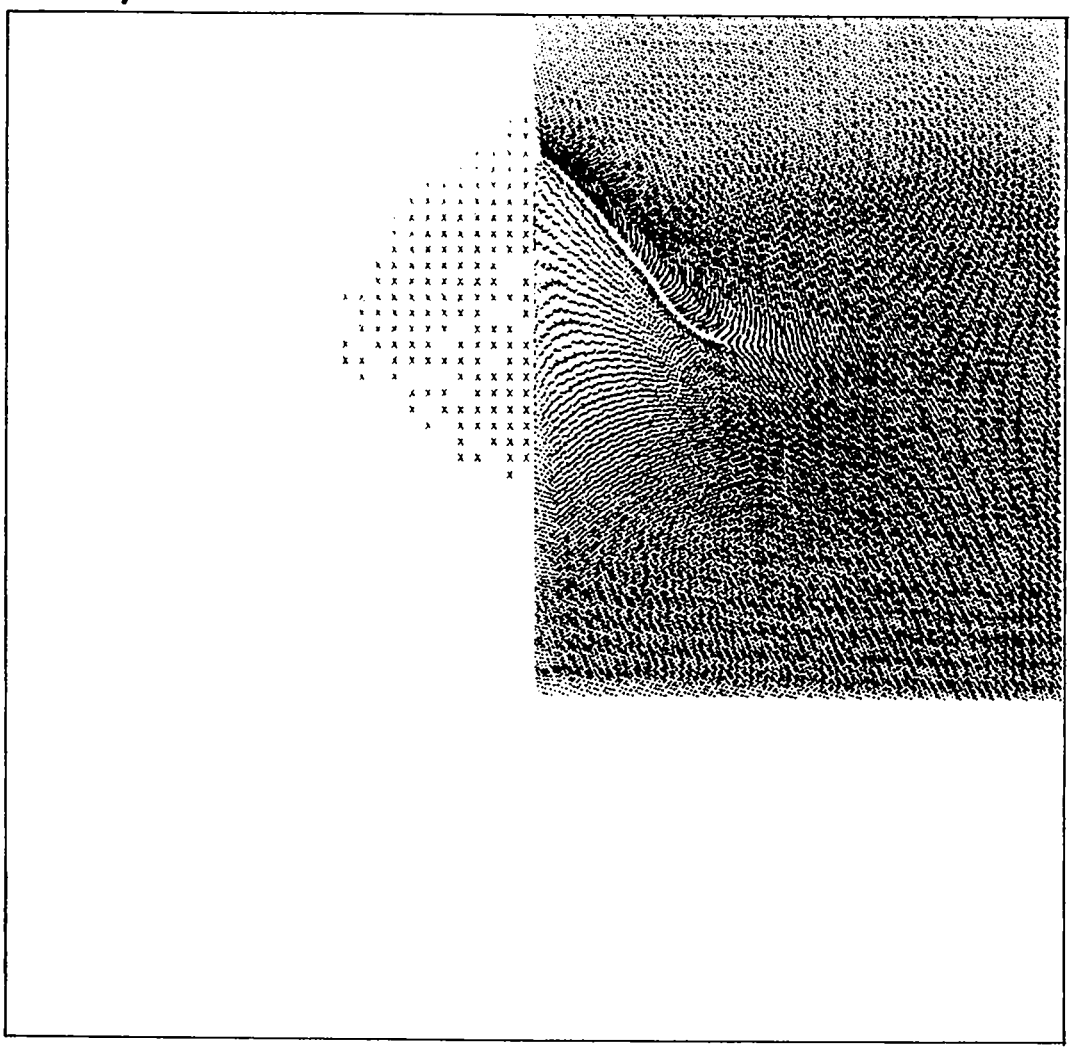

THE TIME IS 2.50000-001 MICROSECONDS AND THE CYCLE NUMBER IS 5.00000+002

Figure 6

THE FORMATION OF A HOT SPOT FROM A 0.0225-cm-RADIUS 0.03-cm-HALF-HEIGHT BICONICAL VOID

The right sides of the following pictures show the particle positions. The position of those cells with a temperature greater than 1400°K is shown on the left half of the pictures with an "x". Chemical reaction is not permitted.

0.005μ sec.

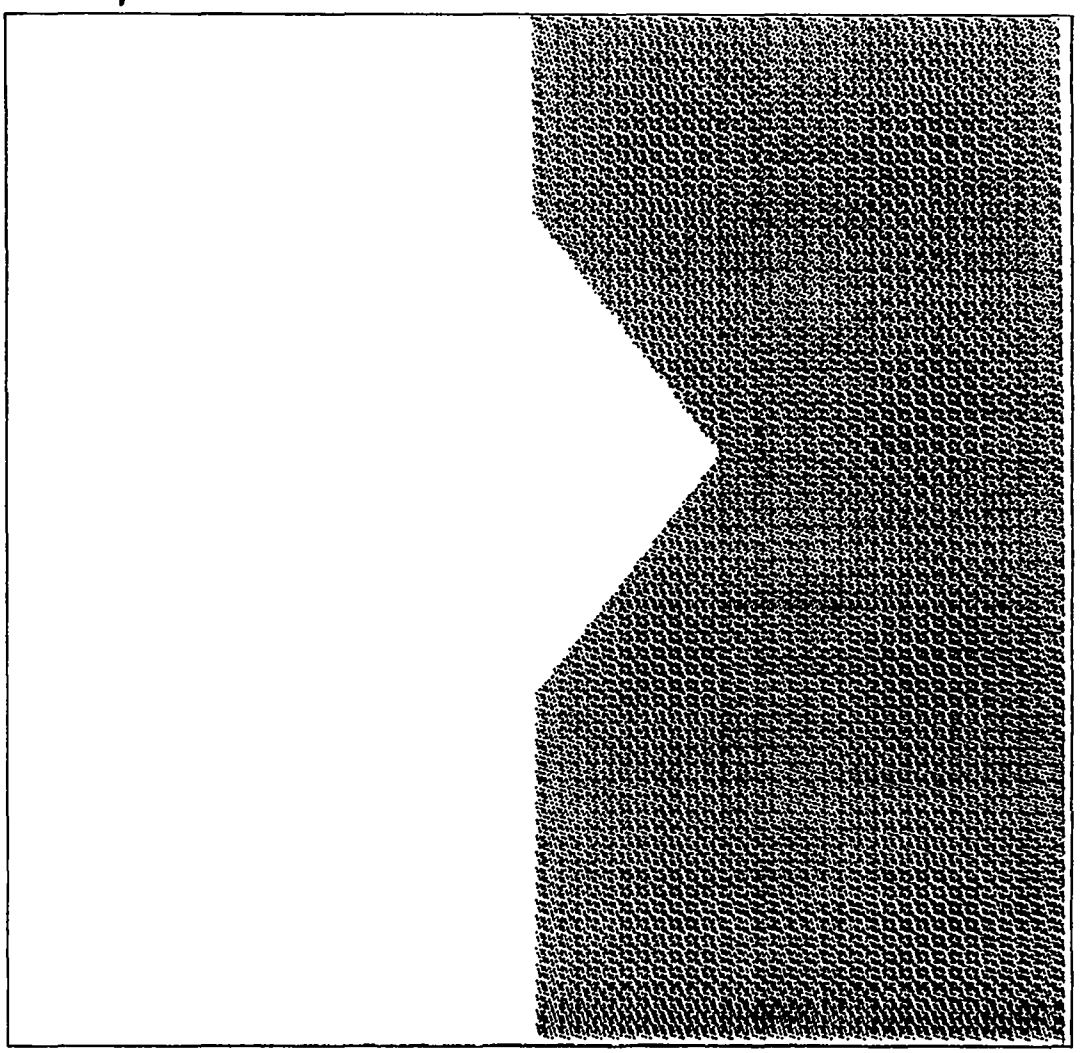

THE TIME IS 5.00000-003 MICROSECONDS AND THE CYCLE NUMBER IS 1.00000+001

0.170μ sec.

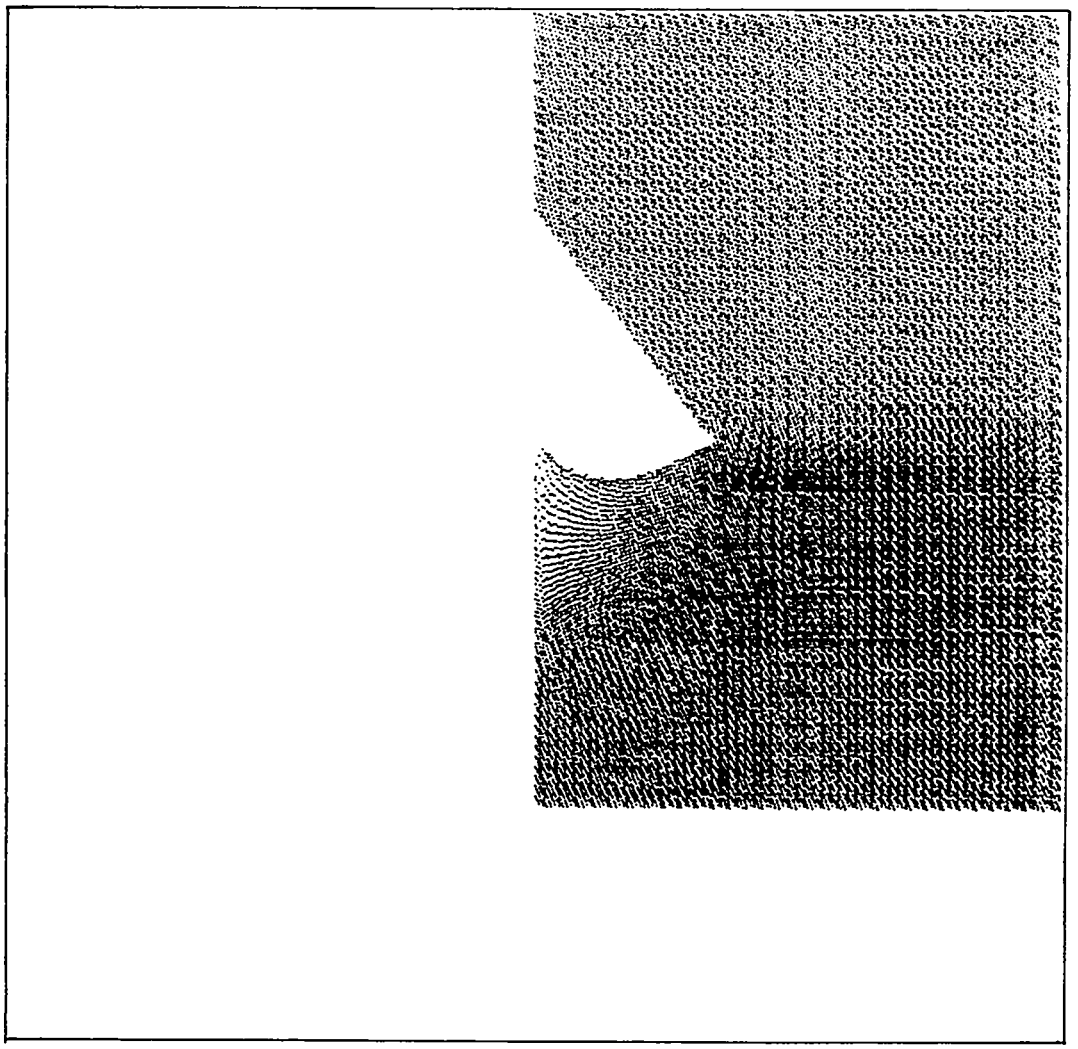

THE TIME IS 1.70000-001 MICROSECONDS AND THE CYCLE NUMBER IS 3.40000+002

0.200μ sec.

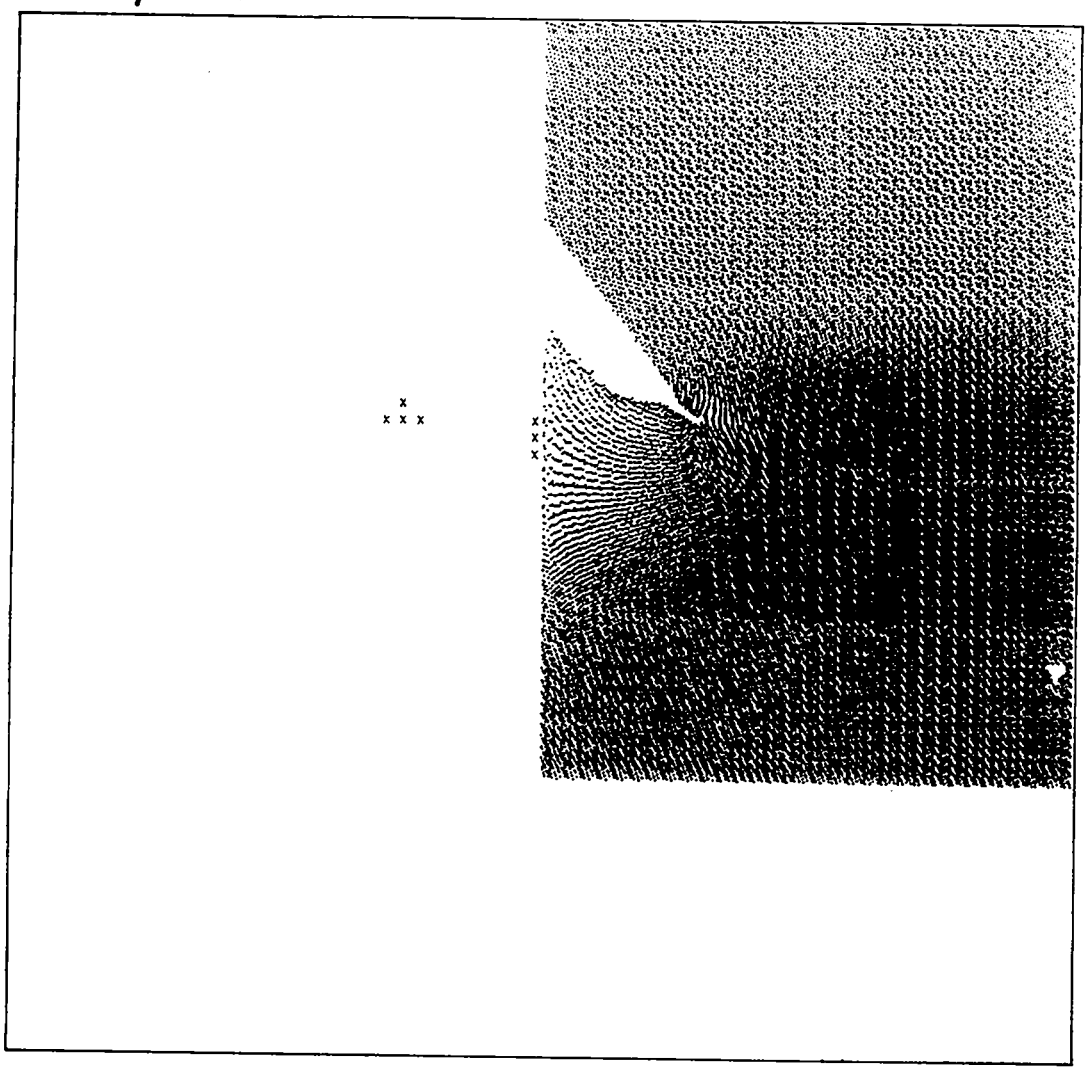

THE TIME IS 2.00000-001 MICROSECONDS AND THE CYCLE NUMBER IS 4.00000+002

0.210 μ sec.

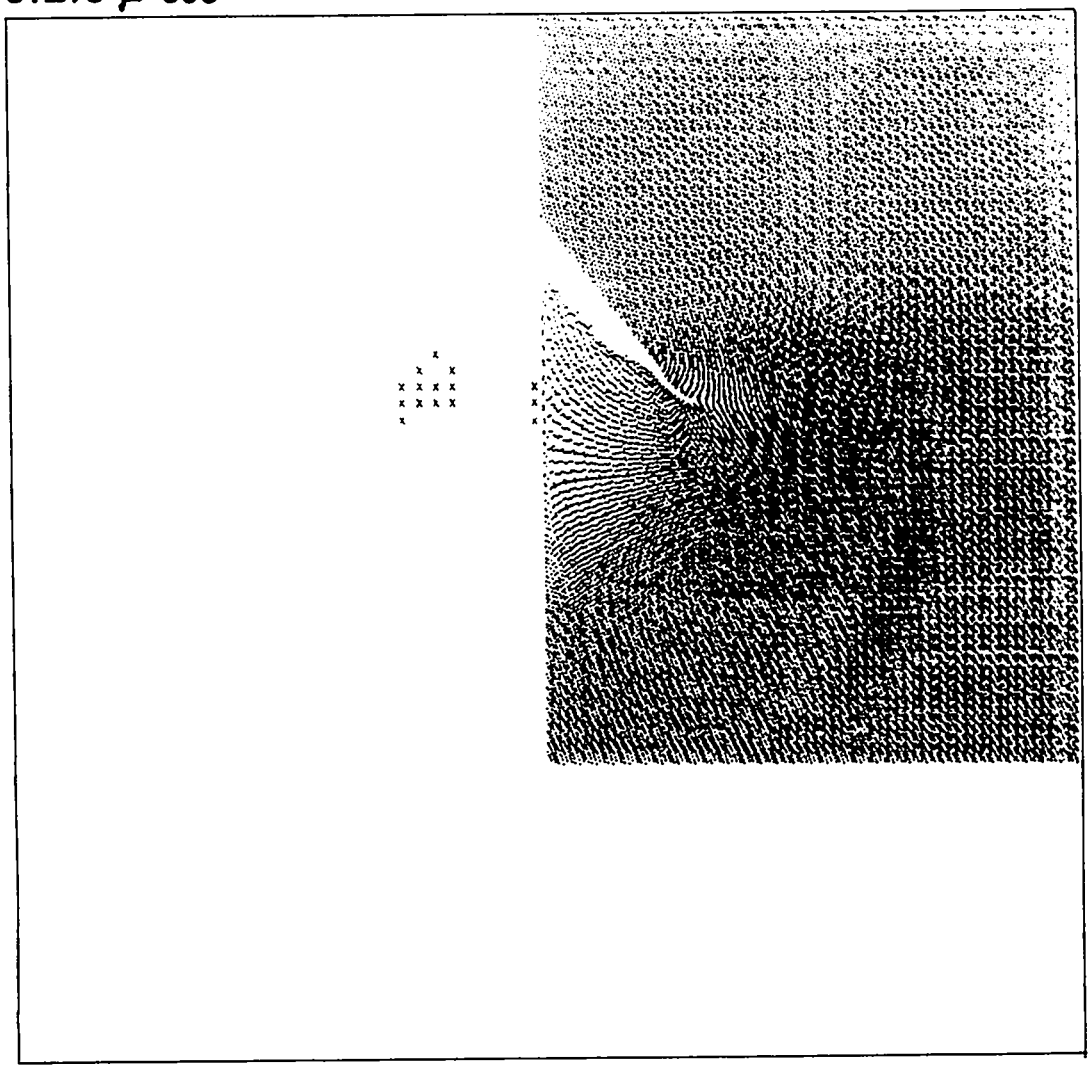

THE TIME IS 2.10000-001 MICROSECONDS AND THE CYCLE NUMBER IS 4.20000+002

0.220μ sec.

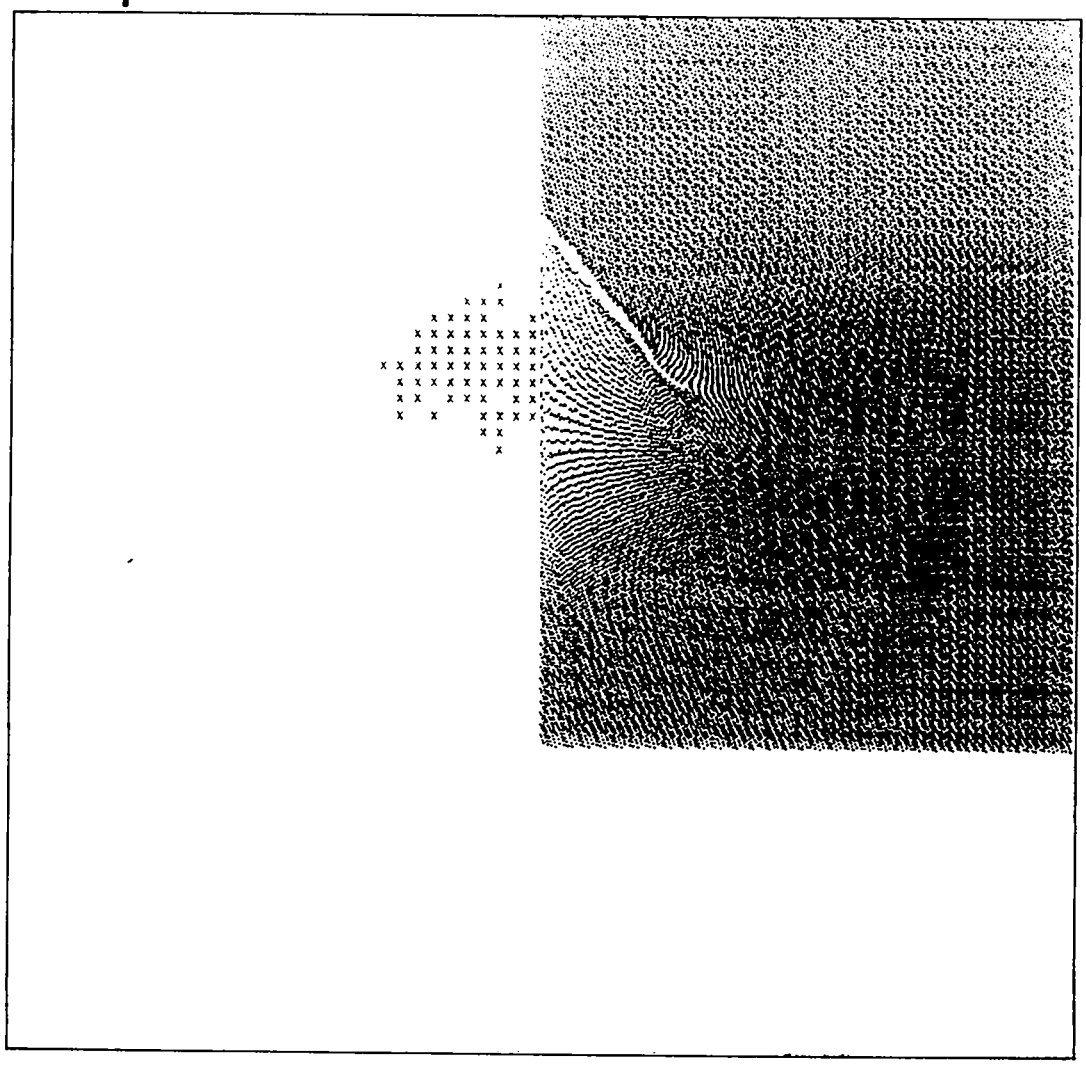

THE TIME IS 2.20000-001 MICROSECONDS AND THE CYCLE NUMBER IS 4.40000+002

0.230μ sec.

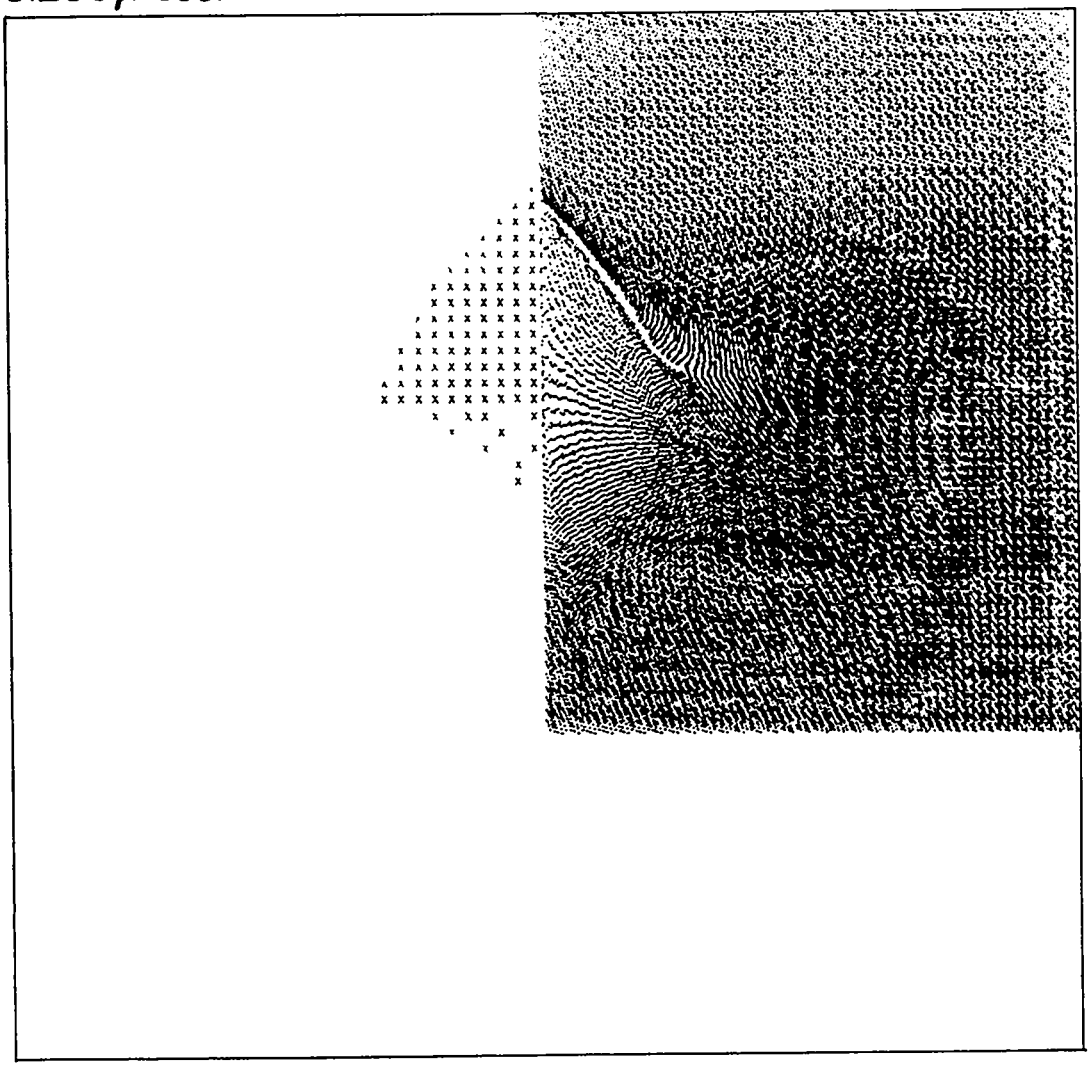

THE TIME IS 2.30000-001 MICROSECONDS AND THE CYCLE NUMBER IS 4.60000+002

0.240μ sec.

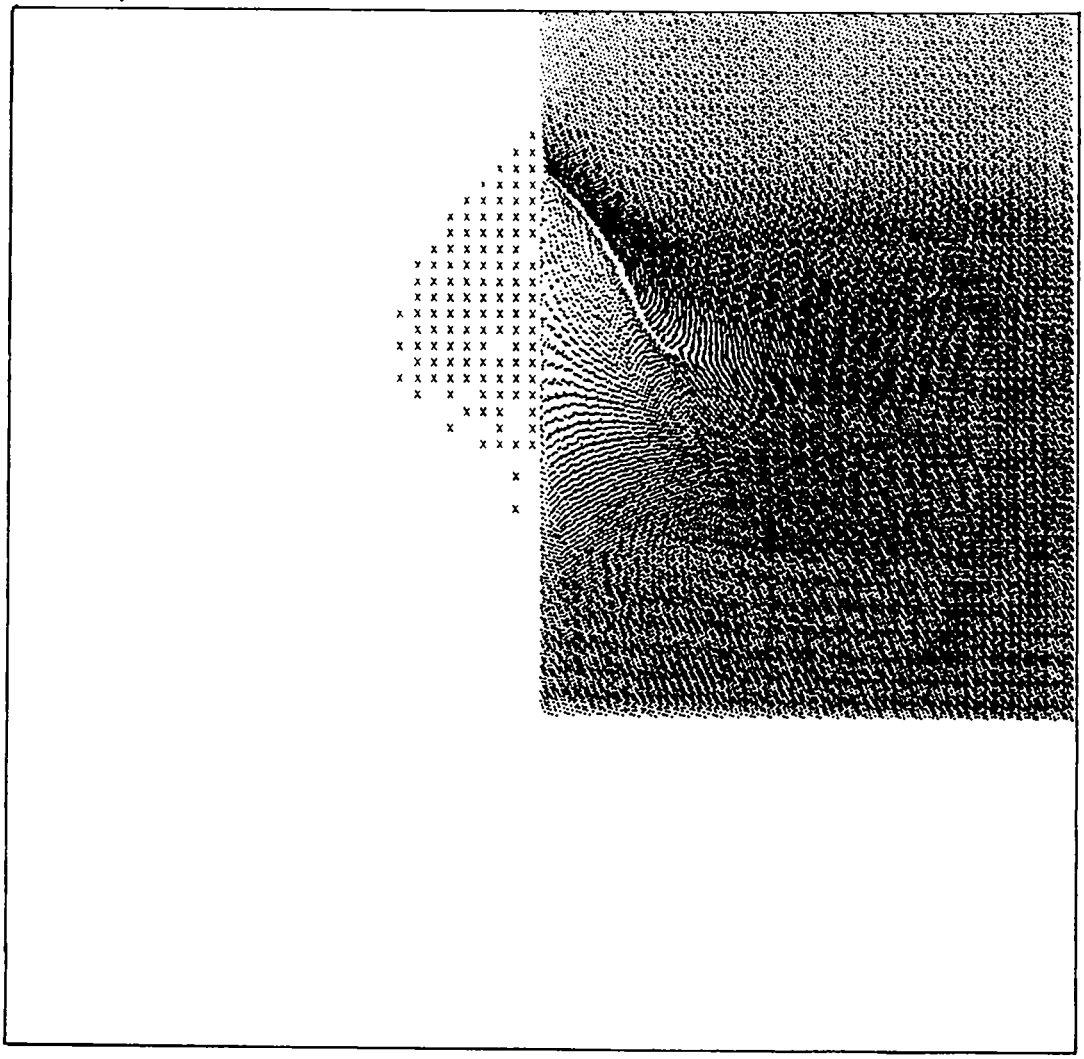

THE TIME IS 2.40000-001 MICROSECONDS AND THE CYCLE NUMBER IS 4.80000+002

Figure 7

THE FORMATION OF A HOT SPOT AND RESULTING PROPAGATING DETONATION FROM A 0.03-cm-RADIUS, 0.03-cm-HALF-HEIGHT BICONICAL VOID

The right sides of the following pictures show the particle cross section of the cylinder. The positions of those cells that have completely decomposed are shown with an "x". Chemical reaction is permitted.

0.200μ sec.

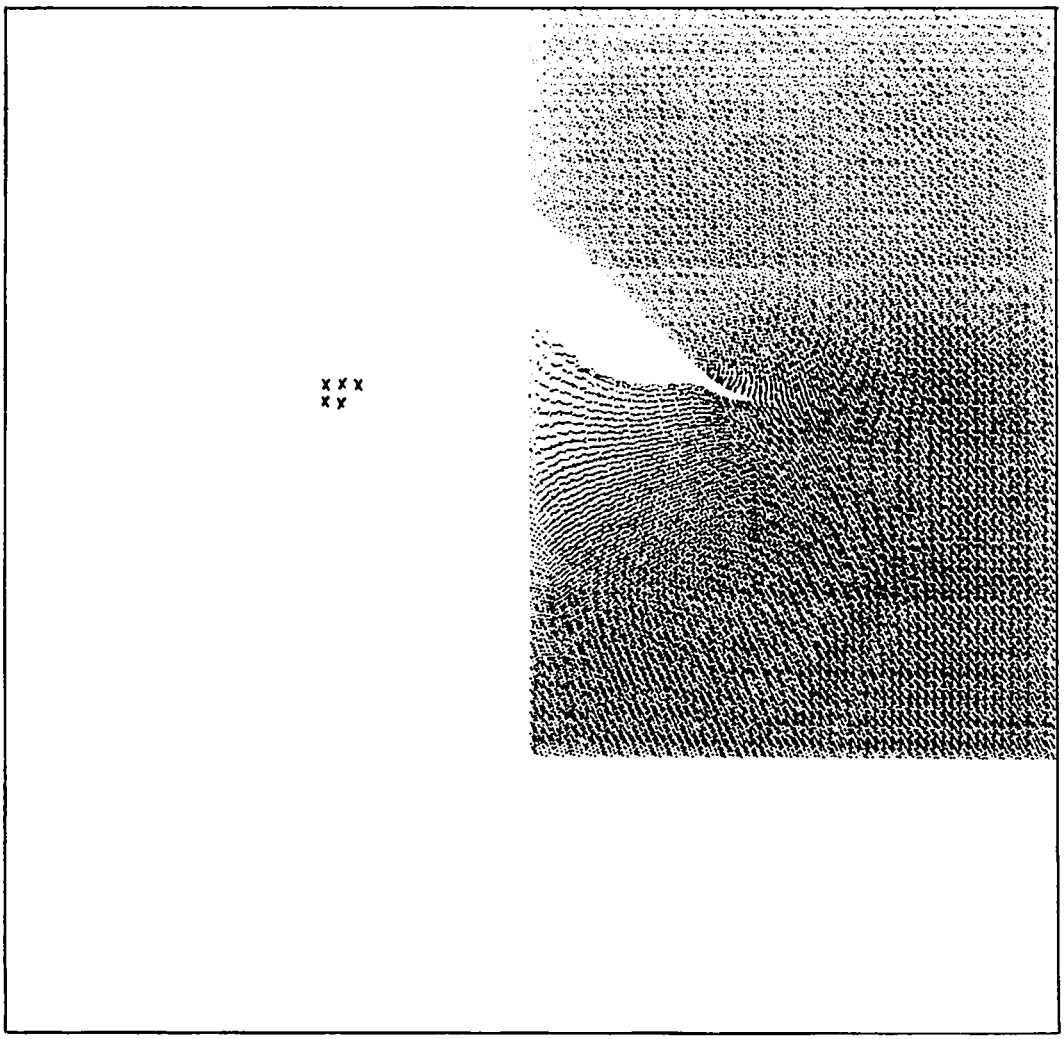

THE TIME IS 2.00000-001 MICROSECONDS AND THE CYCLE NUMBER IS 4.00000+002

0.210μ sec.

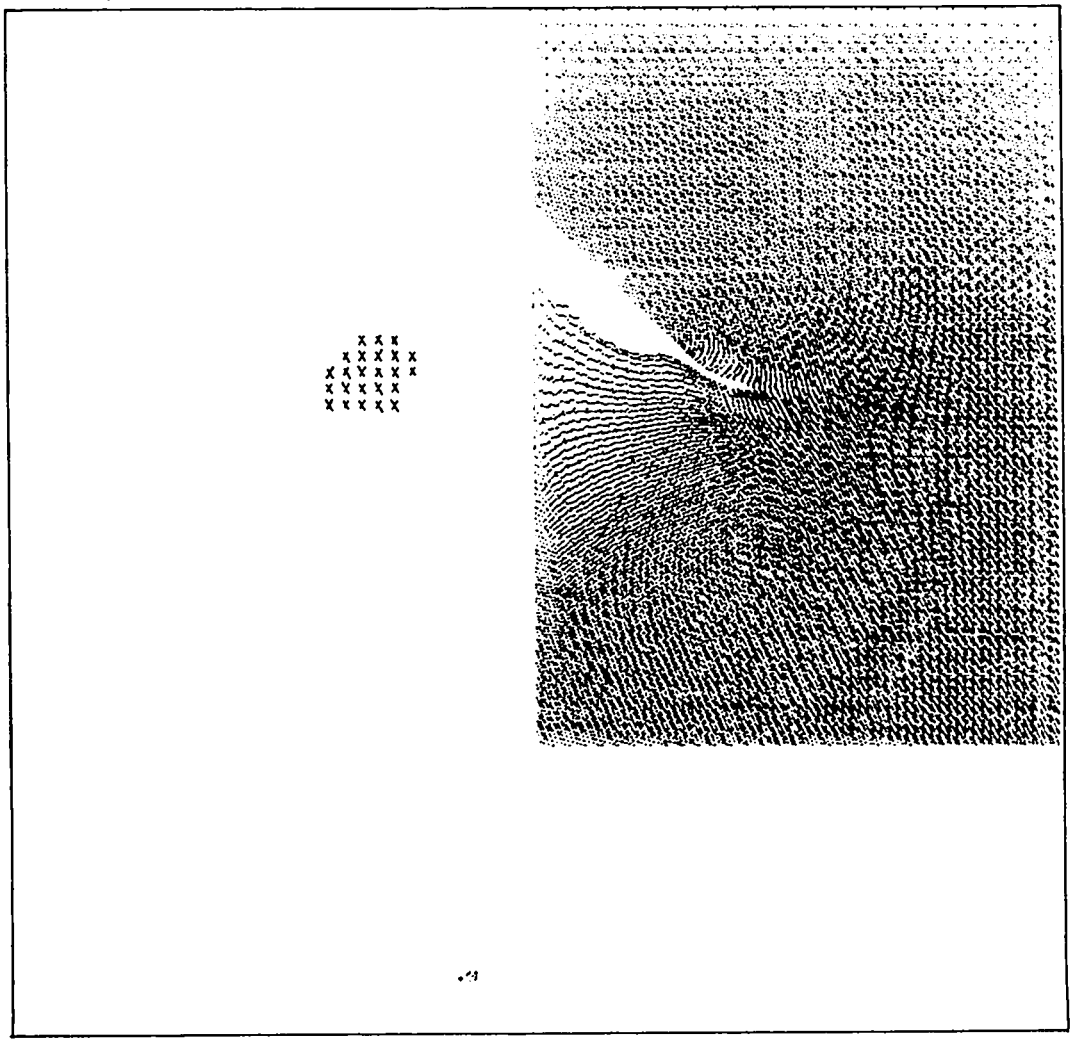

THE TIME IS 2.10000-001 MICROSECONDS AND THE CYCLE NUMBER IS 4.20000+002

0.220μ sec.

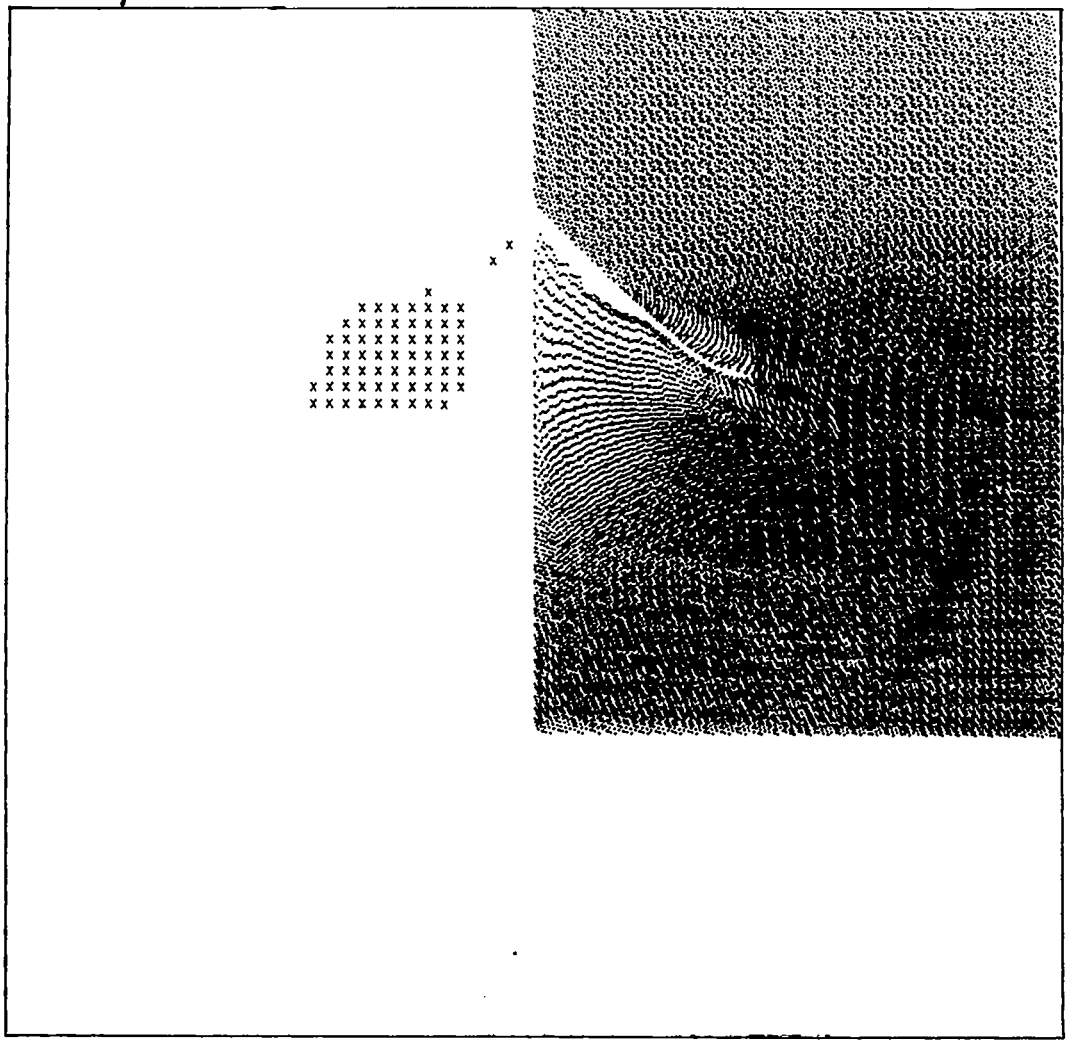

THE TIME IS 2.20000-001 MICROSECONDS AND THE CYCLE NUMBER IS 4.40000+002

0.240μ sec.

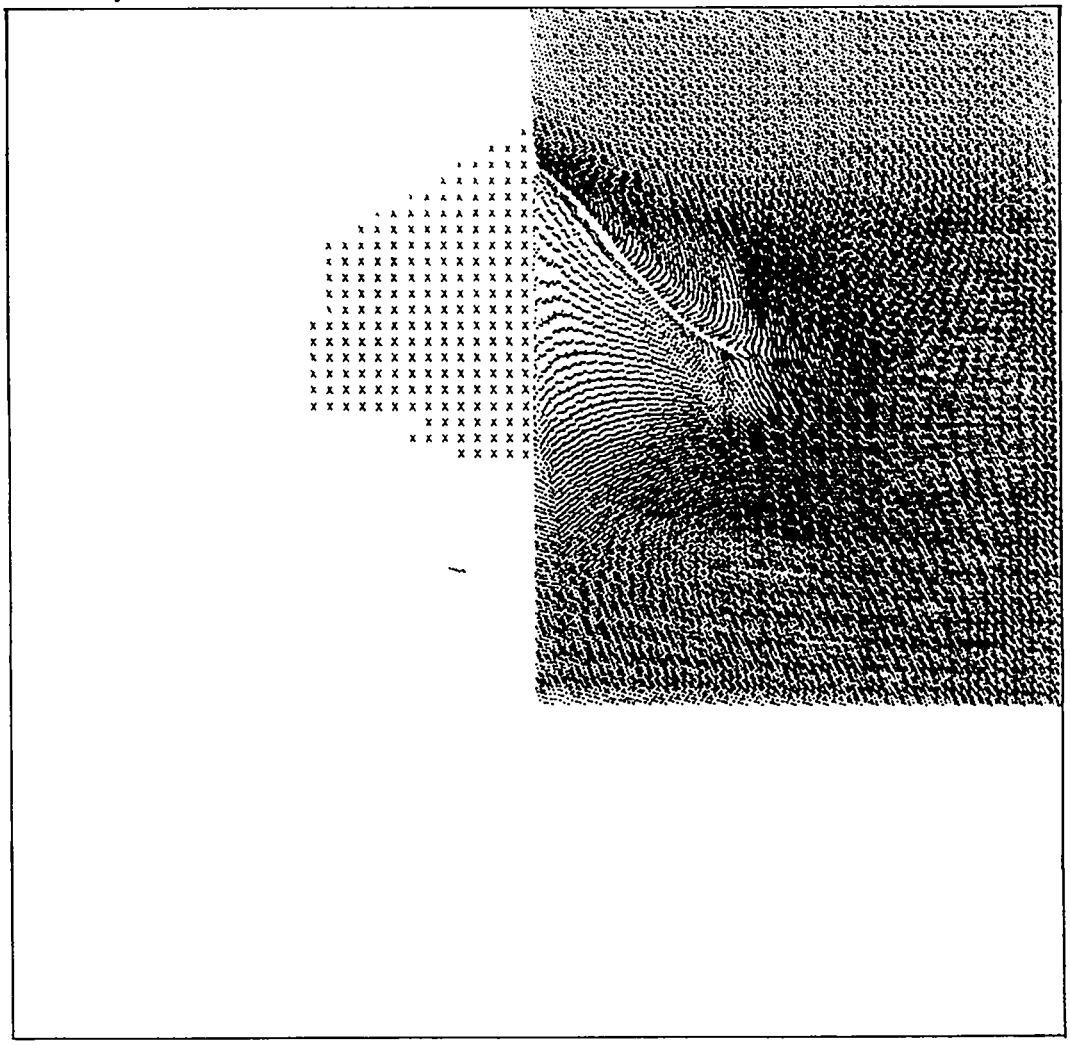

THE TIME IS 2.40000-001 MICROSECONDS AND THE CYCLE NUMBER IS 4.80000+002

0.250μ sec.

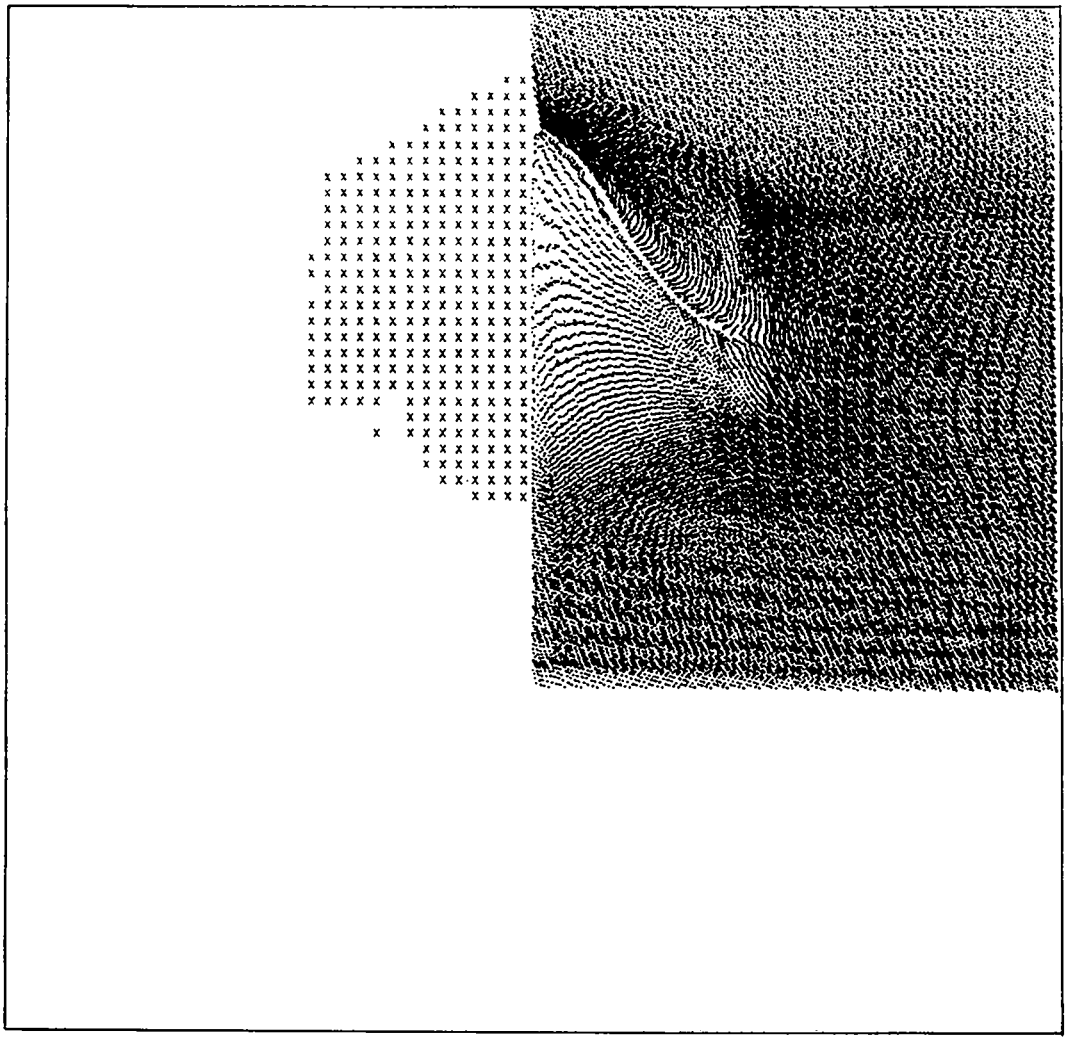

THE TIME IS 2.50000-001 MICROSECONDS AND THE CYCLE NUMBER IS 5.00000+002

0.260μ sec.

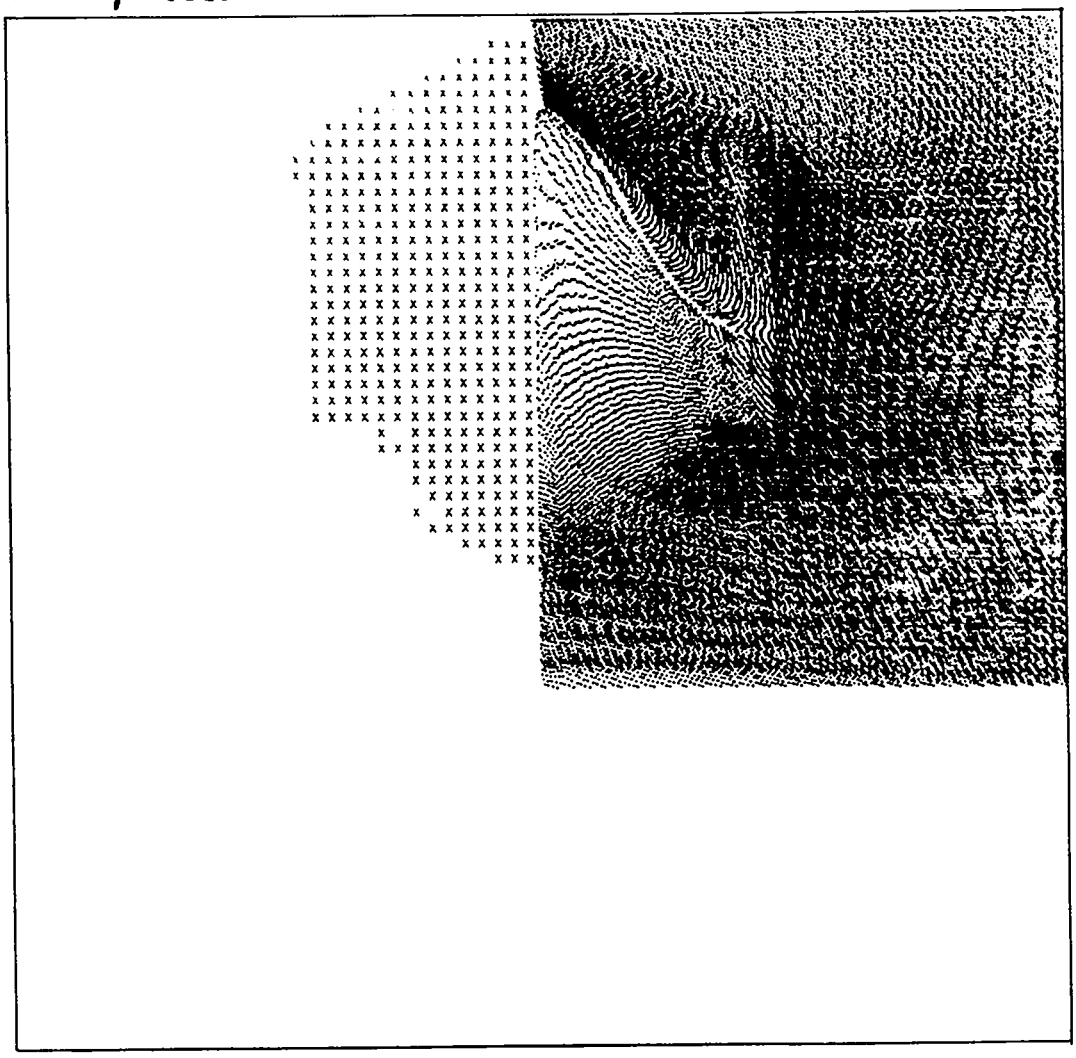

THE TIME IS 2.60000-001 MICROSECONDS AND THE CYCLE NUMBER IS 5.20000+002

IV. ALUMINUM SPHERES IN NITROMETHANE

In this section we shall discuss the results we have obtained with our new two-fluid EIC code for a shock interacting with an aluminum sphere in nitromethane.

The initial and boundary conditions of the calculation were chosen to match the model of a cylinder of nitromethane containing a solid aluminum sphere centered on the axis.

The results of a nonreactive EIC calculation are presented in the form of pictures in Figure 8 for a 0.064-cm-radius, 0.128-cm-high cylinder of nitromethane containing a 0.025-cm-radius sphere of aluminum. The shape of the aluminum sphere and the shock front are shown at various times in Figure 9.

The 85-kbar, 1200°K shock arrives at the lower surface of the aluminum sphere traveling with a shock velocity of 0.45 cm/μsec and a particle velocity of 0.171 cm/μsec. The matching conditions give a pressure of 170 kbar, a particle velocity of 0.093 cm/μsec, a temperature of 500°K, and a shock velocity of 0.66 cm/μsec in the aluminum. The 170-kbar nitromethane has a temperature of about 1500°K. The double-shocked nitromethane energy and temperature are less than the energy and temperature of single-shocked nitromethane at the same pressure.

The shock wave in the aluminum is divergent and faster than the shock wave in the nitromethane. The wave degrades in the aluminum and is about 80 kbar (shock velocity of 0.56 cm/μsec) upon reaching the upper

surface of the sphere. The matching conditions give a 20-kbar shock in the nitromethane above the aluminum sphere. The main shock in the body of the fluid overtakes the weaker shock transmitted through the sphere.

The actual process is much more complex with the velocities and pressures varying about the values assigned to them in this simplified discussion.

The results of a reactive EIC calculation for this system are shown in Figure 10. The formation of the hot spot and resulting propagating detonation is shown. The ringing or layering of the particles at the bottom interface occurs after the time during which the region is an important contributor to the formation of the hot spot.

Figure 8

A 0.025-cm-RADIUS SPHERE OF ALUMINUM IN NITROMETHANE WITH NO REACTION

The formation of a hot spot from a shock interacting with a 0.025-cm-radius sphere of aluminum in nitromethane. The positions of those cells with a temperature greater than 1400°K are shown in the left half of the picture with an "x". Chemical reaction is not permitted. The aluminum particles are printed twice as dark as the nitromethane particles.

0.11 μ sec.

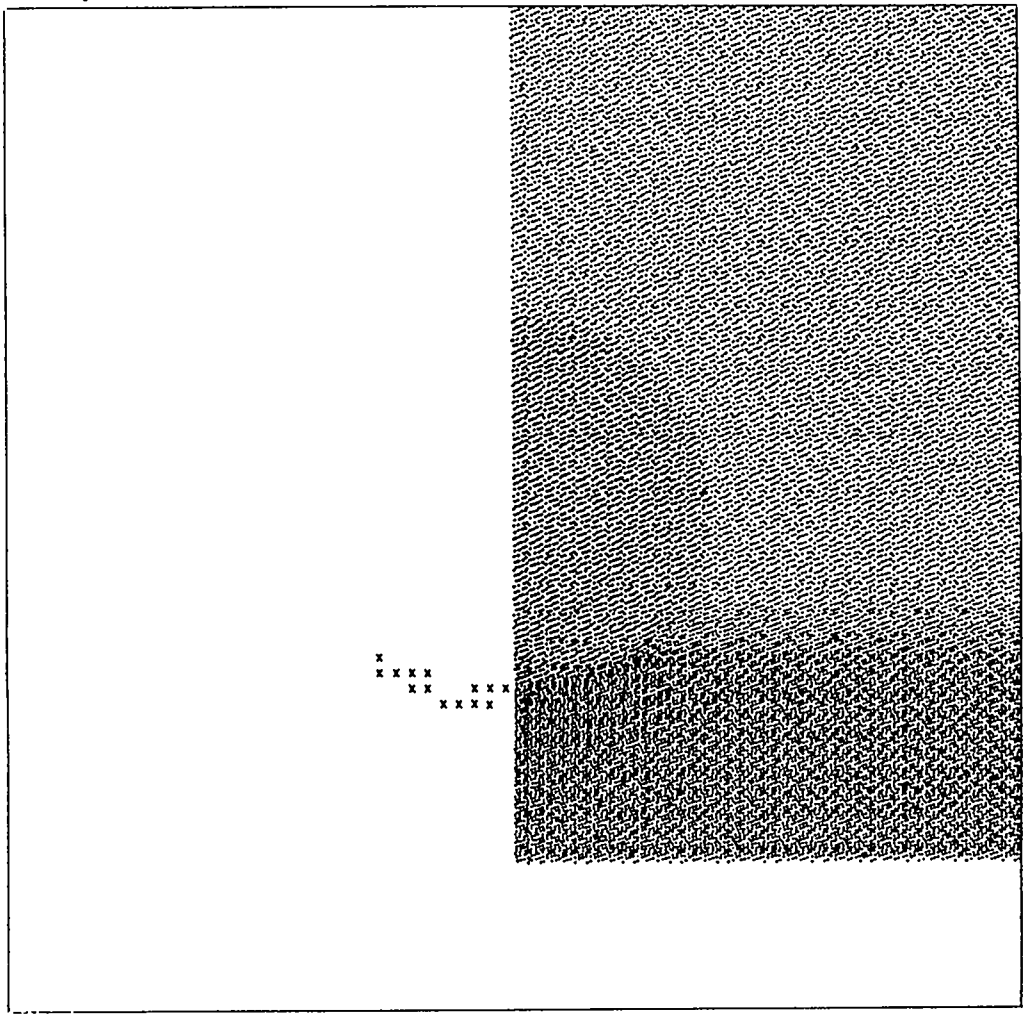

THE TIME IS 1.10000-001 MICROSECONDS AND THE CYCLE NUMBER IS 2.20000+002.

0.16 μ sec.

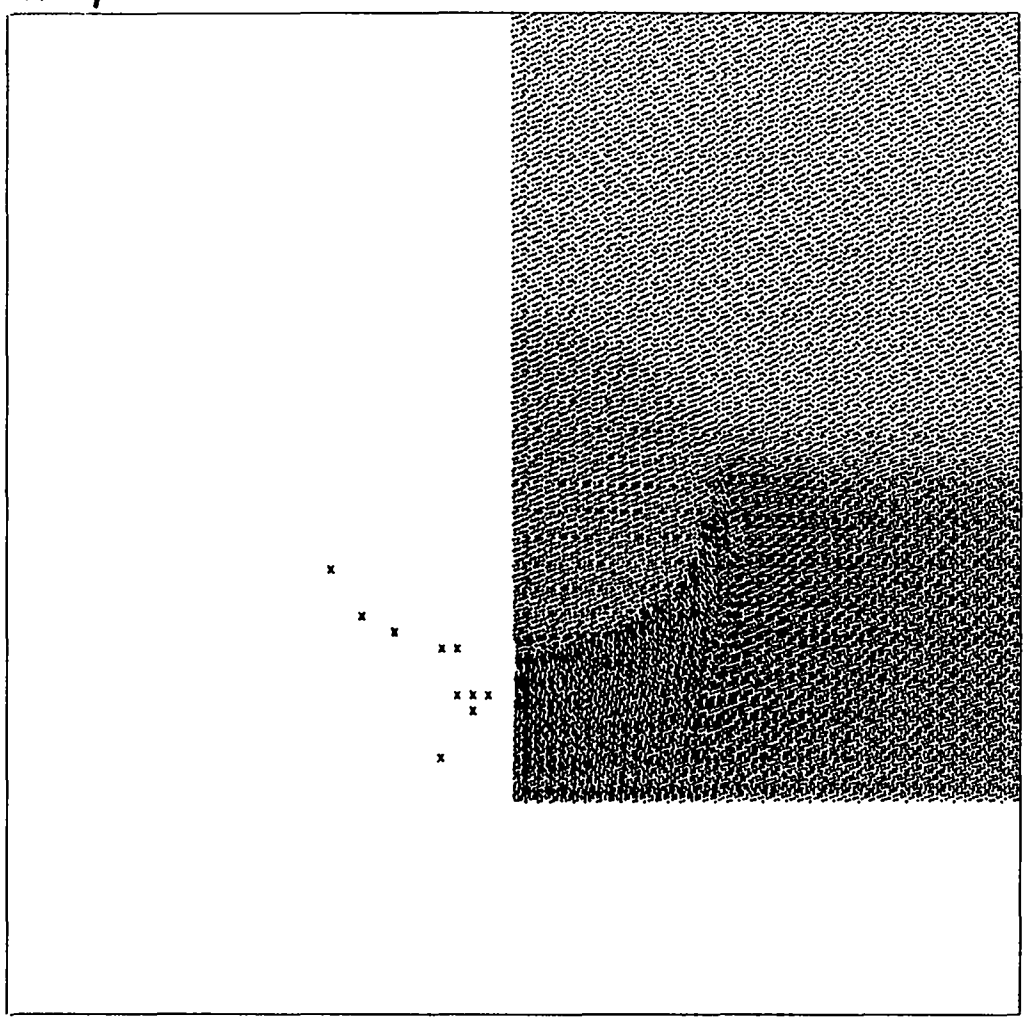

THE TIME IS 1.60000-001 MICROSECONDS AND THE CYCLE NUMBER IS 3.20000+002

0.25 μ sec.

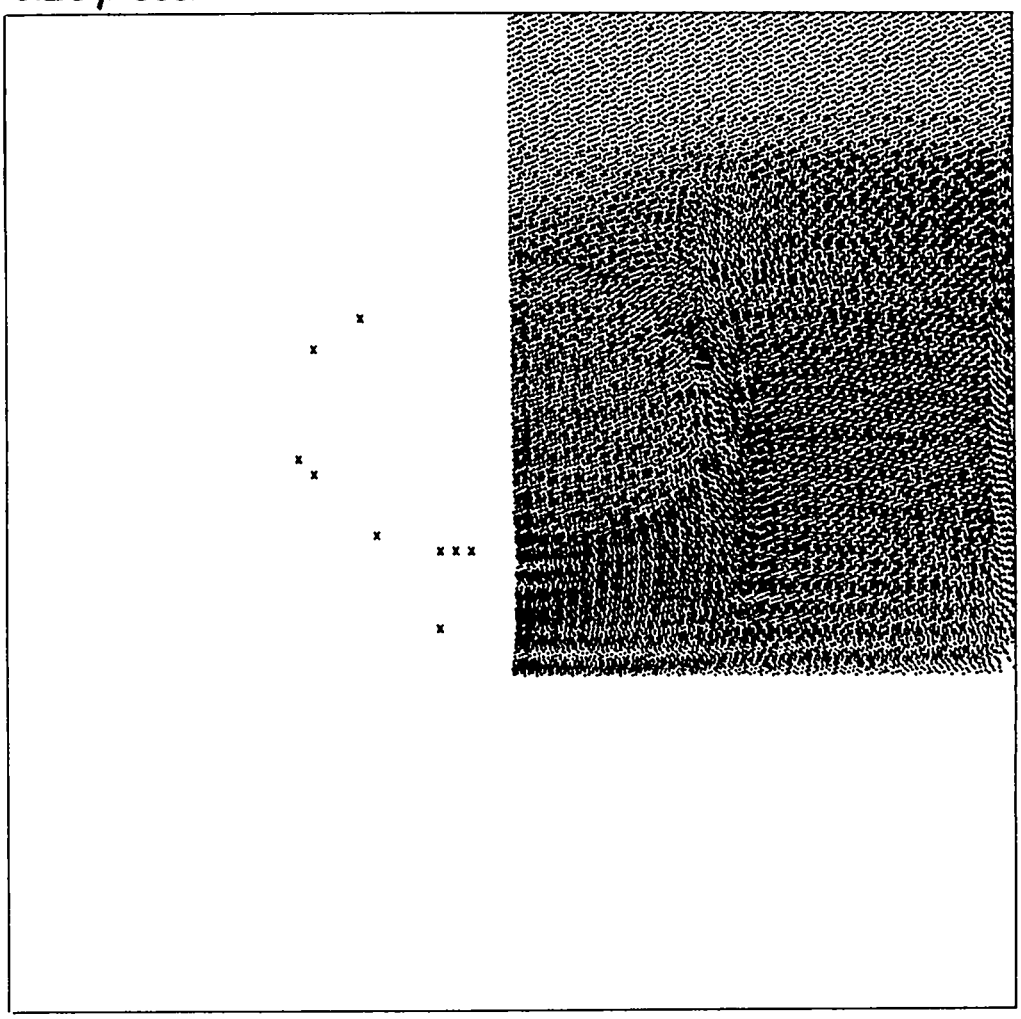

THE TIME IS 2.50000-001 MICROSECONDS AND THE CYCLE NUMBER IS 5.00000+002

0 0.0925 μsec.
1 0.120 μsec.
2 0.145 μsec.
3 0.170 μsec.
4 0.195 μsec.
5 0.210 μsec.
6 0.235 μsec.
7 0.250 μsec.
8 0.270 μsec.

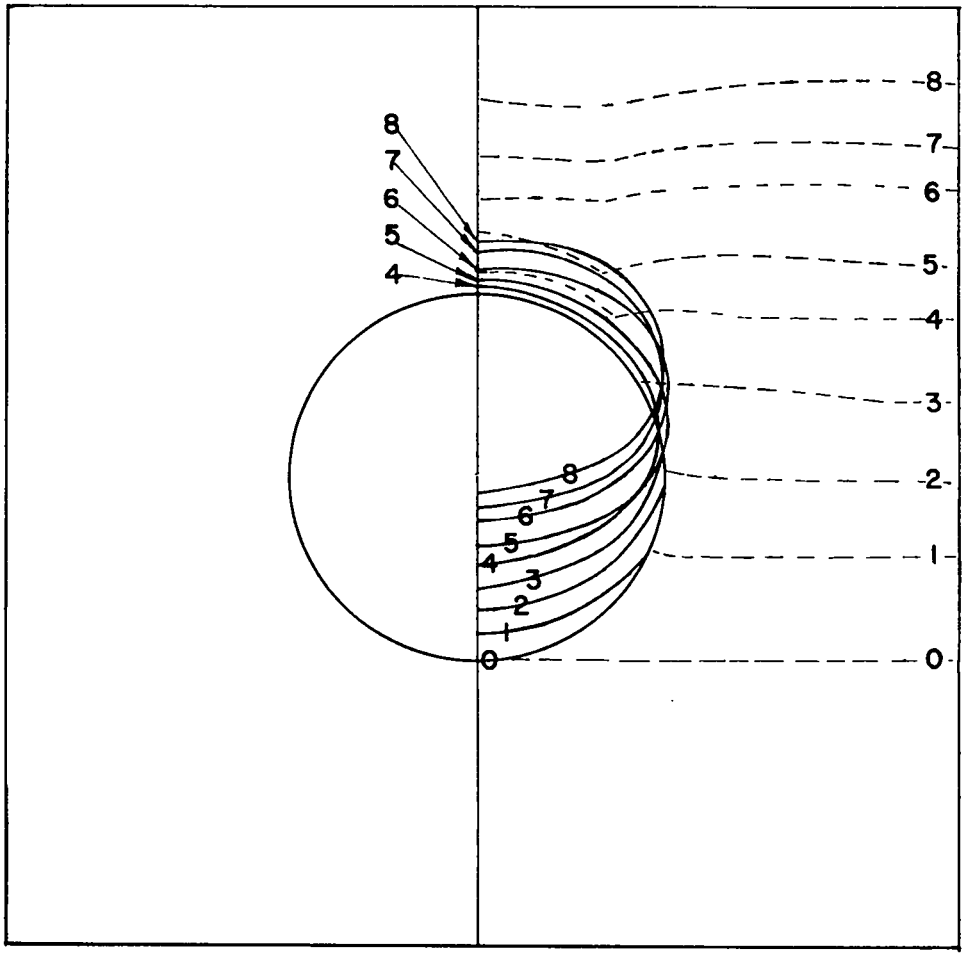

Figure 9. Aluminum sphere shape. The shape of the aluminum sphere is shown with solid lines, and that of the shock front is shown with dashed lines for various times. Chemical reaction is not permitted.

Figure 10

A 0.025-cm-RADIUS SPHERE OF ALUMINUM IN NITROMETHANE WITH CHEMICAL REACTION PERMITTED

The formation of a hot spot and buildup to propagating detonation as a result of a shock interacting with a 0.025 cm-radius sphere of aluminum in nitromethane. The positions of those cells that have completely decomposed are shown in the left half of the picture with an "x". The aluminum particles are printed twice as dark as the nitromethane particles.

0.16 μsec.

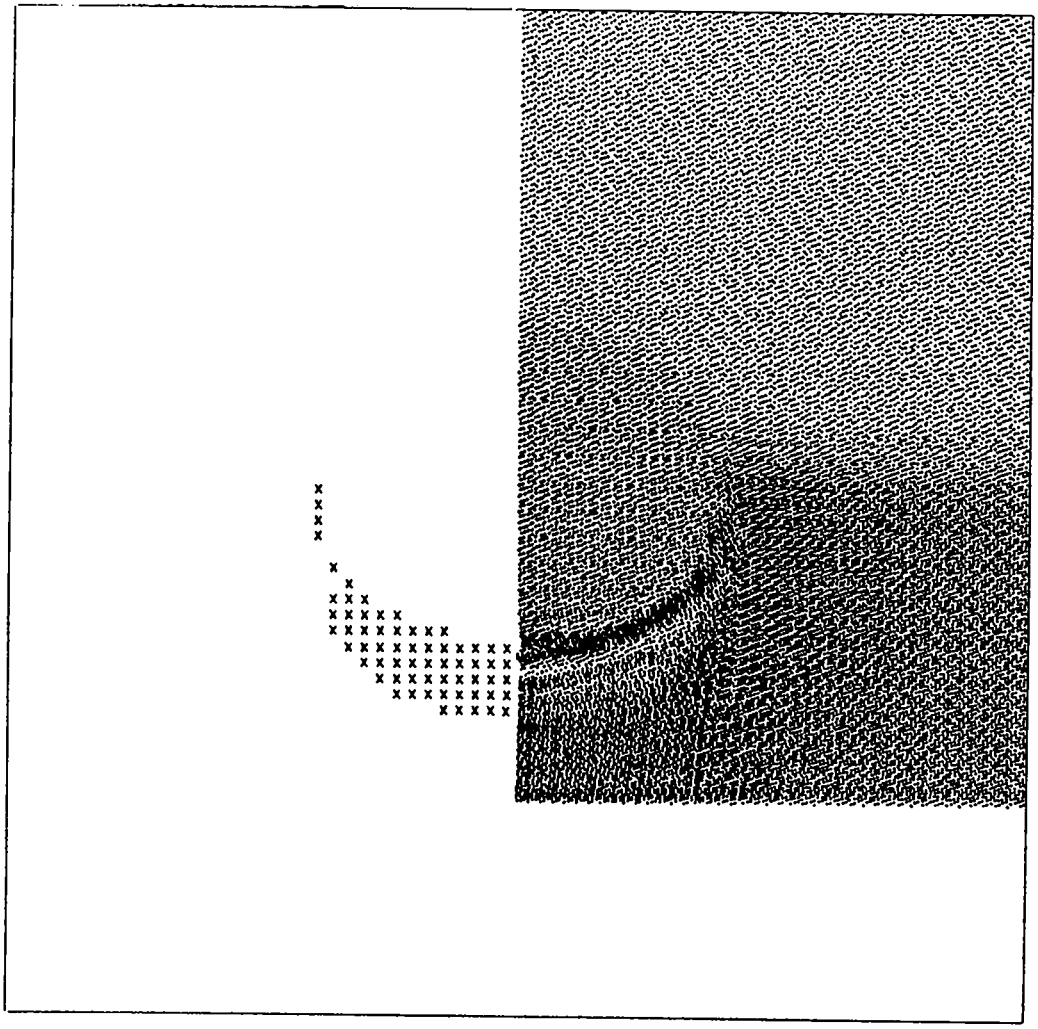

THE TIME IS 1.60000-001 MICROSECONDS AND THE CYCLE NUMBER IS 3.20000+002

0.25μsec.

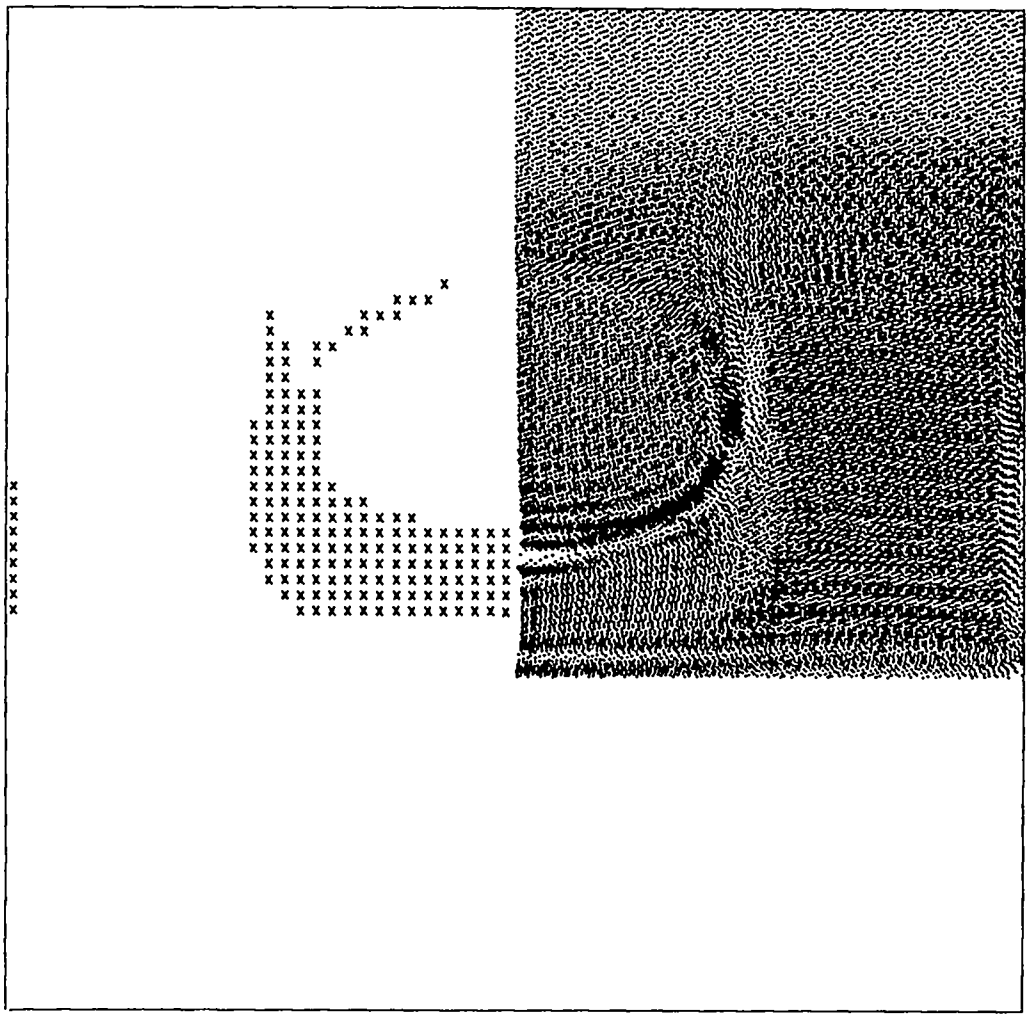

THE TIME IS 2.50000-001 MICROSECONDS AND THE CYCLE NUMBER IS 5.00000+002

V. ALUMINUM CYLINDERS IN NITROMETHANE

In this section we shall discuss the results we have obtained with the EIC code for a shock interacting with an aluminum cylinder in nitromethane.

The initial and boundary conditions of the calculation were chosen to match the model of a cylinder of nitromethane containing a solid aluminum cylinder centered on the axis.

Figure 11 shows the formation of a hot spot when a shock interacts with a 0.032- by 0.032-cm-radius cylinder of aluminum in nitromethane. The 85-kbar, 1200°K shock arrives at the lower surface of the aluminum cylinder traveling with a shock velocity of 0.45 cm/μsec and a particle velocity of 0.171 cm/μsec. The matching conditions give a pressure of 170 kbar, a particle velocity of 0.093 cm/μsec, a temperature of 500°K, and a shock velocity of 0.66 cm/μsec in the aluminum. The pressure in the previously shocked nitromethane below the cylinder is, of course, also 170 kbar, the particle velocity is 0.093 cm/μsec, and the temperature is about 1500°K. The double-shocked nitromethane energy and temperature are less than the energy and temperature of single-shocked nitromethane at the same pressure.

The shock wave in the aluminum is divergent and is about 100 kbar upon reaching the upper surface of the cylinder. The matching conditions give 30 kbar in the nitromethane above the cylinder. The main shock overtakes the initial weaker shock.

The actual process is much more complex with the velocities and pressures varying about the values assigned to them in this simplified discussion.

Figure 12 shows the shape of the aluminum cylinder and the shock fronts at various times.

Figure 13 shows the formation of a hot spot and buildup to propagating detonation from a shock interacting with a 0.032- by 0.032-cm-radius cylinder of aluminum in nitromethane.

Figure 14 shows the formation of a hot spot and failure to build up to propagating detonation from a shock interacting with a 0.002- by 0.002-cm-radius cylinder of aluminum in nitromethane. The hot spot develops in a manner similar to that described previously [2,3] for one-dimensional hot spots.

We did not observe failure of the hot spots formed from the interaction of a shock with a void[1] because the hot spot was formed at the shock front and at a temperature so high (2,000 to 3,000°K) that the reaction was essentially instantaneous in the time and space scale of interest. In the case of the cylinder of aluminum, the hot spot is formed behind the shock front and is at a sufficiently low temperature (1,400 to 1,500°K) that the reaction is not instantaneous in the time and space scale of interest. The resulting hot spot resembles the one-dimensional hydrodynamic hot spot. The hot spot decomposes, sending

a shock wave into the undetonated, previously shocked, explosive. Whether or not it propagates depends upon the initial strength of the shock wave and how well it is supported from the rear. The actual two-dimensional process is much more complex than the one-dimensional approximation.

Figure 11

A 0.032- by 0.032-cm CYLINDER OF ALUMINUM IN NITROMETHANE WITH NO REACTION

The formation of a hot spot from a shock interacting with a 0.032-cm-high, 0.032-cm-radius cylinder of aluminum in nitromethane. The positions of those cells with a temperature greater than 1350°K are shown in the left half of the picture with an "x". Chemical reaction is not permitted. The aluminum particles are printed twice as dark as the nitromethane particles.

0.075 μsec.

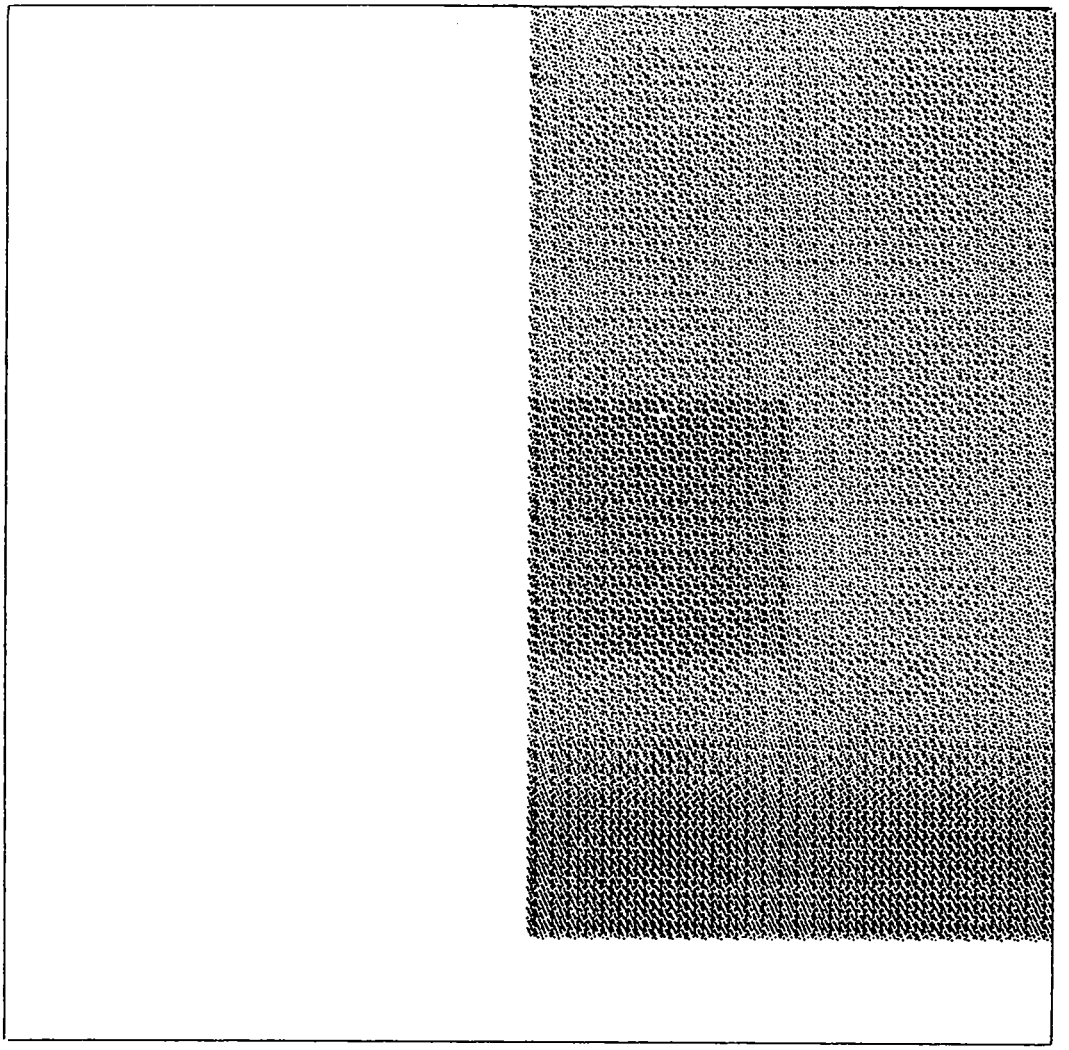

THE TIME IS 7.50000-002 MICROSECONDS AND THE CYCLE NUMBER IS 1.50000+002

0.120 μ sec.

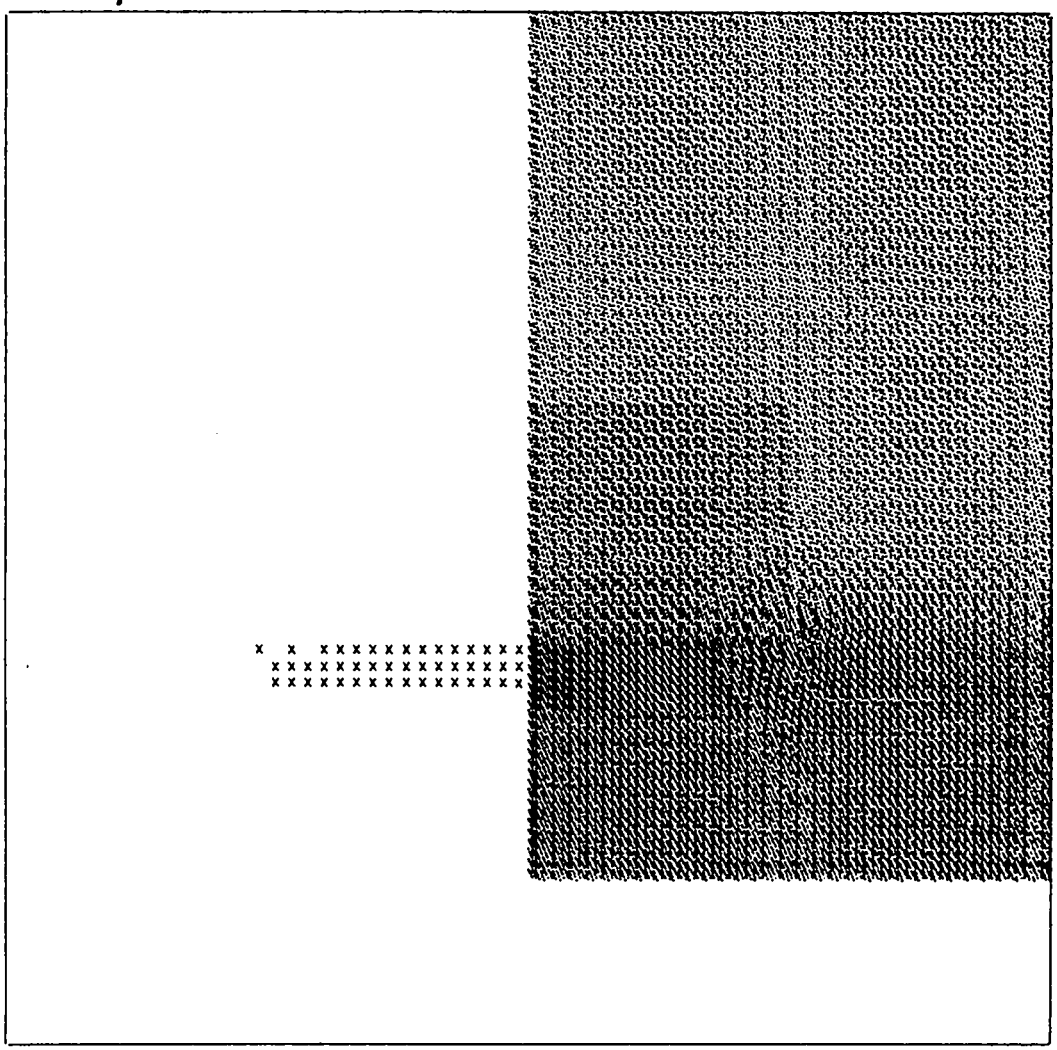

THE TIME IS 1.20000-001 MICROSECONDS AND THE CYCLE NUMBER IS 2.40000+002

0.145 μsec.

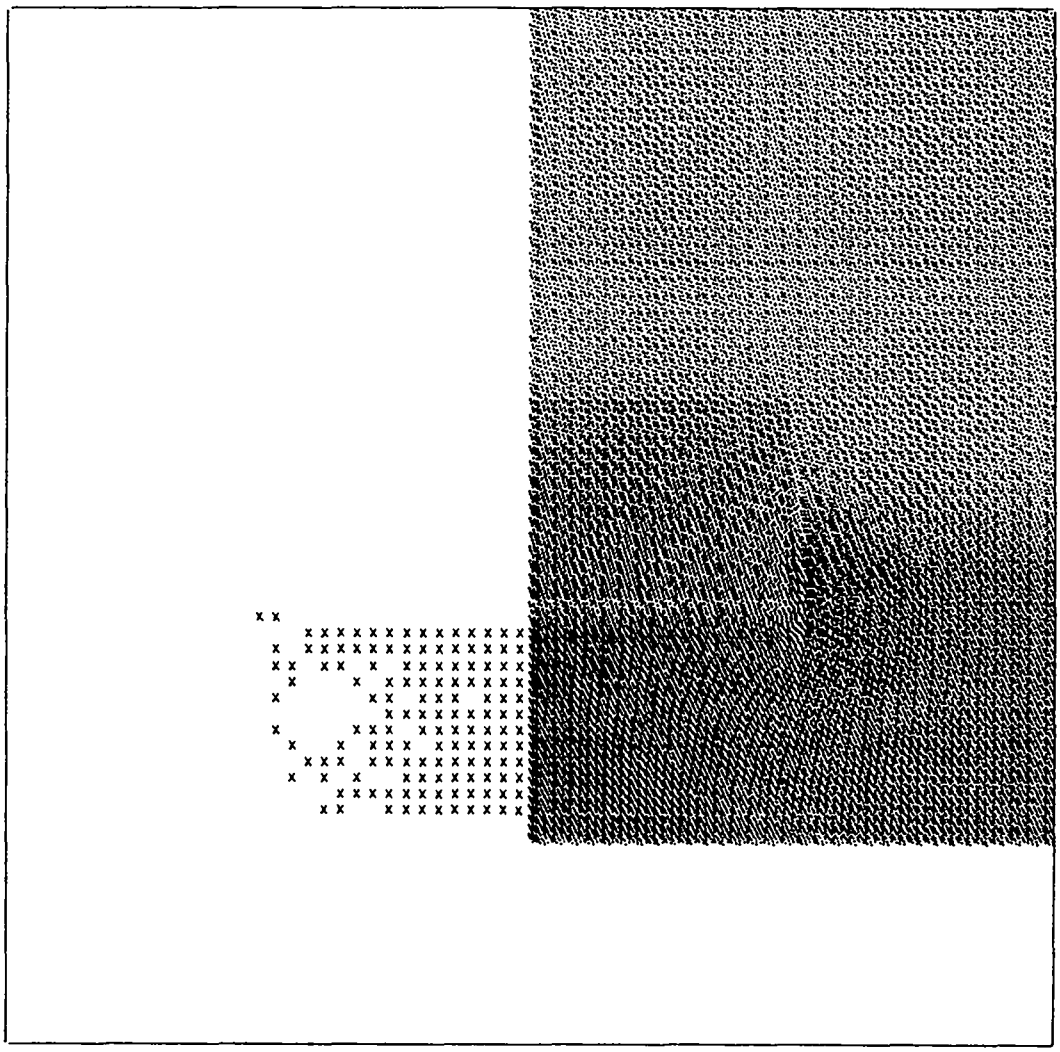

THE TIME IS 1.45000-001 MICROSECONDS AND THE CYCLE NUMBER IS 2.90000+002

0.205μsec.

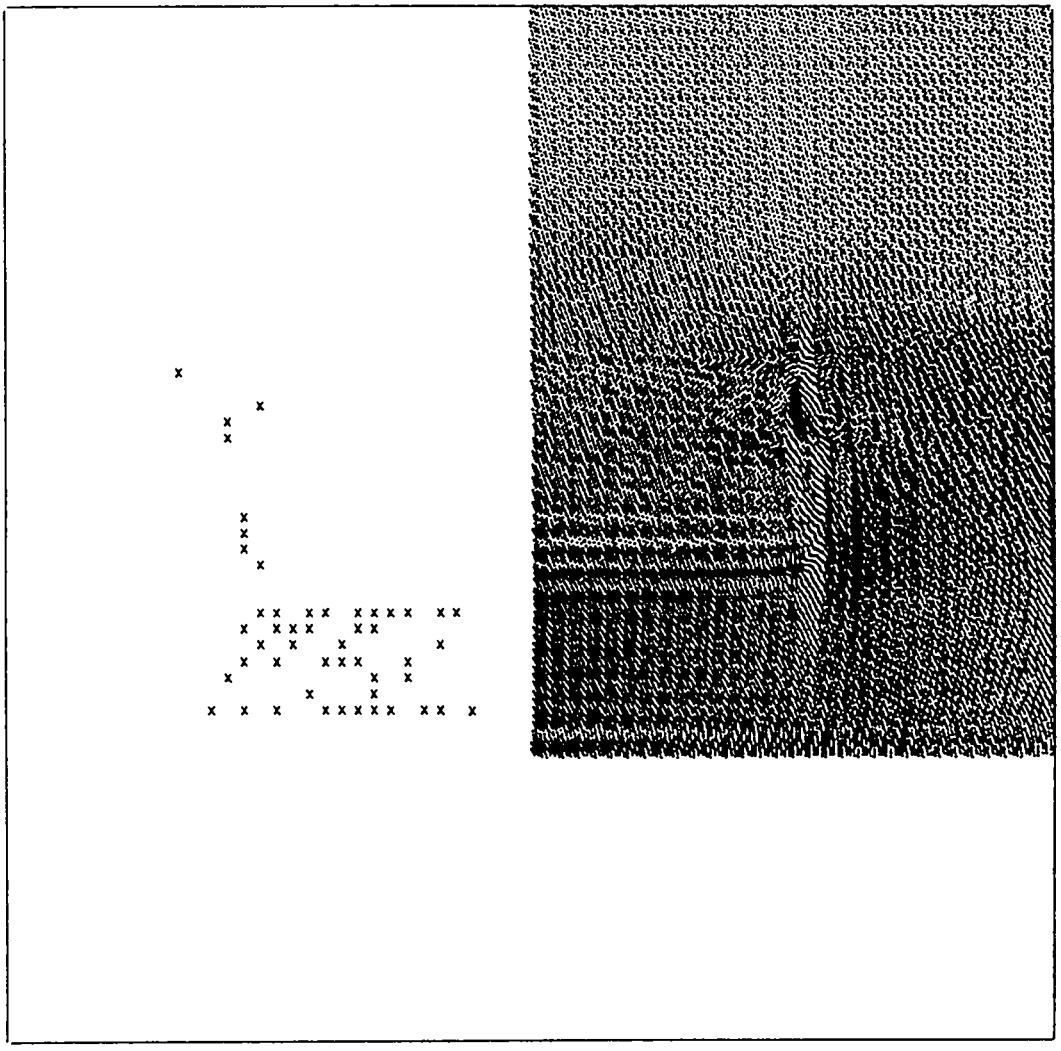

THE TIME IS 2.05000-001 MICROSECONDS AND THE CYCLE NUMBER IS 4.10000+002

1 0.110 μsec.
2 0.140 μsec.
3 0.165 μsec.
4 0.180 μsec.
5 0.215 μsec.

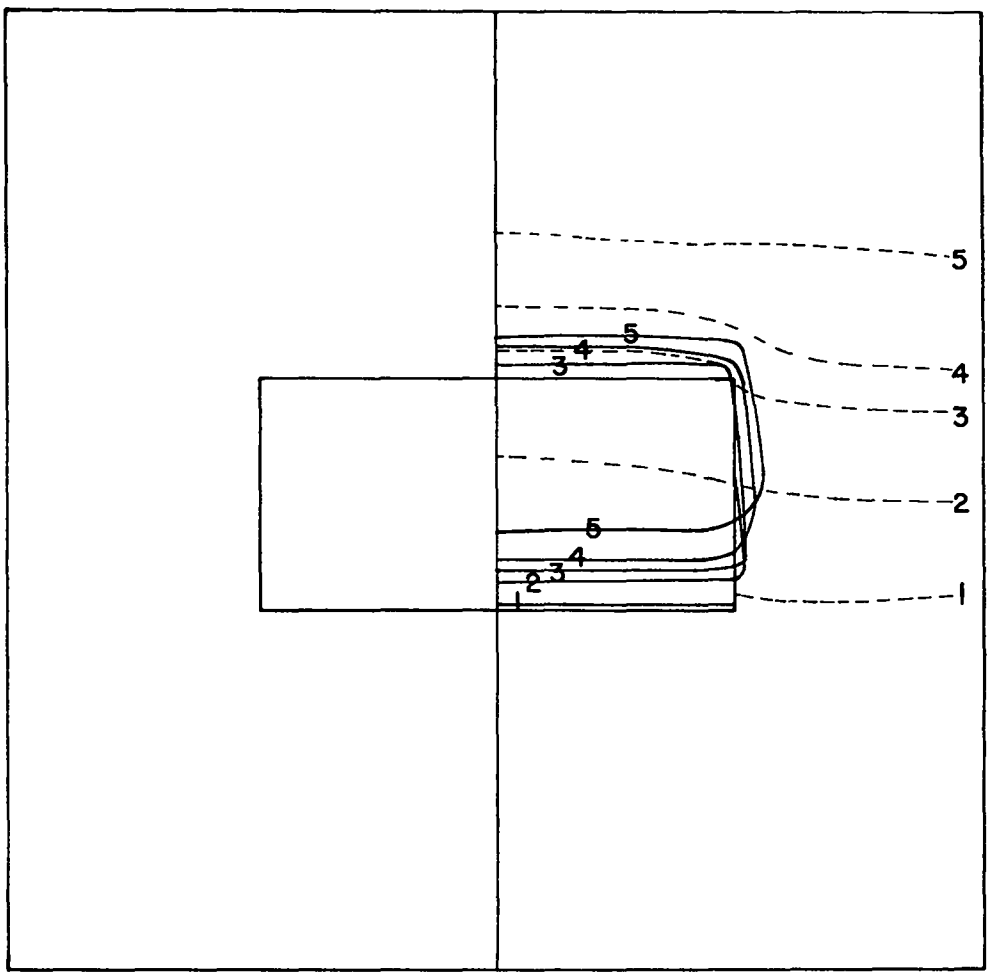

Figure 12. The shape of the aluminum cylinder is shown with solid lines, and the shape of the shock front is shown with dashed lines for various times. Chemical reaction is not permitted.

Figure 13

A 0.032- by 0.032-cm CYLINDER OF ALUMINUM IN NITROMETHANE WITH CHEMICAL REACTION PERMITTED

The formation of a hot spot and buildup to propagating detonation as a result of a shock interacting with a 0.032-cm-high, 0.032-cm-radius cylinder of aluminum in nitromethane. The positions of those cells that have completely decomposed are shown in the left half of the picture with an "x". The aluminum particles are printed twice as dark as the nitromethane particles.

0.140 μsec.

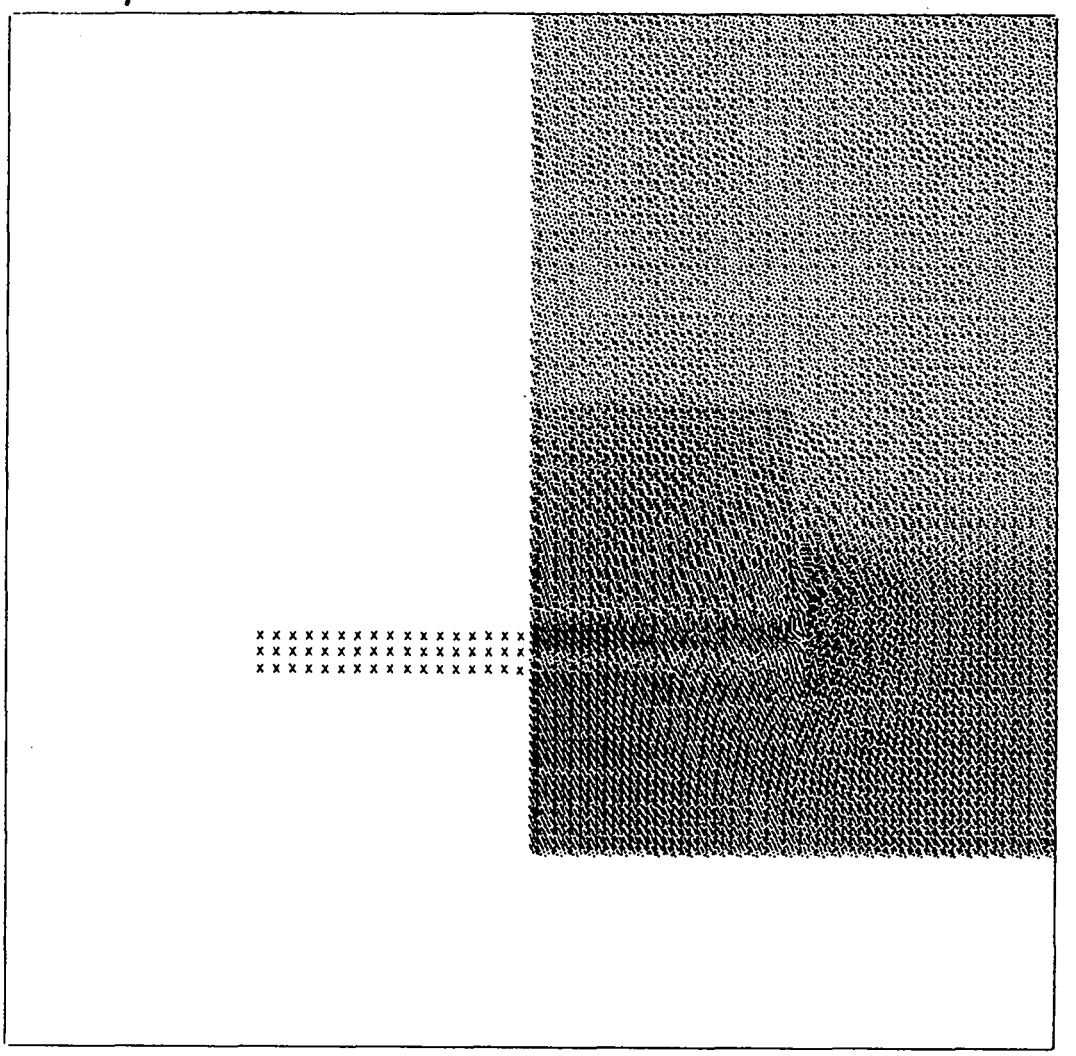

THE TIME IS 1.40000-001 MICROSECONDS AND THE CYCLE NUMBER IS 2.80000+002

0.180 μsec.

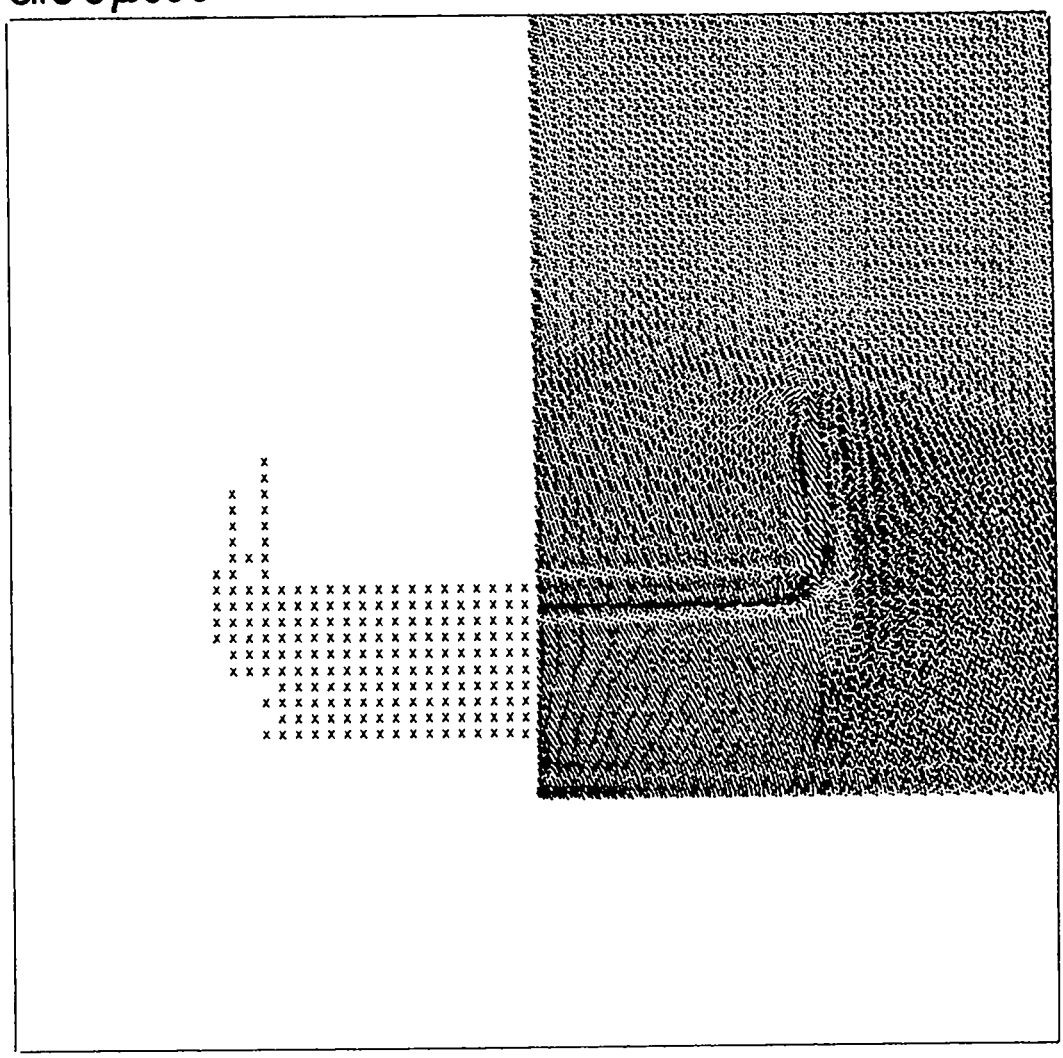

THE TIME IS 1.80000-001 MICROSECONDS AND THE CYCLE NUMBER IS 3.60000+002

0.220 μsec.

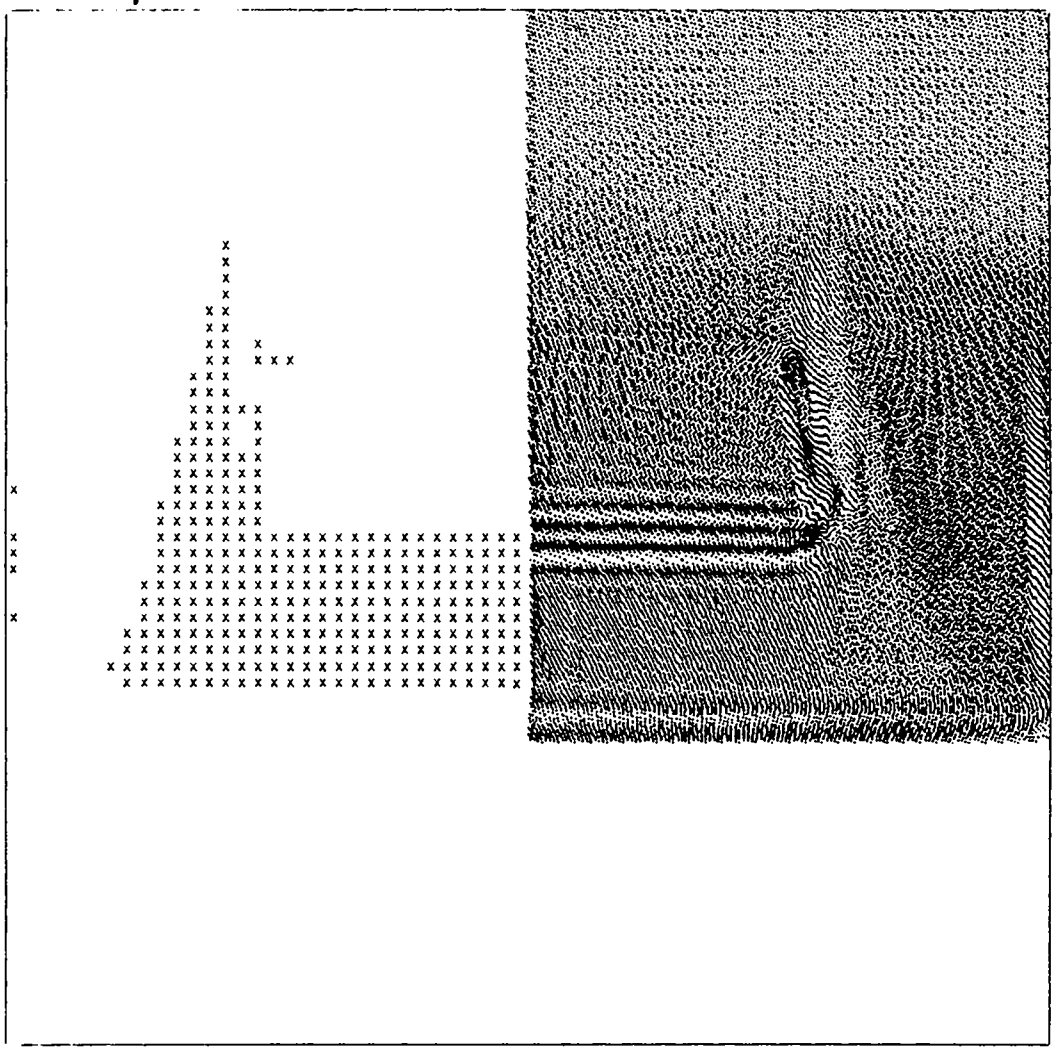

THE TIME IS 2.20000-001 MICROSECONDS AND THE CYCLE NUMBER IS 4.40000+002

Figure 14

A 0.002- by 0.002-cm CYLINDER OF ALUMINUM IN NITROMETHANE

The formation of a hot spot and failure to build up to propagating detonation from a shock interacting with a 0.002- by 0.002-cm cylinder of aluminum in nitromethane. The positions of those cells that have completely decomposed are shown in the left half of the picture with an "x". These results do not scale with the system described in Figure 13. The aluminum particles are printed twice as dark as the nitromethane particles.

0.00875 μsec.

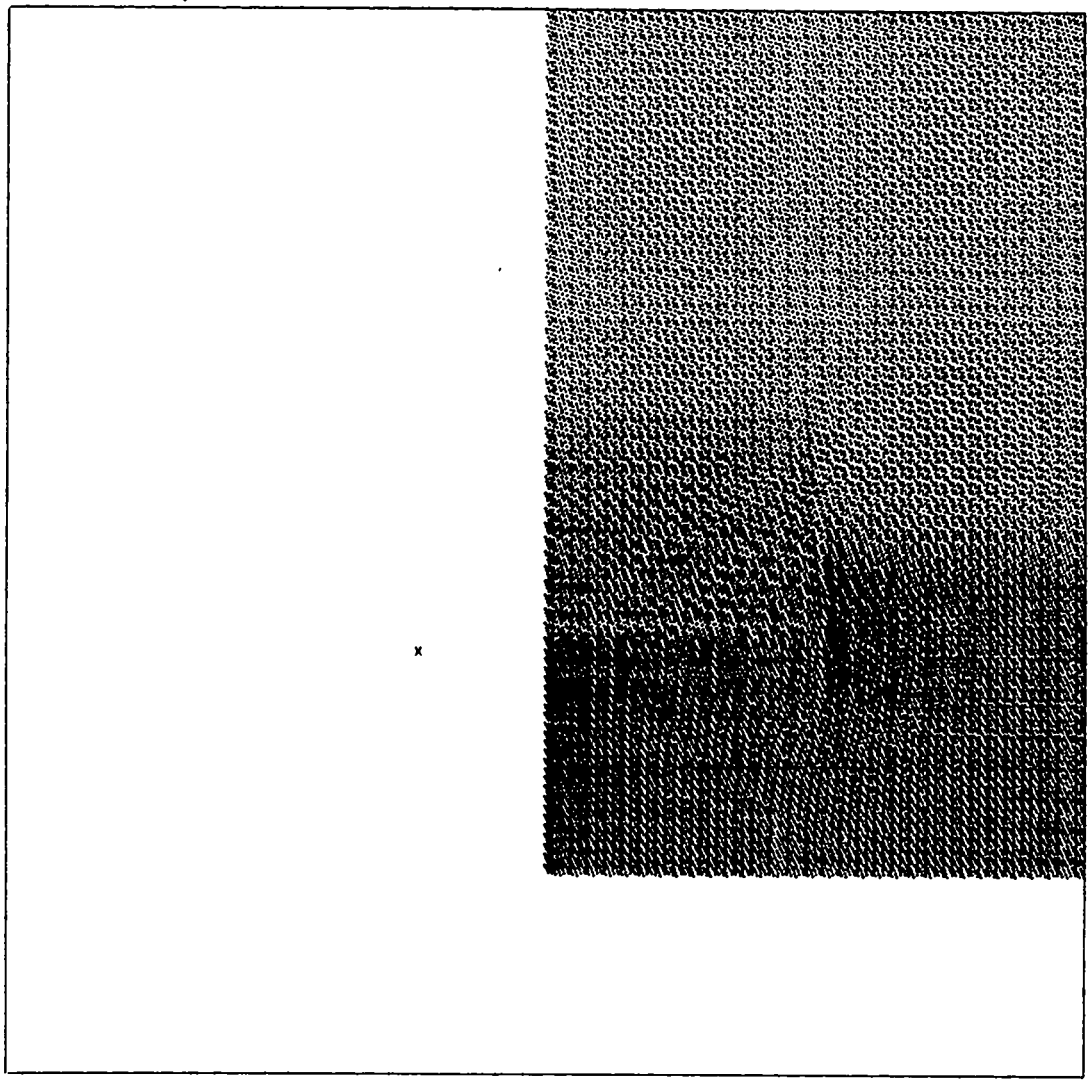

THE TIME IS 8.75000-003 MICROSECONDS AND THE CYCLE NUMBER IS 2.80000+002

0.01125 μsec.

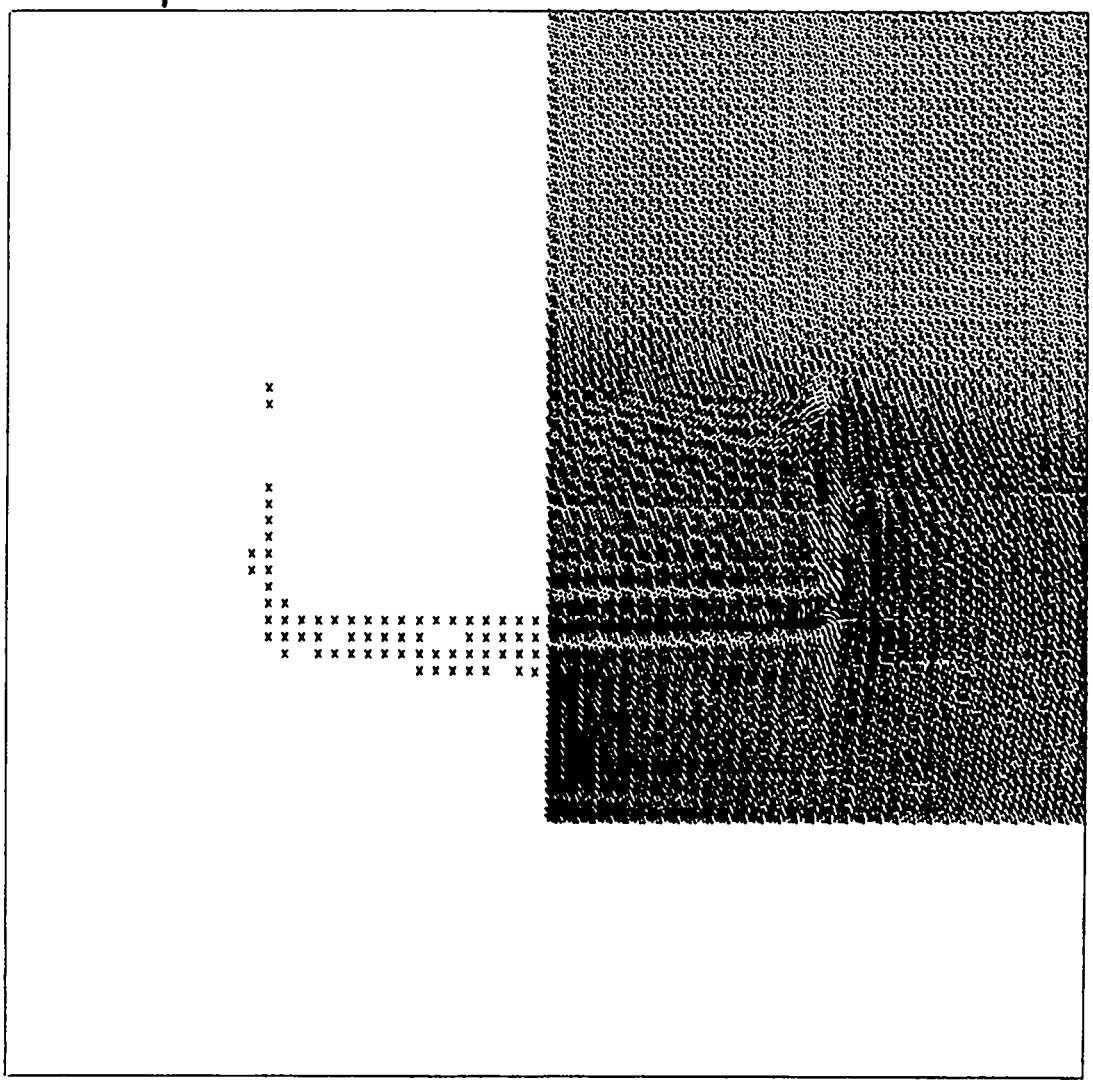

THE TIME IS 1.12500-002 MICROSECONDS AND THE CYCLE NUMBER IS 3.60000+002

0.01375 μ sec.

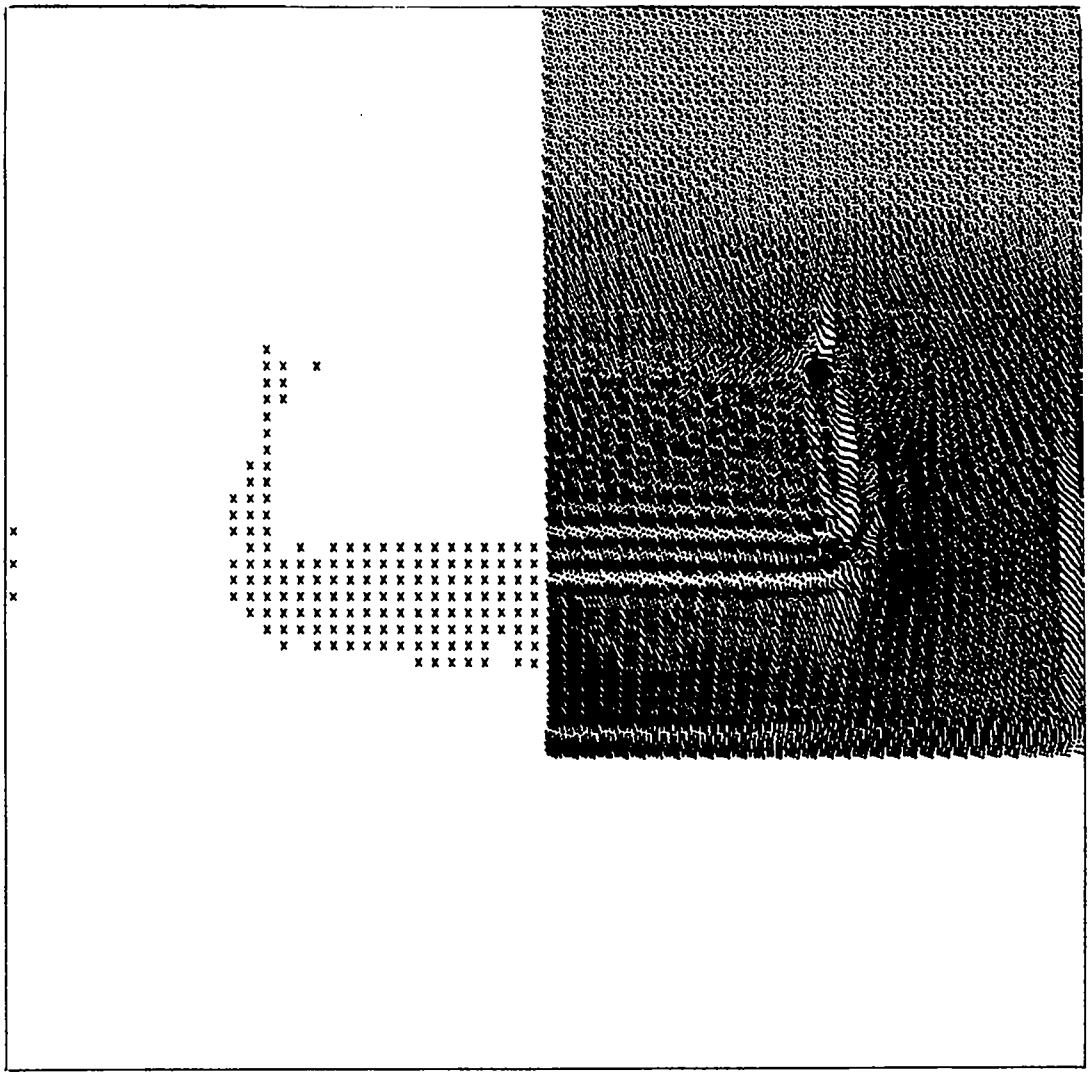

THE TIME IS 1.37500-002 MICROSECONDS AND THE CYCLE NUMBER IS 4.40000+002

VI. CORNERS OF ALUMINUM AND PLEXIGLAS IN NITROMETHANE

Travis[4] has observed early initiation of nitromethane by blocks, sheets, and rods of various plastics and metals. A container of nitromethane was mounted on a booster-attenuator system designed to generate a shock wave, almost plane over an area 10 cm in diameter, which would initiate unperturbed nitromethane with an induction time of about 1.5 μsec. Blocks, sheets, and cylindrical rods were suspended in the nitromethane and the induction times determined. Blocks were mounted with the sides perpendicular to and in contact with the surface of the attenuator plate, thus forming a 90° corner with the plate. Rods were mounted with the axis perpendicular, and sheets with the thinnest side (width) parallel, to the plate surface, either in contact with the attenuator plate or raised a few millimeters above it. For purposes of these discussions the height of the rod and the length and height of the sheets are infinite.

For identical initial shock waves, the relative effectiveness of an inclusion in decreasing the induction time is as follows: The greater the mismatch, the shorter the induction time; the thicker the sheet perpendicular to and either in contact with or above the plate surface, the shorter the induction time, but a maximum thickness exists above which the induction time is not further reduced. A minimum thickness exists below which the induction is not detectably changed by the presence of the discontinuity even though the surface area of the sheet remains essentially constant. This suggests that Helmholtz and Taylor instabilities are not important sources of extra heating. For a copper or aluminum

rod mounted above and perpendicular to the plate surface, the critical radius is greater than 0.005 cm, but less than 0.04 cm. Such observations are in good agreement with the computed results described in the previous section. The induction time is shorter when a rod or sheet is raised above the attenuator surface than when it is in contact with it, forming a corner.

While the EIC calculations are not sufficiently detailed to describe the formation of the low-temperature hot spots formed from corners, they do show us that the shock moves faster in the Plexiglas or aluminum than in the nitromethane so that multiple shocking of the nitromethane occurs and heats the nitromethane near the corner some additional 50-100°K. For example, as a 96-kbar shock emerges from the bottom of a nitromethane-filled Plexiglas box, the nitromethane next to the wall of the box is first shocked to 50 kbar by a laterally moving shock which originates at the wall, and then by an 85-kbar shock transmitted directly through the bottom of the box. The temperature of the double-shocked fluid exceeds the temperature of the single-shocked fluid by some 100°C. Such multiple shocking of the nitromethane heats it sufficiently to produce initiation in the time observed experimentally.

Figure 15 shows the computed results for an aluminum corner in nitromethane, and Figure 16 shows the results for a Plexiglas corner in nitromethane.

Figure 15

A CORNER OF ALUMINUM IN NITROMETHANE

The aluminum particles are printed twice as dark as the nitromethane particles. The horizontal axis is 0.032-cm long, the vertical axis is 0.064-cm high. The aluminum is shocked to 165.9 kbar and a particle velocity of 0.0906 cm/μsec. The nitromethane matched pressure is 85 kbar.

0.025 μsec.

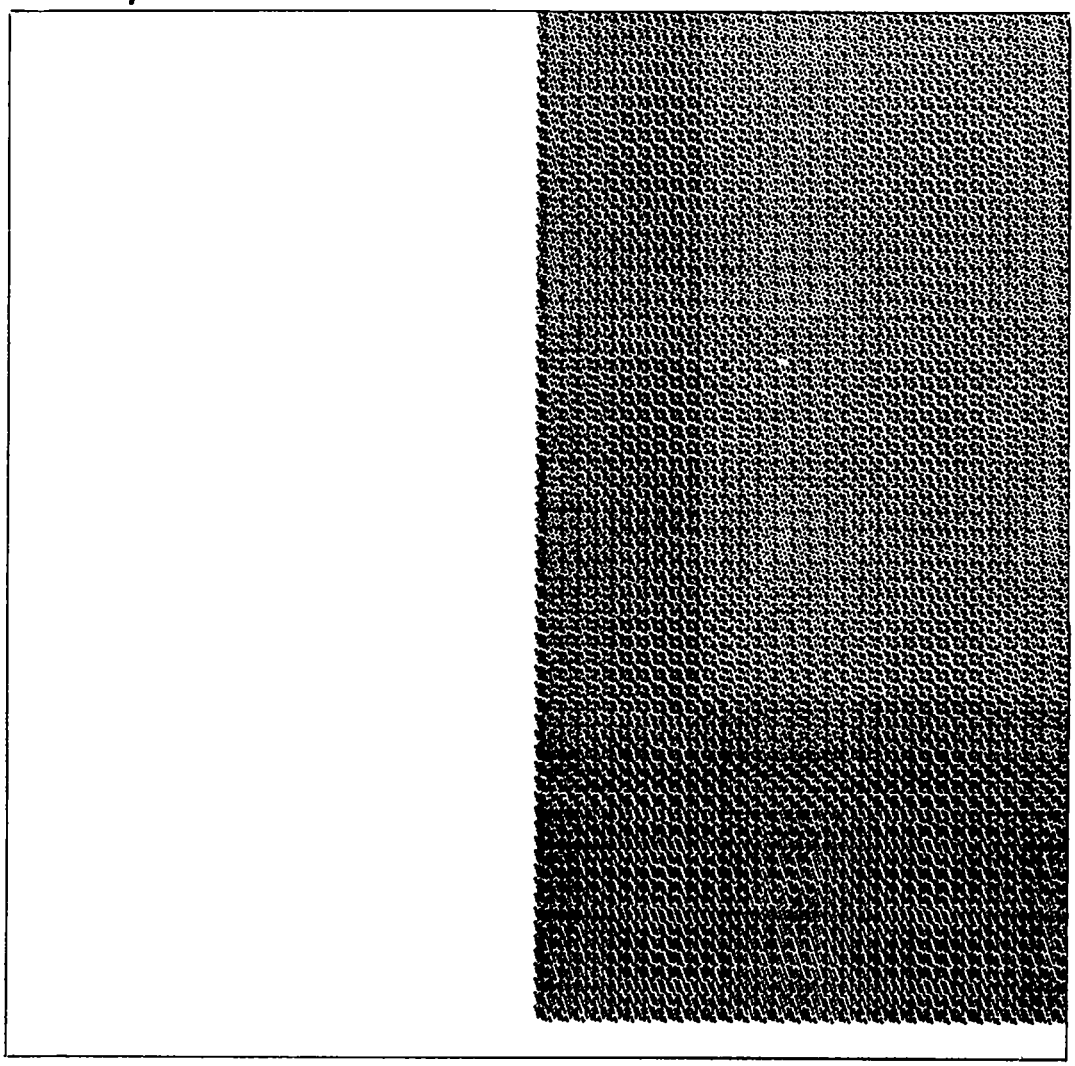

THE TIME IS 2.50000-002 MICROSECONDS AND THE CYCLE NUMBER IS 1.00000+002

0.055 μsec.

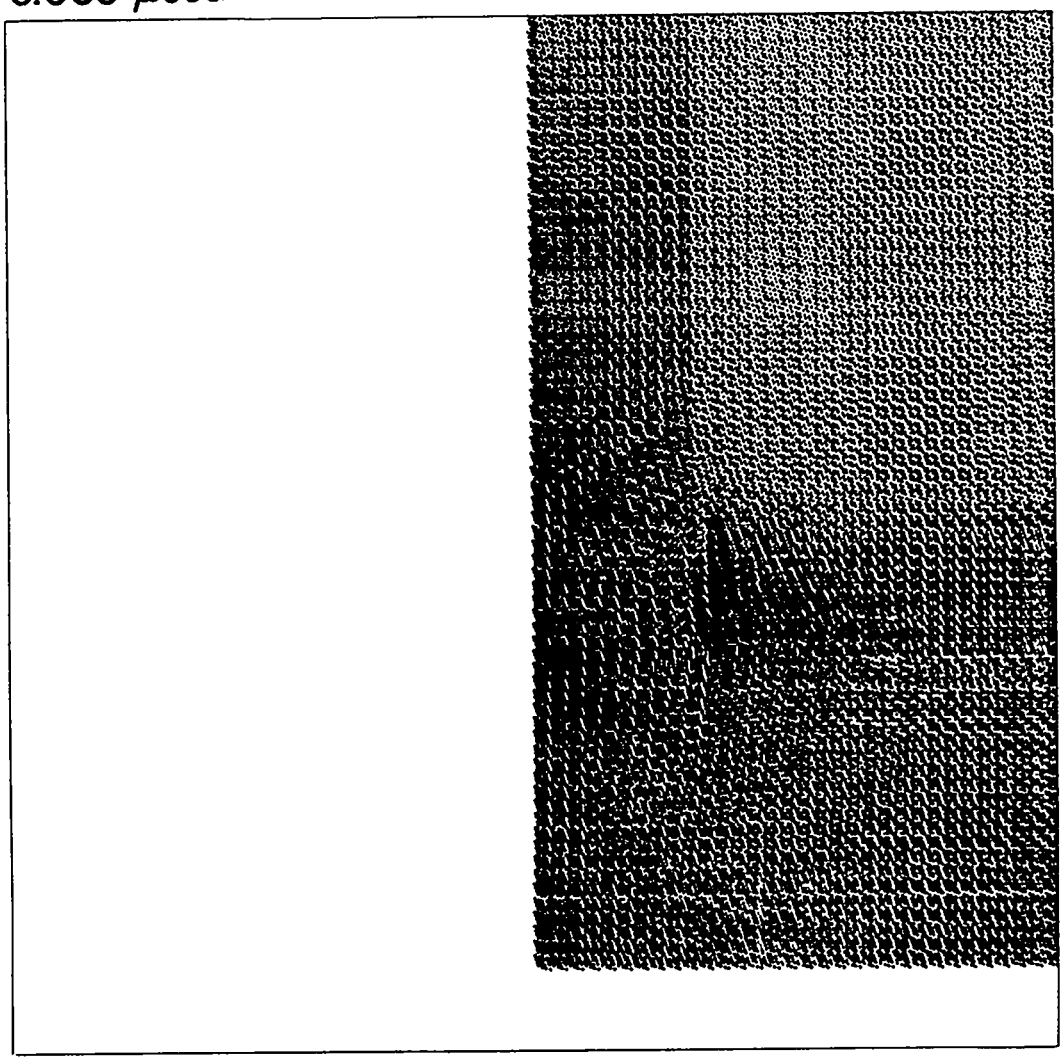

THE TIME IS 5.50000-002 MICROSECONDS AND THE CYCLE NUMBER IS 2.20000+002

0.080 μsec.

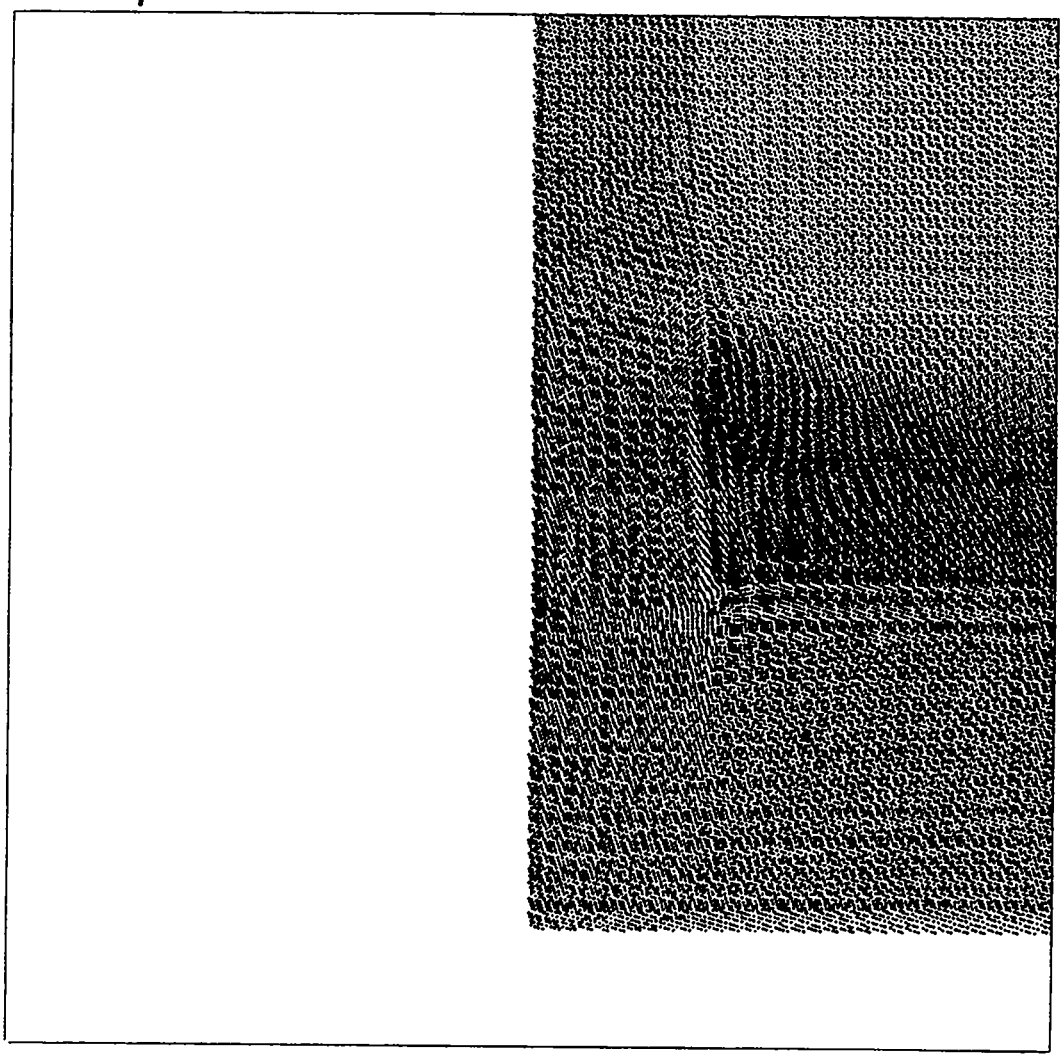

THE TIME IS 8.00000-002 MICROSECONDS AND THE CYCLE NUMBER IS 3.20000+002

Figure 16

A CORNER OF PLEXIGLAS IN NITROMETHANE

The Plexiglas particles are printed twice as dark as the nitromethane particles. The horizontal axis is 0.032-cm long, the vertical axis is 0.064-cm high, and the geometry is plane. The nitromethane has an applied piston pressure of 85.8 kbar and a particle velocity of 0.171 cm/μsec.

0.0625 μ sec.

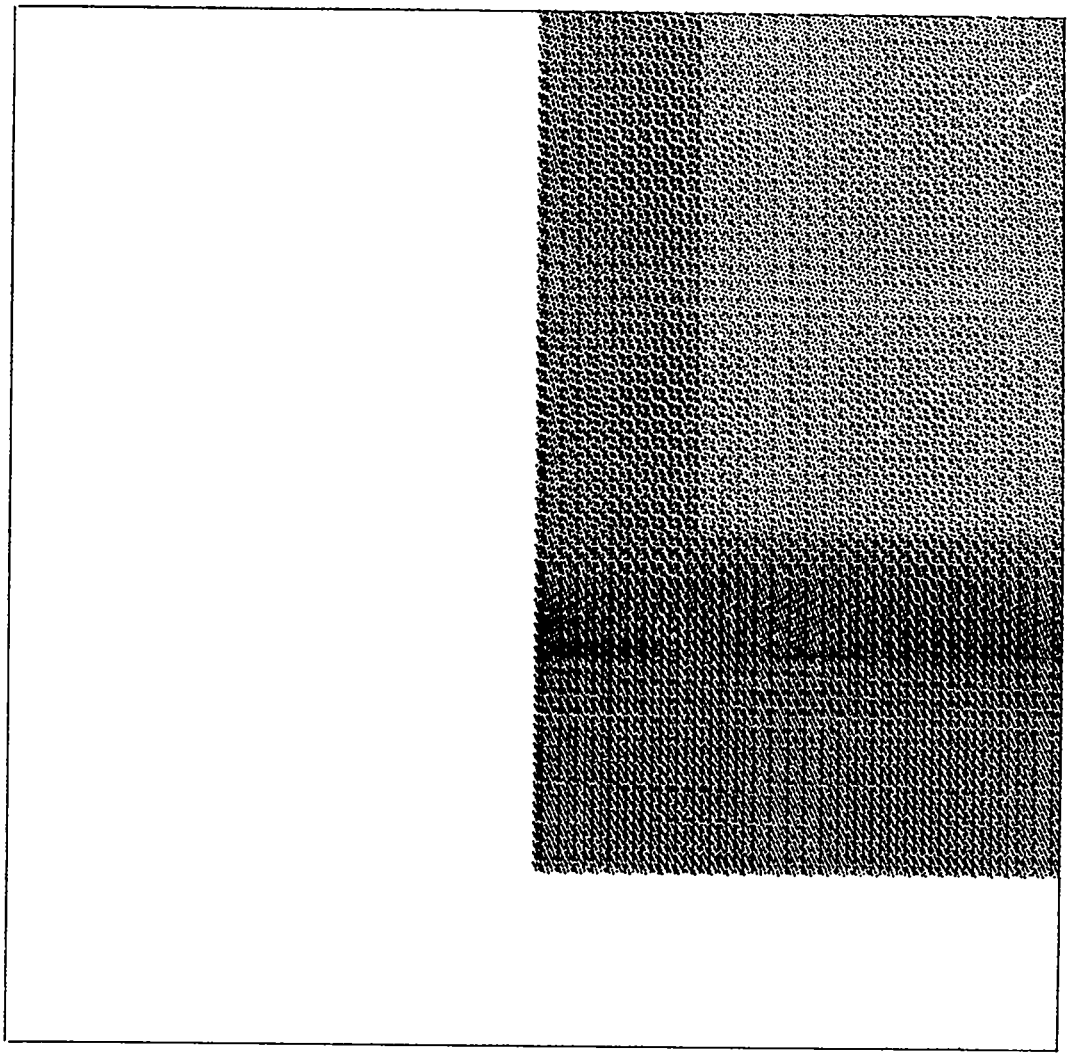

THE TIME IS 6.25000-002 MICROSECONDS AND THE CYCLE NUMBER IS 2.50000+002

0.090 μsec.

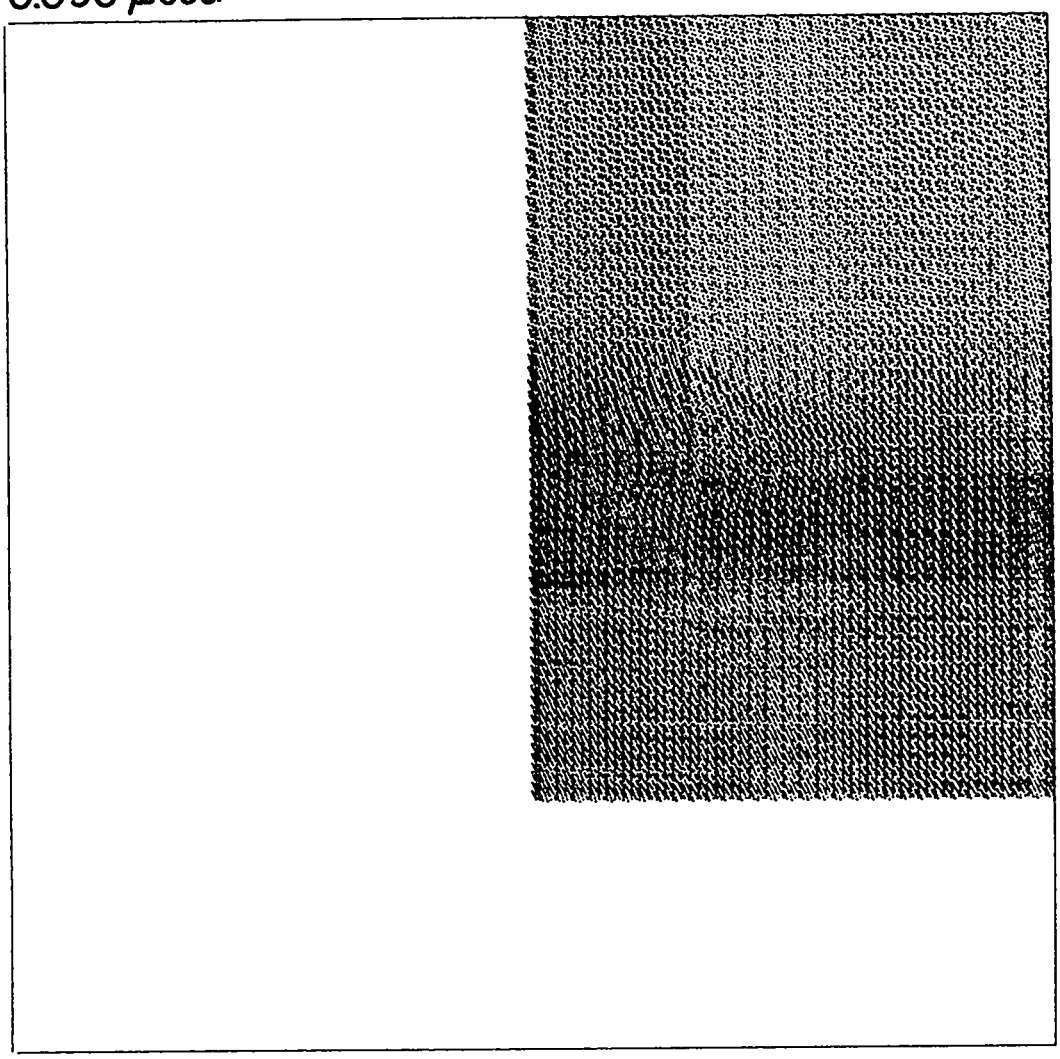

THE TIME IS 9.00000-002 MICROSECONDS AND THE CYCLE NUMBER IS 3.60000+002

0.125 μsec.

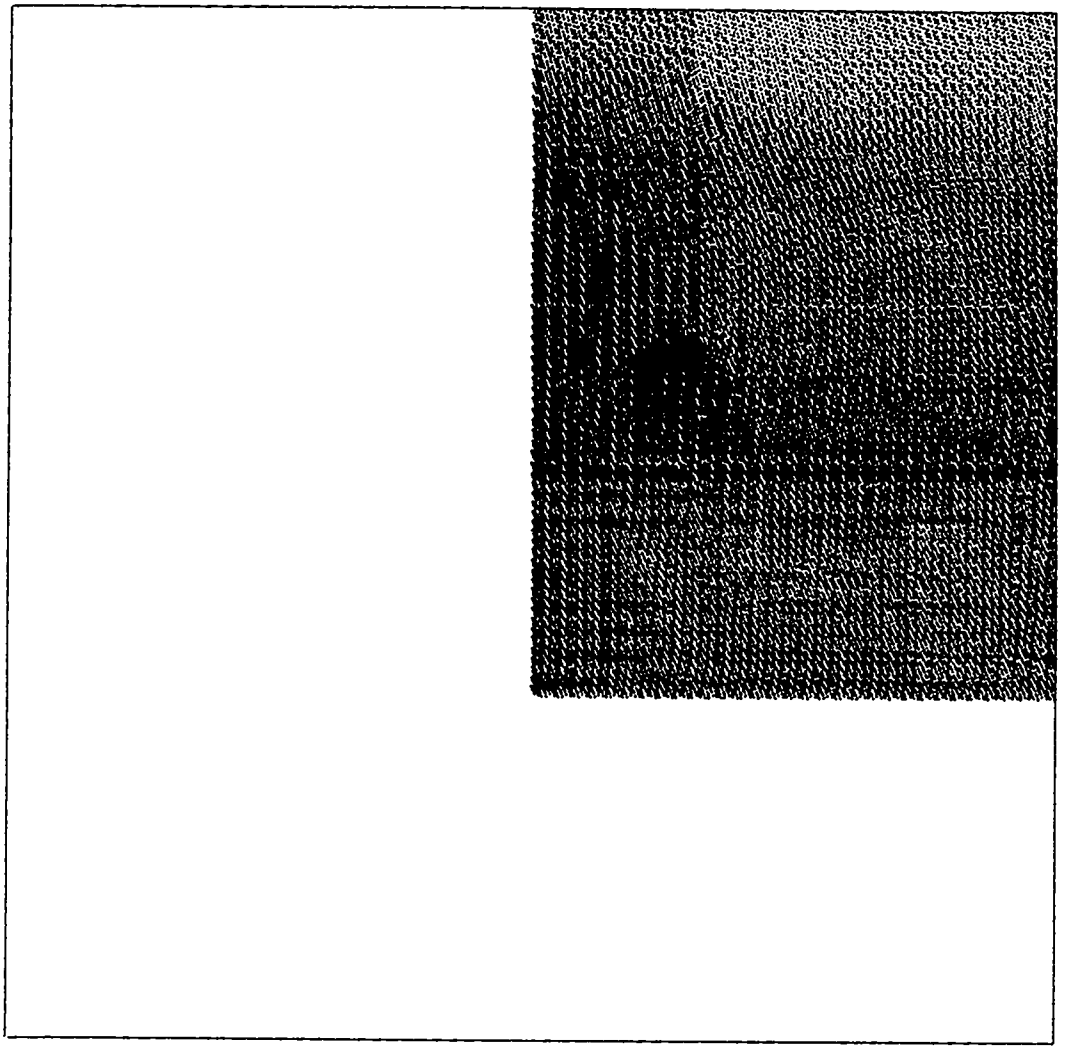

THE TIME IS 1.25000-001 MICROSECONDS AND THE CYCLE NUMBER IS 5.00000+002

VII. CONCLUSIONS

Two-dimensional numerical hydrodynamic calculations of the EIC type with realistic equations of state can be used to compute the interaction of a shock with a void, the formation of a hot spot, and buildup to propagating detonation. Failure can not be expected from the divergent nature of the flow since the reaction is essentially instantaneous in the time and space scale of interest and, therefore, with an appropriate time scale, all quantities are functions of radius/hot-spot radius. Experimental evidence suggests that failure occurs primarily from the side rarefactions cooling the explosive inside the reaction zone.

The interaction of a shock with an aluminum sphere and cylinder has been computed. The computations describe the interaction of a shock with the aluminum discontinuity, the formation of a hot spot, and buildup to propagating detonation. In this case, the hot spot is formed behind the shock front and is at a lower temperature than the hot spot formed by a shock interacting with a void. The one-dimensional hydrodynamic hot spot model is appropriate and the two-dimensional calculations show failure and propagation in approximately the same manner as the one-dimensional hydrodynamic hot spot model.

We conclude that the formation of hot spots from shocks interacting with density discontinuities is well described by two-dimensional reactive hydrodynamics with realistic equations of state. The failure of the resulting hot spot may be treated in those cases where the failure mechanism does not require a detailed reaction zone.

We have increased our understanding of the basic processes involved in the shock initiation of inhomogeneous explosives by studying theoretically the formation of hot spots from shocks interacting with single density discontinuities. The problem of failure of propagating detonation from side rarefactions cooling the explosive inside the reaction zone has not been theoretically described and is probably the next problem that must be solved before further progress is made in understanding the basic processes involved in the shock initiation of inhomogeneous explosives. This suggests that studies of the time-dependent reaction zone and of the phenomenon of failure diameter of explosives may yield further insight into the problems of shock initiation of explosives.

Appendix A

THE HYDRODYNAMIC AND REACTION EQUATIONS FOR AN EXPLOSIVE AND ONE NONREACTIVE COMPONENT

The EIC equations described by Mader[1] are used to solve the fluid dynamics. The procedure is an adaption of the PIC method of Harlow[5]. A cell may contain, for example, undecomposed explosive, detonation products of the explosive, and the nonreactive component. It is necessary to have two mass fractions to describe the composition present in any cell -- the mass fraction (W) of the decomposed explosive relative to the total mass of reactive component and the mass fraction (X) of the nonreactive component relative to the total mass of the cell.

When a particle moves from an old cell to a new cell, the "U" flag of the particle mass is tested to determine if it is a reactive or a nonreactive particle. If a particle goes from cell $\binom{j}{i}$ to cell $\binom{j}{i+1}$ and cell masses have been adjusted, then for:

A. a nonreactive particle

$$X_i^{j\,NEW} = \frac{X_i^j \left(M_i^j + m\right) - m}{M_i^j}$$

$$X_{i+1}^{j\,NEW} = \frac{X_{i+1}^j \left(M_{i+1}^j - m\right) + m}{M_{i+1}^j} \quad .$$

B. a reactive particle

$$W_{i+1}^{j\,NEW} = \frac{W_{i+1}^{j}\left(M_{i+1}^{j} - m\right)\left(1 - \chi_{i+1}^{j}\right) + (m)\,(W_{i}^{j})}{\left(M_{i+1}^{j} - m\right)\left(1 - \chi_{i+1}^{j}\right) + m}$$

$$\chi_{i}^{j\,NEW} = \frac{\left(\chi_{i}^{j}\right)\left(M_{i}^{j} + m\right)}{M_{i}^{j}}$$

$$\chi_{i+1}^{j\,NEW} = \frac{\left(\chi_{i+1}^{j}\right)\left(M_{i+1}^{j} - m\right)}{M_{i+1}^{j}} \quad .$$

NOMENCLATURE

i	cell indices in R direction
j	cell indices in Z direction
m	particle mass
M	cell mass
X	mass fraction of nonreactive component
W	mass fraction of reactive component that is undecomposed

Appendix B

EQUATION OF STATE FOR AN EXPLOSIVE AND ONE NONREACTIVE COMPONENT

The HOM equation of state was used for a cell containing a single component or any mixture of condensed explosive and detonation products, and is described in references 1, 2, and 3. Temperature and pressure equilibrium was assumed for any mixture of detonation products and condensed explosive in a cell.

When there are two components present in a cell, separated by a boundary and not homogeneously mixed, it is reasonable to assume pressure equilibrium, but the temperatures may be quite different. For these systems we assumed that the difference between the total Hugoniot energy and the total cell energy was distributed between the components according to the ratio of the total Hugoniot energies of the components.

If the cell contained all three components, the equation of state was computed assuming temperature and pressure equilibrium for the detonation products and condensed explosive, and pressure equilibrium with the nonreactive component.

The detonation product equation of state parameters used for nitromethane are described in reference 1. The condensed equation of state parameters used for the nitromethane, aluminum, Plexiglas, and water are presented in Table I.

TABLE I - EQUATION OF STATE PARAMETERS

	Nitromethane		Aluminum	
C	+ 1.647	- 001	+ 5.35	- 001
S	+ 1.637	+ 000	+ 1.35	+ 000
F_s	+ 5.41170789261	+ 000	+ 7.96115866874	+ 001
G_s	- 2.72959322666	+ 000	- 3.17533561633	+ 002
H_s	- 3.21986013188	+ 000	- 4.38525371533	+ 002
I_s	- 3.90757138698	+ 000	- 2.64248248960	+ 002
J_s	+ 2.39028184133	+ 000	-5.79734965732	+ 001
γ_s	+ 6.805	- 001	+ 1.7	+ 000
C_v	+ 4.14	- 001	+ 2.2	- 001
α	+ 3.0	- 004	+ 2.4	- 005
V_o	+ 8.86524823	- 001	+ 3.59066427289	- 001
	Plexiglas		Water	
C	+ 2.43	- 001	+ 2.264	- 001
S	+ 1.5785	+ 000	+ 1.325	+ 000
F_s	+ 5.29380243506	- 001	+ 5.69903609370	+ 000
G_s	- 4.24950371368	+ 000	- 2.66572128557	- 001
H_s	- 1.55055576332	+ 001	- 1.53713920377	+ 000
I_s	- 3.08638075572	+ 001	- 7.58607109147	+ 000
J_s	- 1.46708193739	+ 001	- 2.78464374578	+ 000
γ_s	+ 2.157	+ 000	+ 1.65	+ 000
C_v	+ 3.5	- 001	+ 1.0	+ 000
α	+ 1.0	- 004	+ 6.0	- 005
V_o	+ 8.47457627000	- 001	+ 1.0	+ 000

EQUATION OF STATE FOR TWO COMPONENTS IN A CELL SEPARATED BY A BOUNDARY

Knowing I, V, and X, calculate P, T^A, and T^B

(a) $V = X(V^A) + (1 - X)(V^B)$

(b) $P = F^A = P^B$

(c) $I_H = X(I_H^A) + (1 - X)(I_H^B)$

(d) $I^A = (I_H^A) + (I - I_H)\left(\frac{X(I_H^A)}{I_H}\right)$

(e) $I^B = (I_H^B) + (I - I_H)\left(\frac{(1-X)(I_H^B)}{I_H}\right)$

(f) $\frac{\gamma^A}{V^A}(I^A - I_H^A) + P_H^A = \frac{\gamma^B}{V^B}(I^B - I_H^B) + P_H^B$

With relationships (a) and (f) we can iterate for V^A or V^B as a function of the known parameters I, V, and X.

EQUATION OF STATE FOR THREE COMPONENTS

Knowing I, V, X, and W, calculate P, $T^{(1)}$, and $T^{(3)}$

(a) $P = P^{(1)} = P^{(2)} = P^{(3)}$

(b) $T^{(1)} = T^{(2)}$

(c) $V^{(1+2)} = W(V^{(1)}) + (1 - W)(V^{(2)})$

(d) $V = X(V^{(3)}) + (1 - X)(V^{(1+2)})$

(e) $I^{(1+2)} = W(I^{(1)}) + (1 - W)(I^{(2)})$

(f) $I_H^{(1+2)} = W(I_H^{(1)}) + (1 - W)(I_H^{(2)})$

(g) $I_H = X(I_H^{(3)}) + (1 - X)(I_H^{(1+2)})$

(h) $I^{(3)} = (I_H^{(3)}) + (I - I_H)\left(\frac{(X)(I_H^{(3)})}{I_H}\right)$

(i) $I^{(1+2)} = (I_H^{(1+2)}) + (I - I_H)\left(\frac{(1-X)(I_H^{(1+2)})}{I_H}\right)$

(j) $I^{(1+2)} = W(I^{(1)}) + (1 - W)(I^{(2)})$

From equations (c) and (d) one obtains

(k) $V = X(V^{(3)}) + (1 - X)\left[W(V^{(1)}) + (1 - W)(V^{(2)})\right]$.

From reference 1

(l) $P^{(3)} = P_H^{(3)} + \frac{\gamma^{(3)}}{V^{(3)}}\left[I^{(3)} - I_H^{(3)}\right]$

and from equations (a) and (h) one obtains

$$(m)\quad f_1 = P = P_H^{(3)} + \frac{\gamma^{(3)}}{V^{(3)}} \left[(I - I_H) \frac{(X)(I_H^{(3)})}{I_H} \right] .$$

From reference 1

$$(n)\quad P^{(2)} = P_i^{(2)} + \frac{1}{\beta V^{(2)}} \left[I^{(2)} - I_i^{(2)} \right]$$

and from equations (1), (h), and (i) one obtains

$$f_2 = P = \left[I - I_H + \frac{V^{(3)} P_H^{(3)}}{\gamma^{(3)}} + \frac{V^{(1)} P_H^{(1)} W}{\gamma^{(1)}} + (1-W) P_i^{(2)} \beta V^{(2)} \right]$$

$$\left[\frac{V^{(3)}}{\gamma^{(3)}} + \frac{W(V^{(1)})}{\gamma^{(1)}} + (1-W) V^{(2)} \beta \right]^{-1} .$$

From reference 1

$$T^{(1)} = T_H^{(1)} + \frac{(I^{(1)} - I_H^{(1)})(23,890)}{C_V}$$

and from equations (b), (1), and (n) one obtains

$$F_3 = P = \left[\frac{T_H^{(2)} - T_H^{(1)}}{23890} + \frac{P_H^{(1)} V^{(1)}}{C_V^{(1)} \gamma^{(1)}} - \frac{P_i^{(2)} \beta V^{(2)}}{C_V^{(2)}} \right]$$

$$\left[\frac{V^{(1)}}{C_V^{(1)} \gamma^{(1)}} - \frac{\beta (V^{(2)})}{C_V^{(2)}} \right]^{-1} .$$

Taking

$$F = f_1 - f_3 = 0$$

$$G = f_2 - f_3 = 0$$

one may solve for $V^{(1)}$ and $V^{(2)}$ by the Newton-Raphson method. These equations were first derived by W. Gage.

NOMENCLATURE

A	indices for component A, the nonreactive component
B	indices for component B, either condensed explosive or detonation products
H	Hugoniot
I	internal energy
P	pressure
T	temperature
V	volume
W	mass fraction of condensed explosive
γ	$V\ (\partial P/\partial E)_V$
X	mass fraction of component A
1	indices for the reactive condensed component
2	indices for detonation products
3	indices for the nonreactive condensed component
i	isentrope (detonation product)
β	$\frac{1}{V}\ (\partial I/\partial P)_V$

Appendix C

BUBBLE CLOSURE -- A COMPARISON OF EXPERIMENT AND CALCULATIONS

D. Venable[6] has taken "Phermex"[7] radiographs of the interaction of a shock in water with a spherical bubble of air so that we might obtain a check on how well we compute the closure of a bubble using the two-dimensional hydrodynamic code, EIC. The experimental arrangement was a 4-inch-square box of water containing a 1.2-inch-diameter bubble of air lightly confined by thin glass. The shock was generated with 8 inches of Composition B and ran through 0.25-inch Plexiglas before it reached the water. The shock in the water had a shock velocity of 0.529 cm/μsec and a pressure of 121 kbar. The radiographs taken at times of about one-half and three-fourths closure of the bubble are shown in Figure 17. The results of an EIC calculation for a 1.2-inch-diameter spherical void in a 4-inch-radius cylinder of water being shocked to 121 kbar are shown in Figure 18 for the same times as the experimental radiographs in Figure 17. The fluid flow is well described by the calculations.

Figure 17

PHERMEX RADIOGRAPHS OF CLOSURE OF A SPHERICAL BUBBLE IN WATER

The first picture shows the shock wave curvature in a 4-inch-square box of water without a bubble being shocked by 8 inches of Composition B. The second picture shows the bubble about half closed and corresponds to the first calculated picture in Figure 18. The third picture shows the bubble about three-fourth closed and corresponds to the second picture in Figure 18. The outline of the bubble has been sketched on the radiographs since the reproduction is poor.

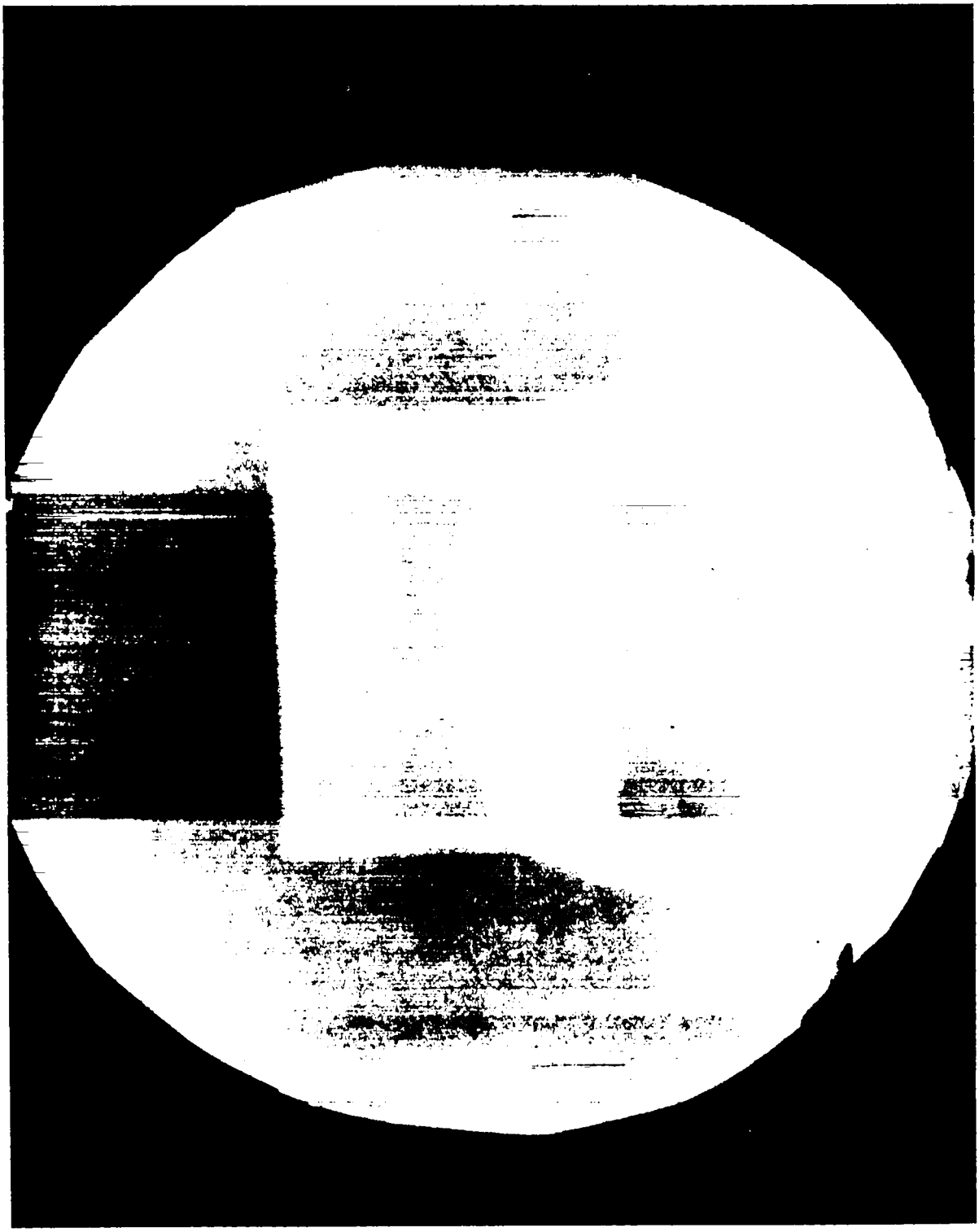

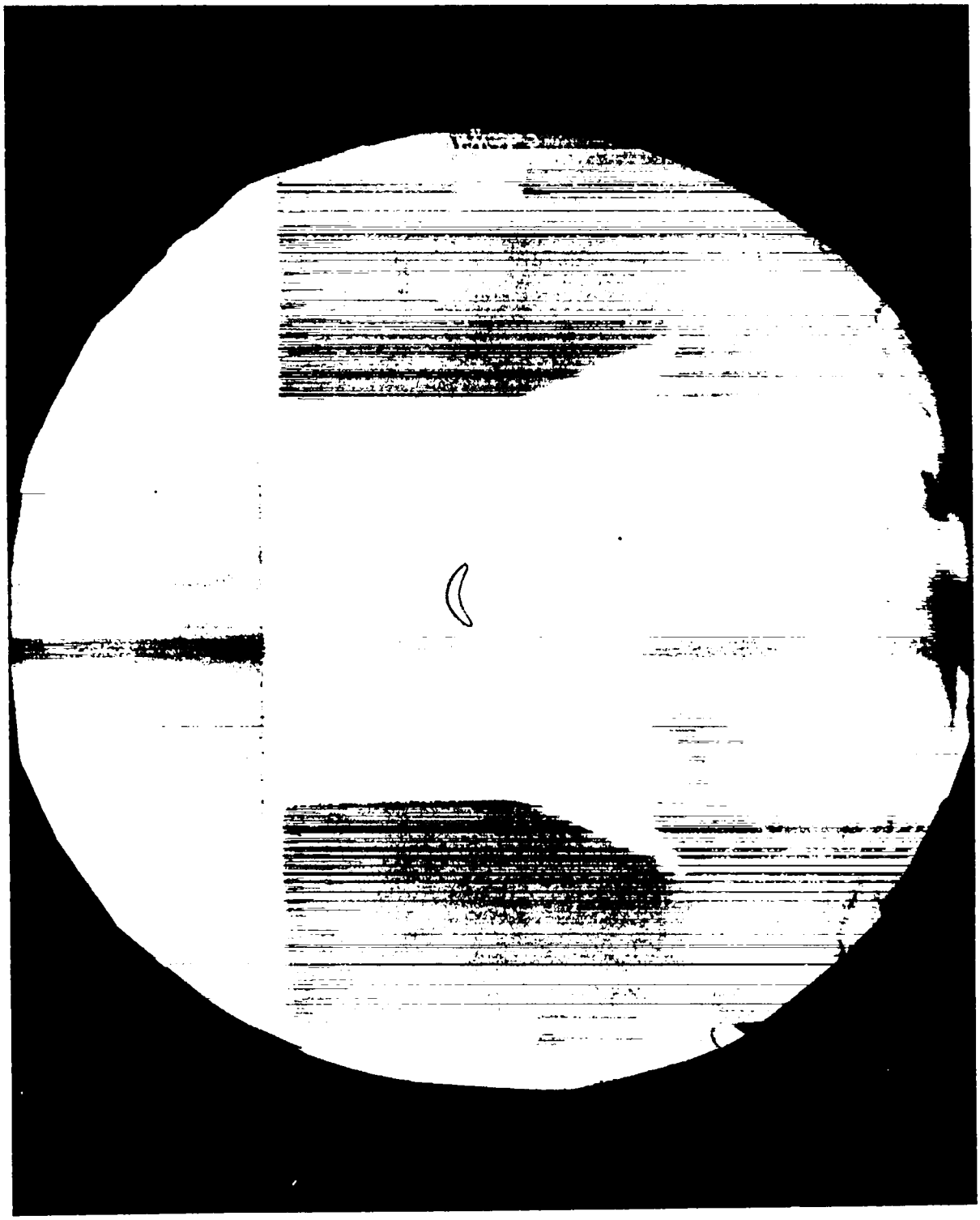

Figure 18

CALCULATED CLOSURE OF A SPHERICAL VOID IN WATER

The pictures show the particle positions for an EIC calculation of a 1.2-inch-diameter spherical void in a 4-inch-diameter cylinder of water being shocked to 121 kbar.

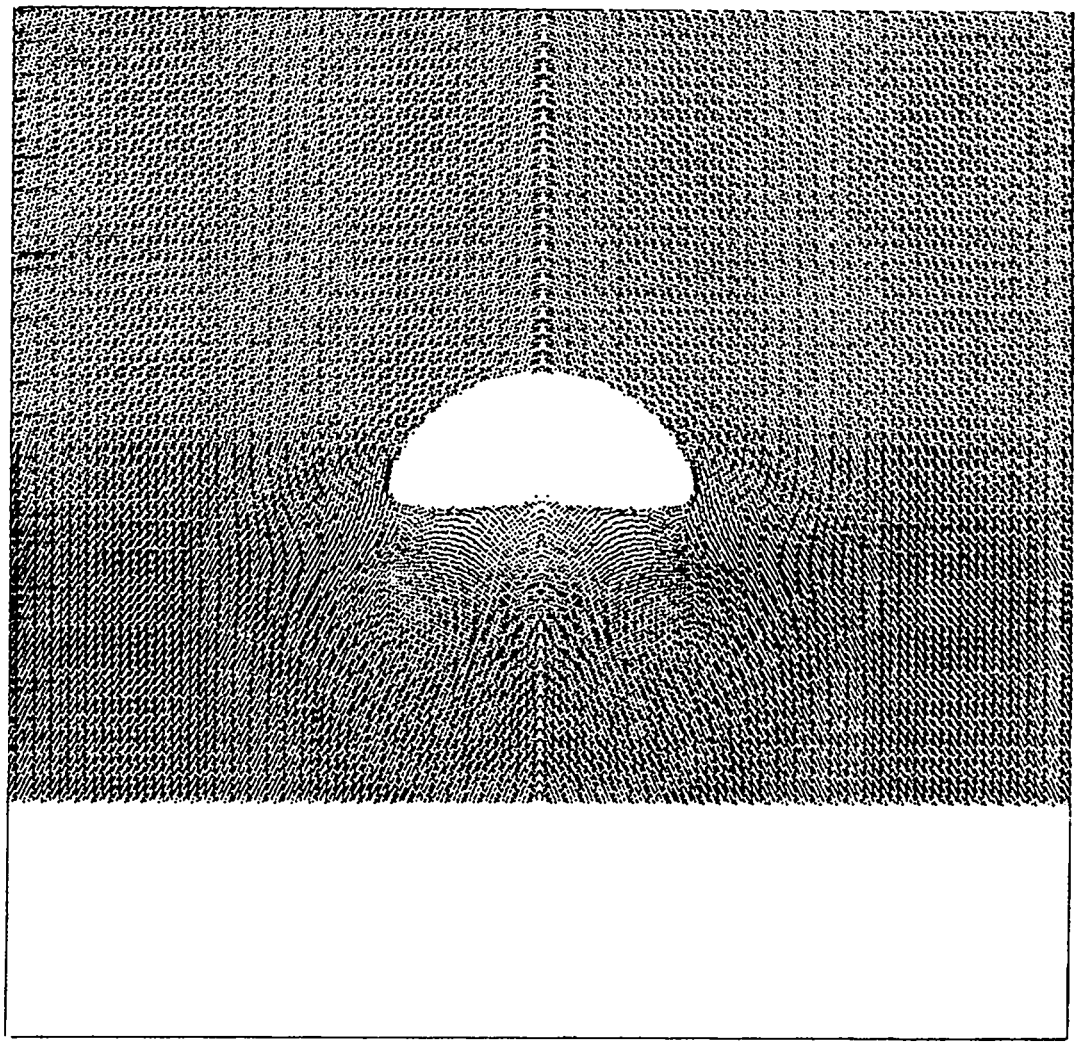

THE TIME IS 1.02000+001 MICROSECONDS AND THE CYCLE NUMBER IS 3.40000+002

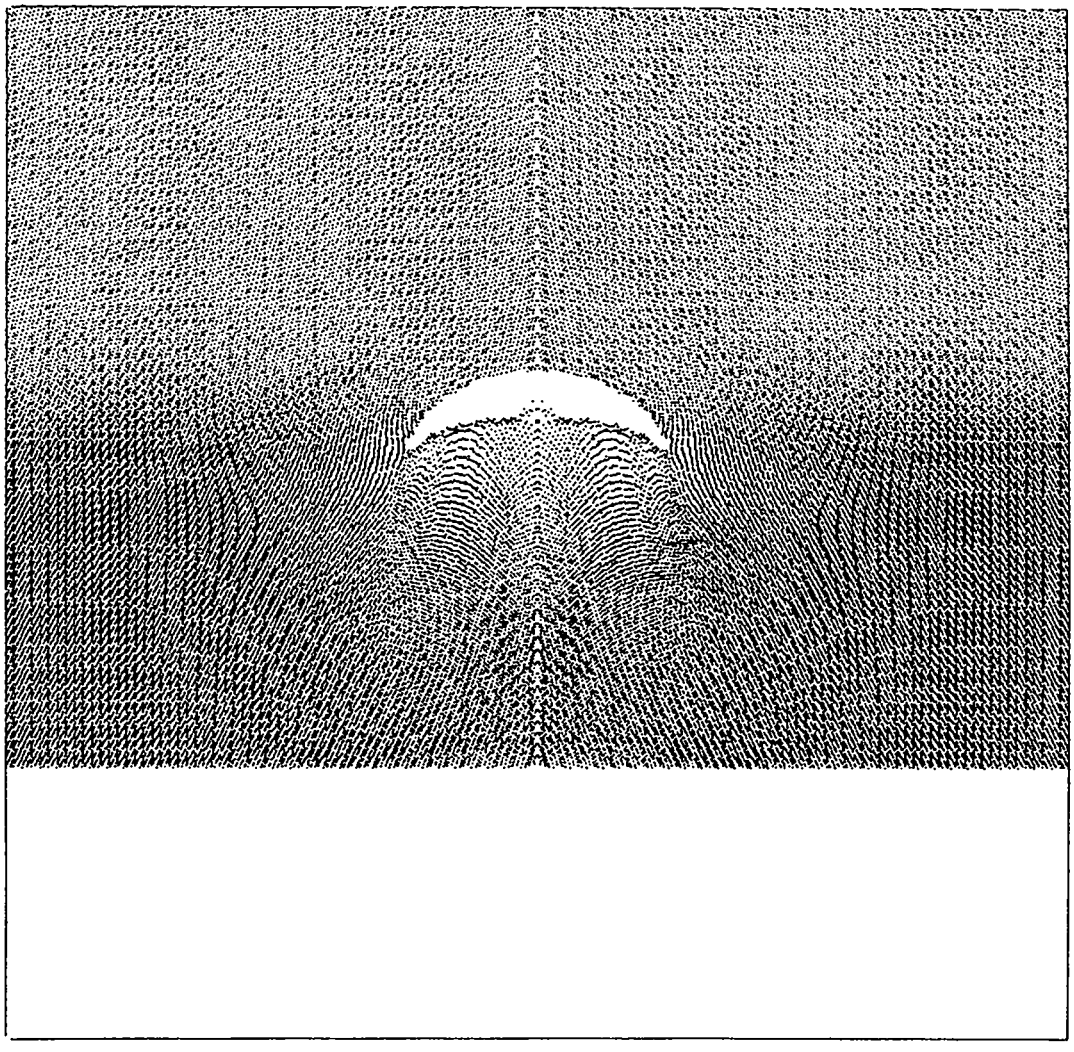

THE TIME IS 1.17000+001 MICROSECONDS AND THE CYCLE NUMBER IS 3.90000+002

Appendix D

THE ONE-DIMENSIONAL APPROACH TO HETEROGENEOUS SHOCK INITIATION

The problem of empirically reproducing, in one-dimensional hydrodynamic problems, the gross features of the shock initiation of heterogeneous explosives has been extensively studied. The results are never satisfactory. For example, many of the models result in complete decomposition of all the explosive behind the shock front long before initiation of propagating detonation occurs.

Our "empirical heterogeneous shock initiation burn" technique described in reference 8 burns too much of the explosive, and the pressures are too low during the buildup to propagating detonation. Where the details of the pressure buildup to detonation are important--as in certain unpublished experiments by Gittings on the contribution of shocked, but not detonating, 9404 to the velocity of metal plates--the empirical technique is useless.

We shall present a detailed interpretation of the experimental data and show that a one-dimensional treatment of the problem is inadequate. This conclusion is hardly surprising.

To assist us in interpreting the experimental data, a code was written to compute the reactive Hugoniots of an explosive using the HOM mixture equation of state[1,2,3,8]. For 9404 we used the unreacted equation of state, $U_s = 0.2423 + 1.883\ U_p$, given by Ramsay[9], and the

completely reacted BKW equation of state given in reference 10.

The computed Hugoniots for 9404 are given in Figure 19 where W is the mass fraction of the undecomposed explosive.

One may use these reactive Hugoniots to estimate the amount of reaction one may be obtaining for an experimentally measured Hugoniot point by determining on which of the reactive Hugoniots the point lies.

Two experimentally measured Hugoniots of partially reacting 9404 are available. The Ramsay Hugoniot[9] may be described by $U_s = 2.46 + 2.53\ U_p$, and the Gittings Hugoniot[11] may be described by $U_s = 2.715 + 2.576\ U_p$. Using these experimental Hugoniots, one obtains the estimates of initial decomposition of 9404 as a function of shock pressure shown in Figure 20.

The experimental data of distance of run to propagating detonation for any initial shock pressure shown in Figure 21 may now be used to obtain the amount of reaction for any distance of run.

It seems reasonable to assume that the explosive will pass through the same P,W,X state points at the shock front regardless of the initial conditions. If this is true, we can describe the complete path of build-up to detonation. For 9404, the path of buildup to propagating detonation is shown in Figures 22, 23, and 24. This is our "experimental" description of the process. The qualitative features of this description are probably realistic; however, one can not expect it to be quantitative because of the assumptions that were necessary.

We made various attempts to reproduce the observed phenomena by

incorporating this description of the process in a one-dimensional hydrodynamic model.

First, we programmed the degree of reaction to be a function of the shock pressure as shown in Figure 20. Initially driving the undecomposed explosive with a 48-kbar shock, we obtained a steady wave of 60 kbar and 8% reaction. This is the steady state solution of the problem.

We programmed the degree of reaction to be a function of the distance the shock has run as shown in Figure 23. We obtained "numerically stable", weak-detonation solutions until more than 50% of the explosive was decomposed, and then finally a C-J detonation developed with larger amounts of reaction. The buildup pressures were much lower than the experimental values.

To obtain a behavior close to the observed one it was necessary to program the degree of reaction, not as a homogeneous rate, but as cells of no reaction or total reaction occurring near the shock front and with the average amount of reaction per unit distance of run given by Figure 23. This is a very crude technique for introducing the two-dimensional nature of the decomposition of the explosive.

We conclude that for reasonable degrees of decomposition of a heterogeneous explosive during buildup to detonation, a one-dimensional model does not satisfactorily reproduce the experimental observations. One apparently needs at least a two-dimensional reaction center model.

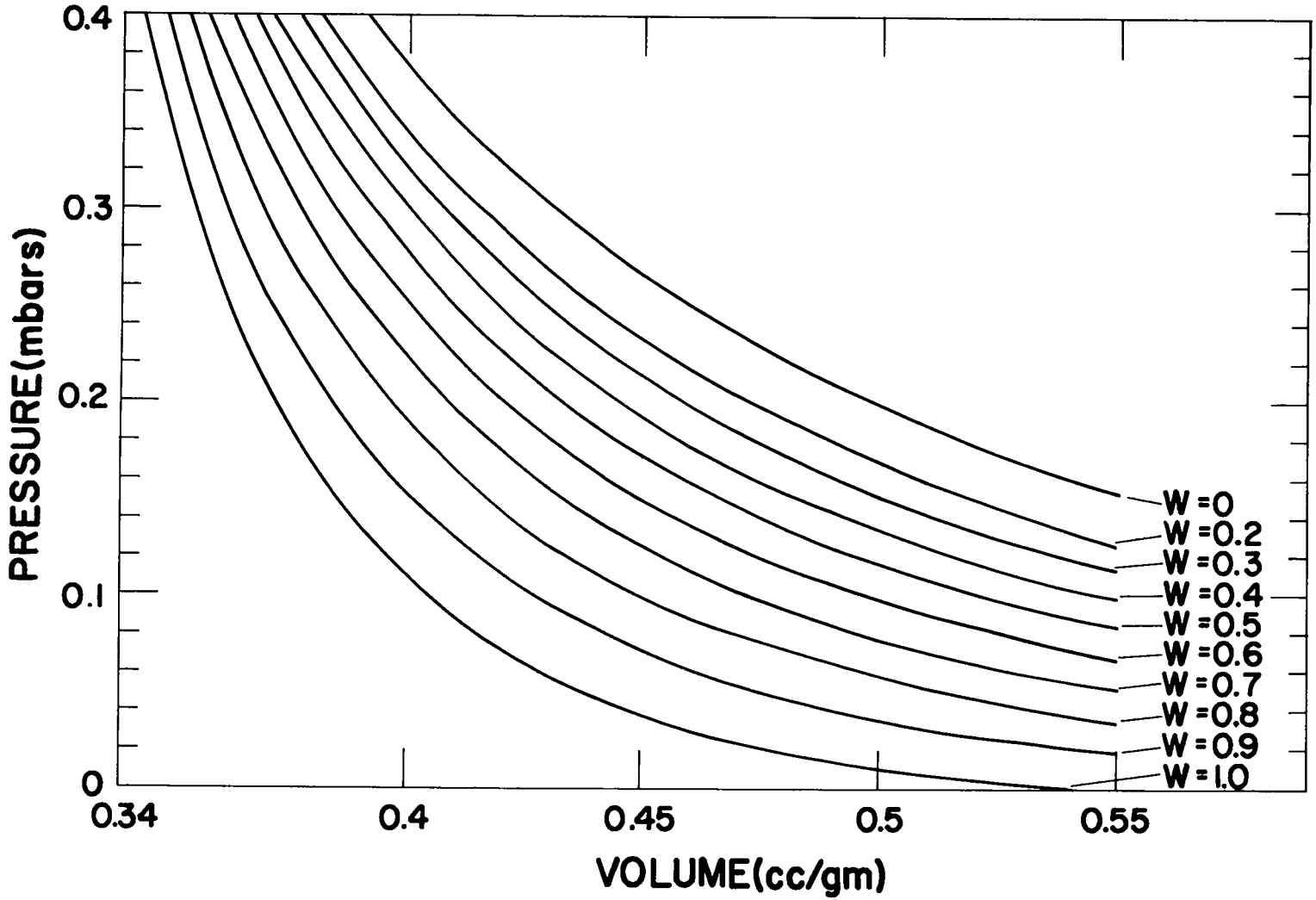

Figure 19. 9404 Hugoniots with various amounts of reaction.

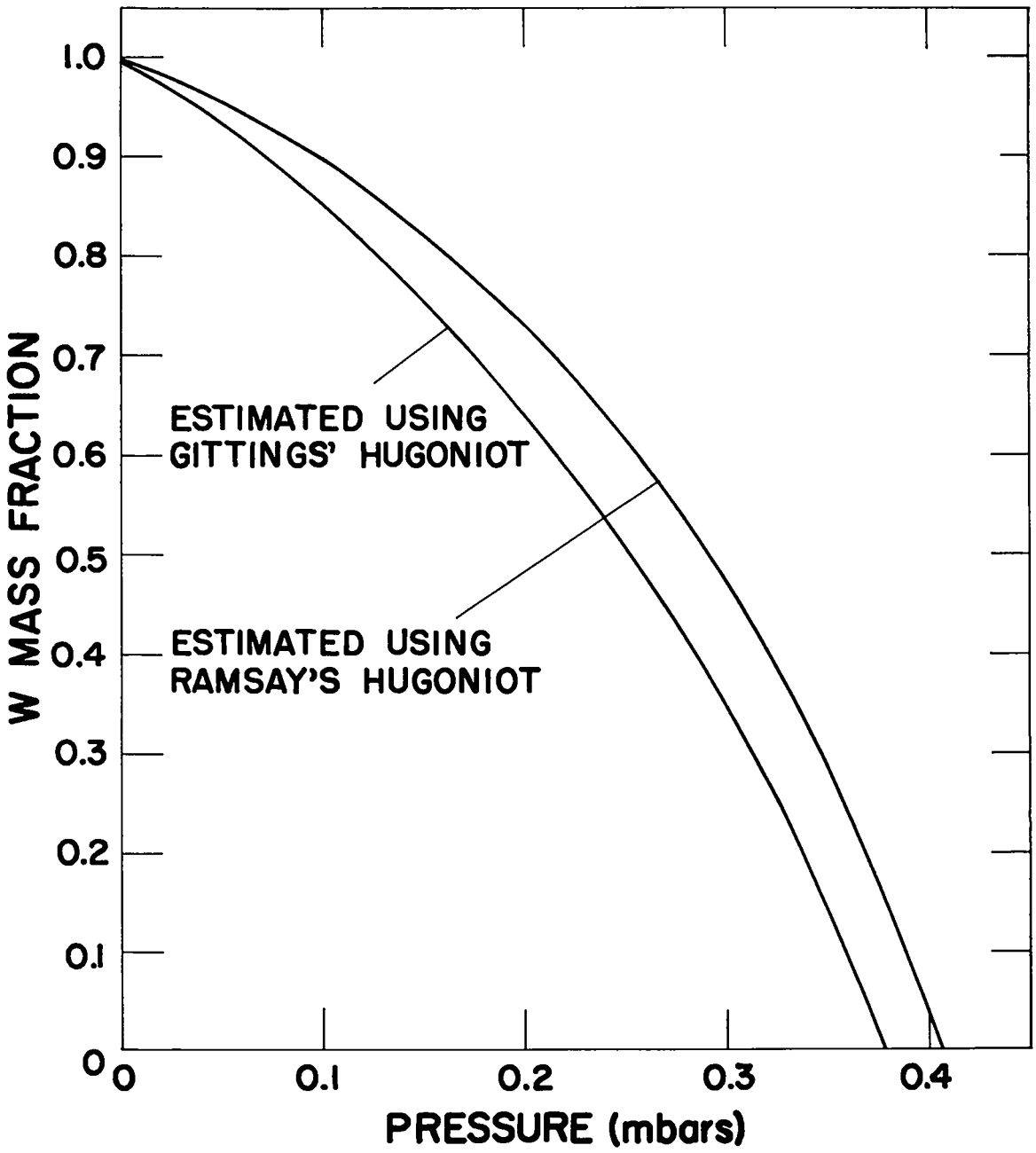

Figure 20. Initial decomposition of 9404 as a function of pressure.

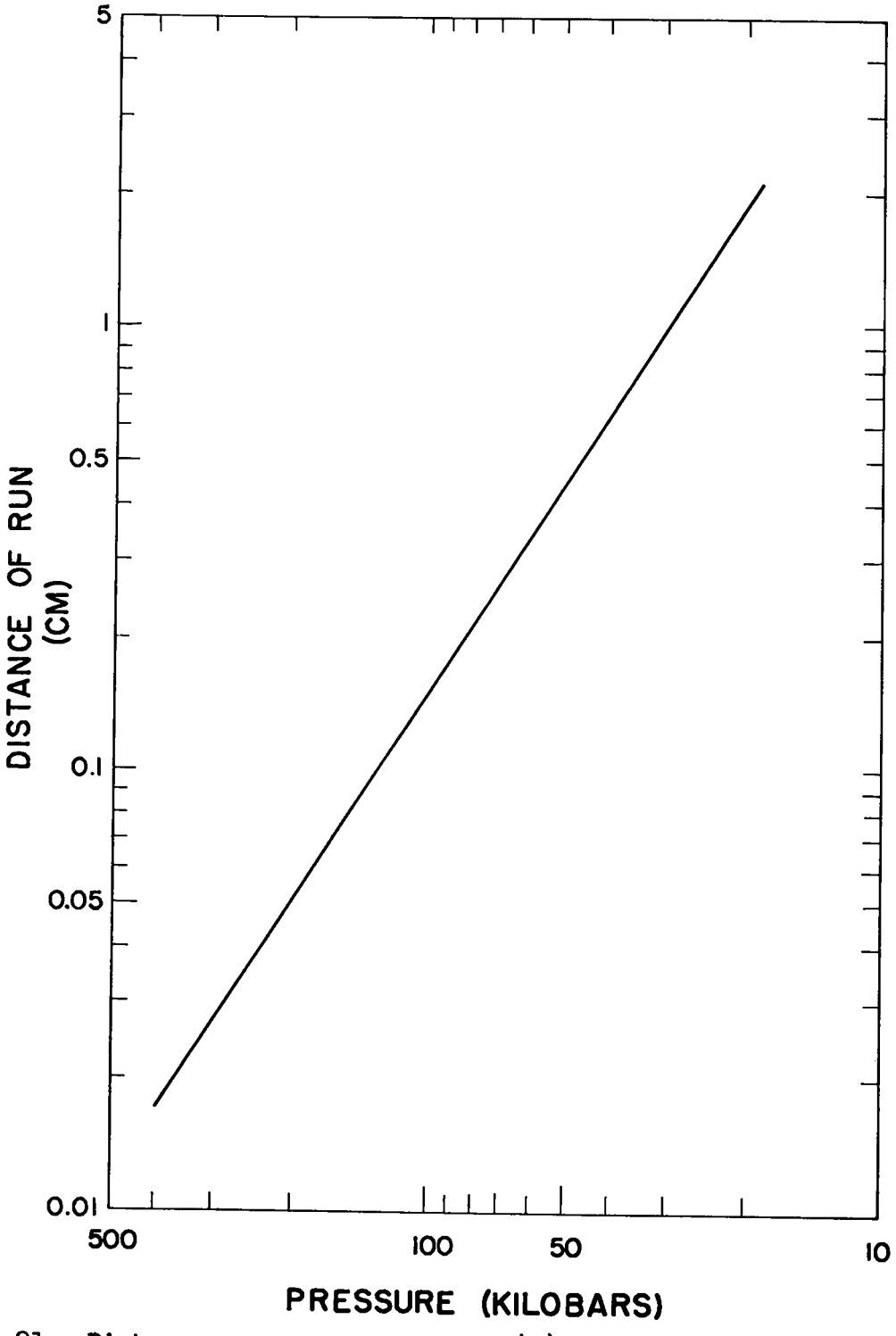

Figure 21. Distance versus pressure for 9404.

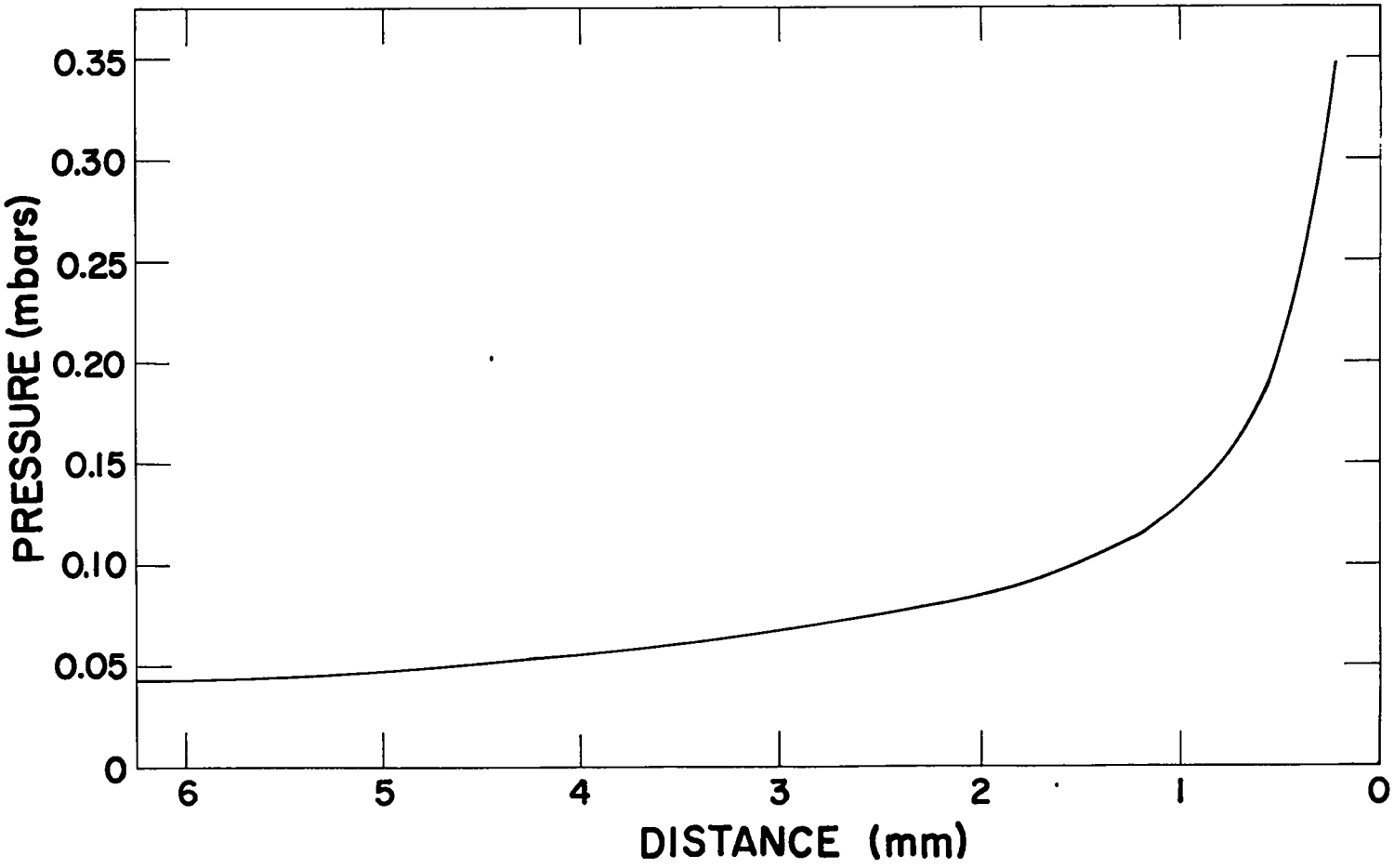

Figure 22. Pressure buildup profile for 9404.

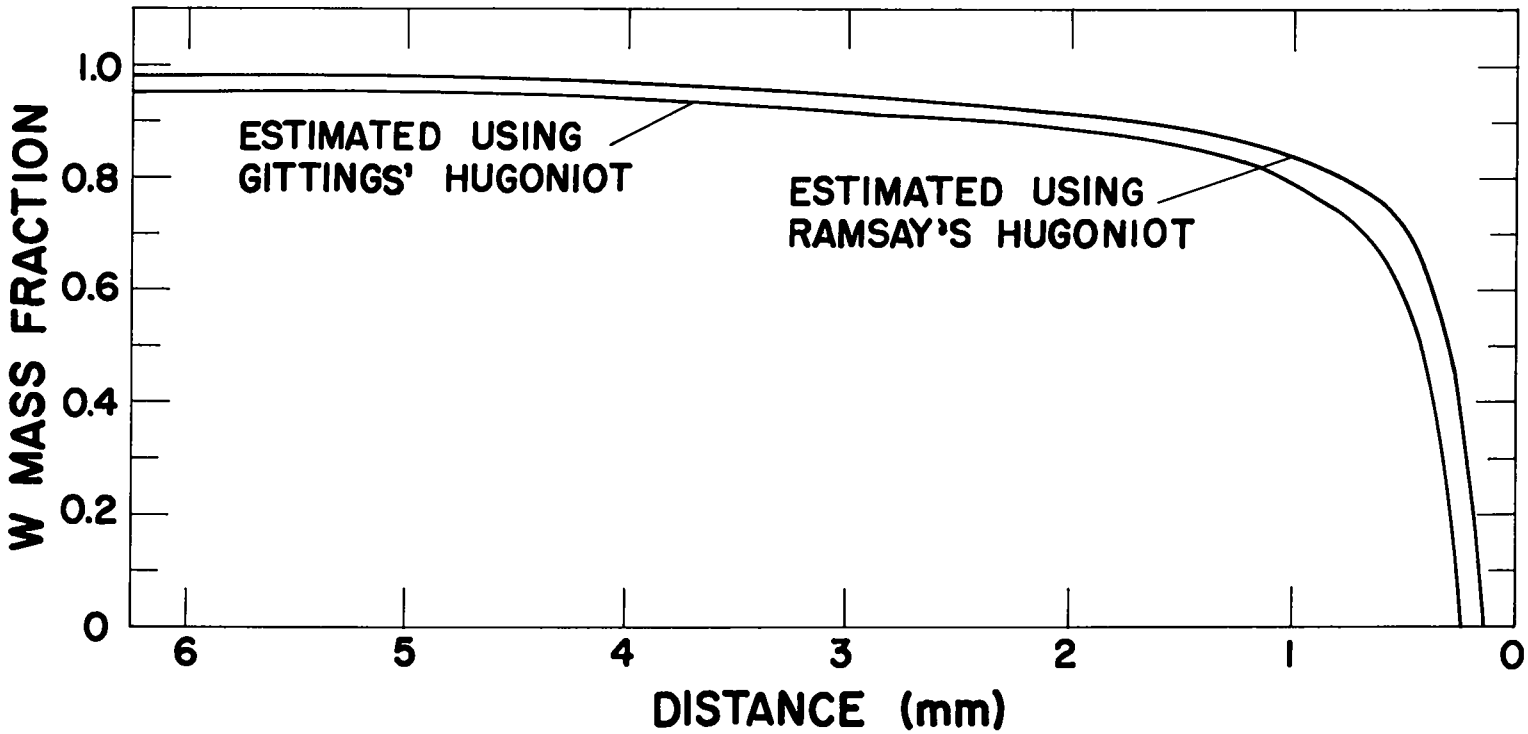

Figure 23. Decomposition buildup profile for 9404.

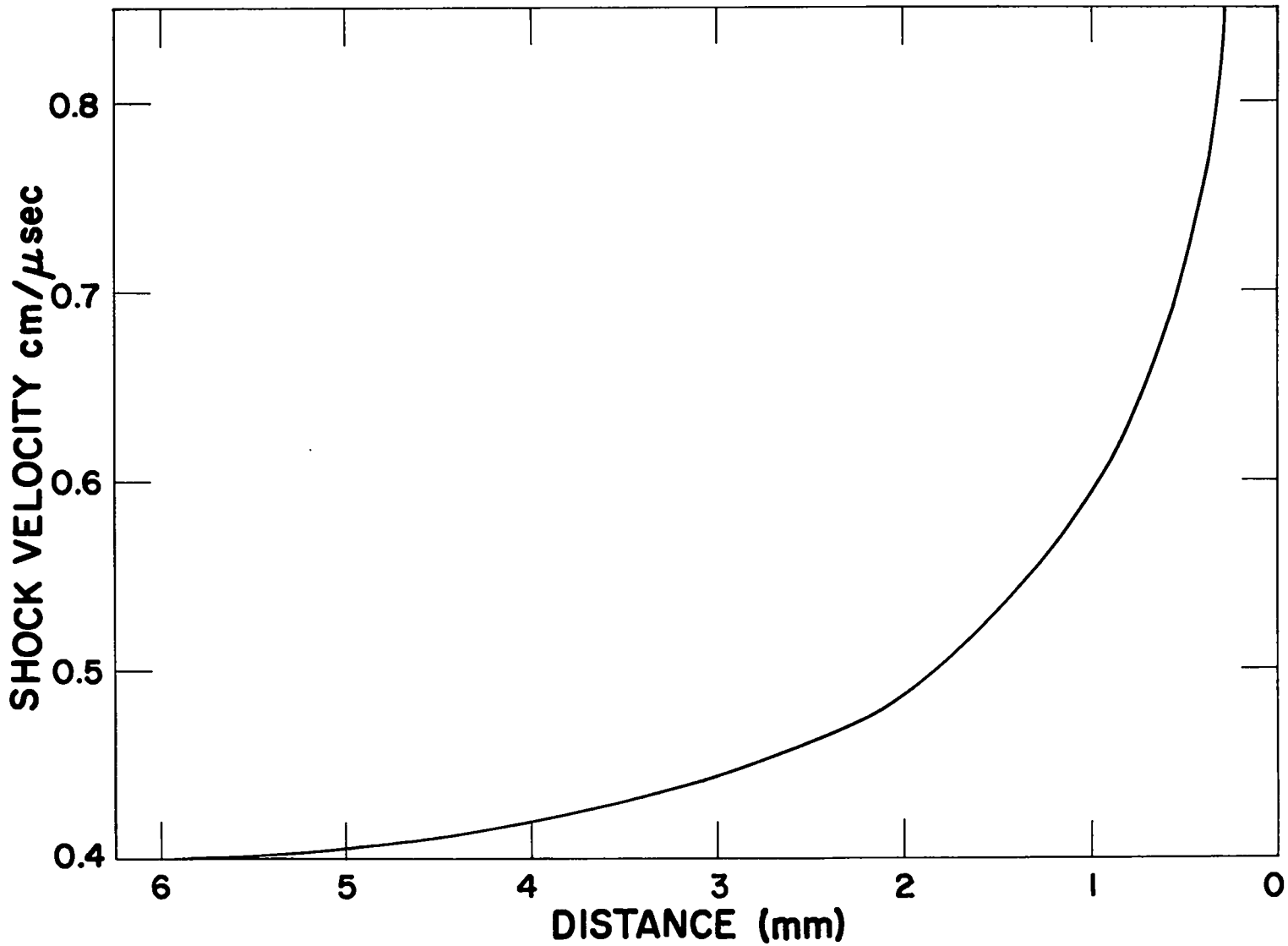

Figure 24. Shock velocity buildup profile for 9404.

LITERATURE CITED

1. Mader, Charles L., "The Two-Dimensional Hydrodynamic Hot Spot", Los Alamos Scientific Laboratory report LA-3077 (1964).

2. Mader, Charles L., "Shock and Hot Spot Initiation of Homogeneous Explosives", Phys. Fluids 6, 375 (1963).

3. Mader, Charles L., "The Hydrodynamic Hot Spot and Shock Initiation of Homogeneous Explosives", Los Alamos Scientific Laboratory report LA-2703 (1962).

4. Travis, J. R., private communication.

5. Harlow, F. H., "The Particle-In-Cell Computing Method for Fluid Dynamics", in Methods in Computational Physics, Alder, Fernbach, and Rotenberg, Eds. (Academic Press, New York, 1964), Vol 3, pp. 319-343.

6. Venable, D., private communication.

7. Venable, D., "PHERMEX", Physics Today 17, No. 12 (1964).

8. Mader, Charles L., "STRETCH SIN - A Code for Computing One-Dimensional Reactive Hydrodynamic Problems", Los Alamos Scientific Laboratory report GMX-2-R-63-1 (1963), TID-18571.

9. Ramsay, J., private communication.

10. Mader, Charles L., "Detonation Properties of Condensed Explosives Computed Using the Becker-Kistiakowsky-Wilson Equation of State", Los Alamos Scientific Laboratory report LA-2900 (1963).

11. Gittings, E., private communication.